SPRINGER BRIEFS IN APPLIED SCIENCES AND TECHNOLOGY · MANUFACTURING AND SURFACE ENGINEERING

Vijayan Krishnaraj
Redouane Zitoune
J. Paulo Davim

Drilling of Polymer-Matrix Composites

Springer

SpringerBriefs in Applied Sciences and Technology

Manufacturing and Surface Engineering

Series Editor

J. Paulo Davim

For further volumes:
http://www.springer.com/series/10623

Vijayan Krishnaraj · Redouane Zitoune
J. Paulo Davim

Drilling of Polymer-Matrix Composites

Springer

Vijayan Krishnaraj
PSG College of Technology
Tamil Nadu
India

J. Paulo Davim
Department of Mechanical Engineering
University of Aveiro
Aveiro
Portugal

Redouane Zitoune
Clement Ader Institute
Toulouse University
Toulouse
France

ISSN 2191-530X ISSN 2191-5318 (electronic)
ISBN 978-3-642-38344-1 ISBN 978-3-642-38345-8 (eBook)
DOI 10.1007/978-3-642-38345-8
Springer Heidelberg New York Dordrecht London

Library of Congress Control Number: 2013939825

Printed on acid-free paper

Springer is part of Springer Science+Business Media (www.springer.com)

Contents

Part I

Part I

Chapter 1
Introduction

1.1 Composites: A Brief History

The technologically advancing society is continuously challenging the limits of conventional materials and placing newer demands on material performance. Extreme and sometimes conflicting requirements are forcing us to engineer materials that are not possible by conventional alloying methods. Composite materials form a material system composed of a mixture or combination and are insoluble in each other. Composite material comes under one class of engineered material developed specifically to meet such a challenge. Glass fibre reinforced resin matrix composites were first introduced in the early 1940s. Since then, the use of composites is growing steadily in various industries such as aircraft, marine, automobile, sporting goods, etc.

Some of the advantages of composites include high specific strength, high specific stiffness, fatigue strength and impact resistance, thermal conductivity, corrosion resistance, and good dimensional stability. Composite materials are usually designed to possess certain specific properties desirable in that application. Unusual combination of properties not easily obtainable with alloys such as higher fracture toughness, higher oxidation and corrosion resistance, directional properties, good resistance to heat, cold and moisture, ease of fabrication and low cost could be brought out; of course, not all together simultaneously. Modern composite materials, depending on the matrix materials used, can be classified as polymer matrix composites (PMC), ceramic matrix composites (CMC) and metal matrix composites (MMC) [1–4].

1.1.1 Polymer Matrix Composites

Polymer matrix composites (PMC) are found to be the most commonly used advanced composites because of their low cost, high strength, and simple manufacturing techniques. These composites consist of a polymer reinforced by smaller-

V. Krishnaraj et al., *Drilling of Polymer-Matrix Composites*,
SpringerBriefs in Manufacturing and Surface Engineering,
DOI: 10.1007/978-3-642-38345-8_1, © The Author(s) 2013

diameter fibres. PMCs can be grouped into three different categories. The grouping is based, to a large degree, on the type of fibre reinforcement utilized in the composite matrix. A variety of polymers may be used for each type of PMC. The three groups are glass fibre-reinforced polymer (GFRP), carbon fibre-reinforced polymer (CFRP), and aramid fibre-reinforced polymer composites (AFRP) [1]. Glass fibre reinforced plastics are most commonly used materials in view of their relatively high specific strength and low cost. The other materials provide higher specific strength, higher specific stiffness and light weight. They are, however, expensive and are used only for those applications where performance and not cost is the major consideration. Aramid is used instead of carbon where strength, lightness and flexibility are major considerations and are not so important on stiffness and high temperature performance. Polyester resins are lower in cost and are not as strong as the epoxy. Their use in composite includes boat hulls, structural panels, appliances, etc. Epoxy, in addition, has a lower shrinkage after cure. It is used commonly in carbon and aramid fibre composites. Maximum usable temperatures of polymeric matrix composites are relatively low, as the matrix materials is prone to softening or chemical decomposition at moderate temperatures.

1.1.2 Ceramic Matrix Composites

Ceramic matrix composites are being developed mainly to improve fracture toughness, in addition to their higher specific modulus and elevated temperature and mechanical properties that are superior to metals. Continuous fibres, discontinuous fibres or particulates can be used as reinforcing material. The common fibre materials used are alumina and silicon carbide. Other CMCs include carbon/carbon composite in which high strength carbon fibres are embedded in a graphite matrix. The low density of carbon in combination with the extraordinary strength of carbon fibres offers potential for the development of high specific strength material.

1.1.3 Metal Matrix Composites

Metal matrix composites are used for applications requiring higher operating temperature than that are possible with polymer matrix composites. Most of these alloys are developed especially for use in aerospace industry; but newer applications are found in auto industry such as in automobile engine parts, brake drums, brake shoes etc. Continuous fibres provide the highest stiffness and strength for metal matrix composites.

The discontinuous and particulate MMCs are of low cost that provide higher strength, stiffness and better dimensional stability over metal alloys. They provide

increased wear resistance and contribute towards the difficulty in machining these materials. These alloys are used for sporting equipment, automobile engine parts; missile guidance parts etc. even though they are costlier today.

1.1.4 Classification of Composites Based on Fibre Reinforcement

Fibres are the most important class of reinforcements, as they satisfy the desired conditions and transfer strength to the matrix constituent influencing and enhancing their properties as desired. The performance of the fibre composites is judged by its length, shape, orientation, composition of the fibres and the mechanical properties of the matrix. Based on the reinforcement shape and position, the composites can be classified as:

1. Laminar Composites
2. Flake composites
3. Filled composites
4. Particulate composites.

1.2 Principles for Using Fibre Reinforced Composites

There are four major principles that should be considered in using fibres as composite reinforcement. Mechanical properties depend on the combined effect of the amount of fibre reinforcement used and its arrangement in the finished composite. Chemical, electrical and thermal performance is influenced by the resin system used as the matrix. Material selection and design and production requirements determine the proper fabrication process to be used. The cost, performance and the value achieved in the finished composite depend upon good design and judicious selection of raw materials and process.

1.2.1 Amount and Arrangement of Fibre Used

Strength of the finished product is directly related to the amount of fibre in the finished product. Generally speaking, strength increases directly in proportion to the amount of fibre used. A component containing 80 % fibre and 20 % resin by weight is almost four times stronger than a part containing opposite amounts of these two materials. Equally important is the arrangement of fibre in the finished product. When all the strands are laid parallel to each other, maximum strength

and modulus are obtained in the fibre direction. Such a parallel arrangement is used in the design of rocket motor cases, golf and fishing rods. When half the strands are laid at right angles to the other half, strength is highest in those two directions, although strength is less than with parallel arrangement, it is still considerable. Woven fabric/Chopped strand mat laminates find application in boats, airplane wing tips and swimming pools. When fibres are arranged in a random manner, strength is no longer concentrated in one or two directions. Safety helmets, chairs, electrical parts, luggage and machine housings utilize this arrangements. This random arrangement results in equal but lower strength in all directions. This condition is called isotropic.

1.2.2 Resin Mix

The major resins used in fibre reinforced plastics vary in resistance to corrosion and heat. Formulation of the resin mix also influences corrosion and heat resistance but has a less pronounced effect. By varying ingredients such as filler, pigment and catalyst system, each resin mix can be made to vary in performance. Resin also helps to prevent abrasion of the fibres by maintaining the position of the fibres and keeping them separated. For example polyester resins are used in approximately 85 % of all glass fibre reinforced plastics because they are economical. Other resins in use are epoxies, phenolics, silicones, melamines, acrylics and polyesters modified with acrylics. Some thermoplastic resins such as nylon, polystyrene, polycarbonate and fluorocarbons are also reinforced with fibres.

1.2.3 Processes

Processes vary in their capacity to utilize different arrangements of glass, different amounts of glass and different resins. A given combination of raw materials required to meet performance criteria in a given application narrows the choice of processes to those which can successfully and economically form the raw material into a completed part. Production flexibility of a process is often the single most important economic factor. For example if a large number of parts are to be made from one mould the lowest total cost is achieved by using presses and moulds and automating materials handling. Conversely, if only a few parts are required, a process minimizing investment in moulds and other equipment would be the logical choice. Continuous forming, being used for bench slats, FRP paneling etc. can greatly improve the economics of large volume items.

1.2.4 Economy

Economical cost and performance result from good design based on judicious selection of both raw materials and process. Proper materials must be combined in a process or processes so that potential performance is realized at an economical cost of manufacturing. Design of the part must take advantage of the material's maximum capabilities. Wide application of glass fibre reinforced plastic in engineering field and the less processing cost are the reasons for selecting this material for the present investigation.

1.3 Major Fabrication Processes of FRP Composites

Many processes are available to produce the desired combination of design performance and economics of glass fibre composites. Each process has its own usefulness for combining different kinds and amounts of glass and resin. The basic processes can be categorized into two classes: open mould and closed mould processes [4]. The open mould processes include hand lay-up, spray-up, vacuum pressure bag, autoclave, filament winding and continuous pultrusion. Closed mould processes include matched die moulding, injection moulding and resin transfer moulding. The predominant fabricating processes used in making laminates and structures are briefly explained below.

1.3.1 Hand Lay-Up Process

Hand lay-up process is the oldest and simplest fibre reinforced plastic forming process. In fabrication, the fibres and resin are placed in or on the mould and the entrapped air is removed with squeezing rollers. Layers of fibres and resin are added to build up to design thickness. If a high quality surface is desired, a gel coat is applied on the mould prior to lay-up. The line diagram of a simple hand-lay up process is shown in Fig. 1.1. The lay-up normally cures at room temperature but heating may be used to accelerate cure. The exposed surface is generally rough but it can be made smoother by wiping on cellophane or other suitable releasing films such as Mylar or polyvinyl alcohol. Resins used in hand lay-up are usually polyesters or epoxies.

Fig. 1.1 Hand lay-up process (www.dehler.com)

1.3.2 Filament Winding Process

Filament winding uses continuous reinforcement to achieve efficient utilization of fibre strength. Roving or single strands are fed from a creel through a bath of resin and wound on a suitably designed mandrel. Pre-impregnated roving may also be used. Special winding machines lay down fibres in a predetermined pattern to give maximum strength in the direction required. When the desired number or layers have been applied, the wound mandrel is cured at room temperature or in an oven. A method of filament winding is illustrated in Fig. 1.2.

Fig. 1.2 Filament winding process (UPS, Toulouse)

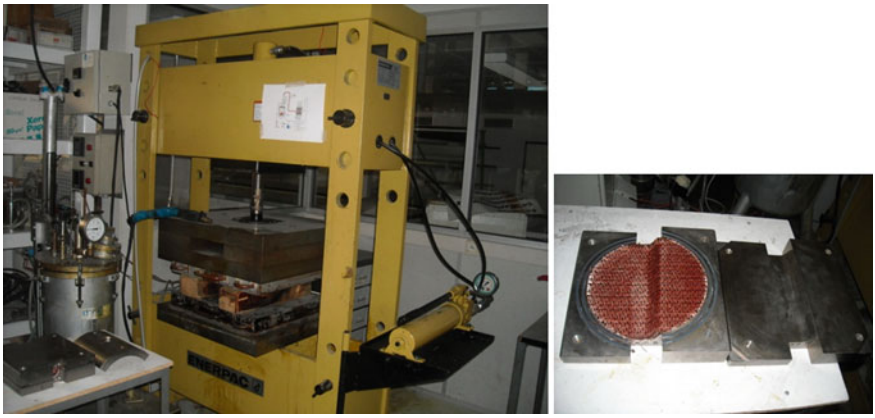

Fig. 1.3 Resin transfer moulding machine with mould (UPS, Toulouse)

1.3.2.1 Resin Transfer Moulding

Resin transfer moulding is similar to an injection moulding process. It uses a two-sided mould set that forms the surfaces of the part. The distinguishing feature of resin transfer moulding is that the reinforcement materials are placed inside the cavity and the mould is closed prior to supplying the resin. Resin transfer moulding includes numerous varieties which differ in the mechanics of how the resin is introduced to the reinforcement in the mould cavity. These variations include everything from vacuum infusion (for resin infusion see also boatbuilding) to vacuum assisted resin transfer moulding (VARTM). This process can be performed at either ambient or elevated temperature (Fig. 1.3).

1.3.3 Autoclave Moulding

Autoclave moulding is a process used to impart a controlled heat and pressure to cure mould prepared based on the required layup sequence. Application of pressure permits higher density and removal of volatiles from the resin during the curing cycle. Both surfaces of the component can be formed a two-sided mould. On the base side is a rigid steel mould and on the upper side is a flexible film made of nylon. Reinforcement materials can be placed manually in the mould based on the requirement. It may be a continuous fibre or prepreg. Prepregs are nothing but fibres with resin available in the form of tapes. The upper mould is installed and vacuum is applied to the mould cavity (Fig. 1.4). The assembly is placed into an autoclave for curing. This process is generally performed at elevated pressure and elevated temperature. This helps in reaching higher volume fraction with low void content. This process helps to avoid reaction with the atmosphere during the curing cycle and also helps in attaining maximum structural efficiency.

Fig. 1.4 Autoclave moulding (UPS, Toulouse)

1.4 Significance of FRP Machining

1.4.1 Conventional Machining

In recent years the fibre reinforced composite materials are increasingly used in various fields of Science and Engineering because of their unique properties. As a result there is a strong need to understand the issues associated with the manufacture of composite components. The existing manufacturing technique of fabricating to near-net shape is incomplete unless the component is subjected to secondary machining operations like trimming, finish grinding, drilling holes/cavities etc. based on the requirement.

Conventional machining on FRP composite material plays a vital role in meeting dimensional accuracy and good surface quality requirement. The process is cheaper compared to NTM techniques. Because of the potential application there is a strong need to understand the issues associated with conventional machining of FRP composite materials.

Among the machining processes, drilling is most frequently used in industries due to the need for assembly of components in mechanical structures. However, the properties of FRP materials like anisotropy, non homogeneity, and abrasiveness provide problems like excessive tool wear, poor surface finish, delamination, fibre pullout, dimensional variation, etc. These limitations motivated the present research, a study on the problems of drilling on FRP materials.

1.4.2 Non-Traditional Machining

Non-traditional machining (NTM) techniques were used in many of the applications as a secondary machining operation. However, NTM processes also pose

Fig. 1.5 CNC machine used for machining composites with vacuum system (UPS, Toulouse)

Fig. 1.6 System used for drilling fuselage in aerospace industries (www.sae.org)

some limitations. As the equipment costs are very high, the process is considered to be highly expensive for small-scale production. Also, they are material oriented. Any NTM process cannot be used to work on any FRP material. Aramid is the suitable material for laser machining, because of closeness in properties of fibre and resin. To use electric discharge machining (EDM) process, the material should be electrically conductive. Abrasive water jet machining produces higher noise levels. In laser machining problems like delamination, uneven kerf and thermal cracks are observed. These processes are incapable of producing blind holes/cavities. As these processes are highly expensive, they are suitable for application in industries where manufacturing cost is of secondary importance (Figs. 1.5 and 1.6).

1.5 Summary

The performance of machined components, especially of fibre reinforced plastics (FRP) in high strength applications, is often critically dependent on the quality of surface produced by machining since the surface layer may drastically affect the strength and chemical resistance of the material. The deterioration in the surface quality or the damage caused by the machining operation is due to the anisotropic nature of the fibrous composites. Drilling of holes to facilitate the assembly of parts is one of the most important machining operations. Drilling of composites poses conditions and requirements that are not usually encountered in metal machining. The mechanism of material removal in orthogonal machining of FRP is not yet completely understood till date and therefore the oblique cutting mechanism of fibrous laminated FRP composites poses new set of problems never encountered earlier.

When drilling composites, the major concern is that of the damage caused to the workpiece. The principal mechanism of damage is largely delamination. Delamination is generally regarded as a resin or matrix dominated failure behavior, which occurs in the inter-ply region. A number of research initiatives have been undertaken for developing an up to date understanding of the drilling process in the context of FRP composite materials, but still a lot remain uncovered. As known, during the application of the composites, the presence of holes or cut-outs for various purposes must be considered. For example, when the hole is produced by machining after fabrication of the composites material, a reduction in strength is expected by reason of cutting the fibre bundle, loosening, and de-bonding of fibre around the hole. The mechanism of the material removal in an oblique cutting process such as drilling, the variation of the forces with time and their influence on accompanying damage, the optimal drill point geometry for minimizing the drilling forces, the effect of manufacturing processes on quality of holes and the subsequent damage are discussed in the forthcoming chapters.

References

1. Kaw AK (2006) Mechanics of composite materials, 2nd edn. CRC Press, NY
2. Bhagwan BD, Broutman LJ (1990) Analysis and performance of fibre composites, 2nd edn. Wiley, London
3. Matthews FL, Rawlings RD (1999) Composite materials: engineering and science. Woodhead Publishing, Cambridge
4. Mazumdar SK (2002) Composites manufacturing: materials, product, and process engineering. CRC Press, NY

Chapter 2
Drilling of Composites

2.1 Introduction

The cutting process consists of removing a layer of material from blank to obtain a component of the required shape and dimensions and with specified quality of surface finish. During the process of material removal there is a relative motion between the workpiece and cutting tool. Such a relative motion is produced by a combination of rotary and translatory movement either of the work pieces or of cutting tool or both. The relative motion depends on the type of cutting operation. The cutting operation carried out on any machine tool is based on the theory, which is the same for all processes [1]. The importance of the cutting process may be further appreciated by the observation that nearly every device in use in our complex society has one or more machined surfaces or holes.

The main aspect of machinability is to discuss in detail the force, torque, tool life, and surface finish. Though there are a number of interrelated factors which affect the machinability of the material, the most important factors are the cutting parameters, the properties of the work and tool materials and the geometry of the cutting tool. The cutting parameters are the speed, feed and depth of cut. The tool parameter involves the tool material, tool coating and tool geometry. However, the work design parameter is concerned with the FRP composite material. Though the machining technique on FRP composite material is similar to that of metals, the fibre content, stacking sequence of fibre in composite, nature of the matrix play an important role in deciding the machinability of the material and on the quality of the machined surface.

It is a typical feature of the production of fibre reinforced plastic (FRP) composite component to their net shape almost completely in the transition from soft to hard material stage. This takes place by a phase change or by the curing of the thermoplastic or thermosetting matrix inside or on the top of a mould. In spite of this near net shape production technology in general, a finish machining of cured FRP will become necessary, because the required dimensional accuracy and the surface quality may not be achieved at a reasonable effort in the curing cycle. Due to the in homogeneity, anisotropy and abrasive nature of the FRP composite

V. Krishnaraj et al., *Drilling of Polymer-Matrix Composites*,
SpringerBriefs in Manufacturing and Surface Engineering,
DOI: 10.1007/978-3-642-38345-8_2, © The Author(s) 2013

material, the machining behavior of FRP composites is quite different from that of metals. The present section of the chapter highlights a comparative discussion about the mechanism of drilling, and also a brief description about the influence of various factors on the machinablity of the work material.

2.2 Drilling Operation

The most common tool used in drilling is conical point twist drills with two flutes, as shown in Fig. 2.1. This tool has three distinct types of cutting surfaces, i.e. a chisel edge, two main cutting edges and two marginal cutting edges. The principal elements of the drill point are lip, chisel edge, helix angle, point angle, chisel edge angle, rake angle, clearance angle etc. Lip is the main cutting edge of the drill and is formed by the interaction of the flank and flute surface. For efficient cutting, the lip should be straight, equal in length and symmetrical with the axis of the drill. The chisel edge is the point end of the web and it is formed by the interaction of the flank surfaces. The helix angle practically determines the rake angle at the cutting edge of the drill. As the helix angle decreases the rake angle also decreases and makes the cutting edge stronger. The most commonly used point angle is 118°, however for FRP materials the preferred point angle is 135°. The drill properly ground to this angle gives satisfactory results for a wide variety of materials. Reducing the point angle leads to an increase in the width of cut (Length of cut increases) and it is generally adopted for brittle materials. Larger the chisel edge angle more is the clearance on the cutting lip, which generally varies from 130° to 145°.

The rake angle depends mainly on the flute, helix angle, point angle and the radius at which it is measured. The actual value of the relief angle during drilling also

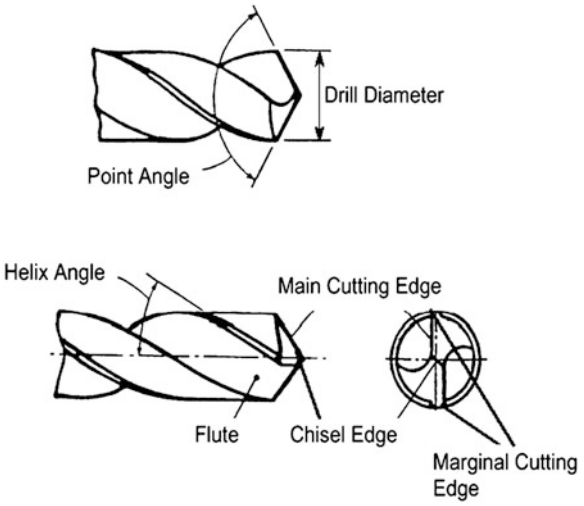

Fig. 2.1 Standard twist drill geometry

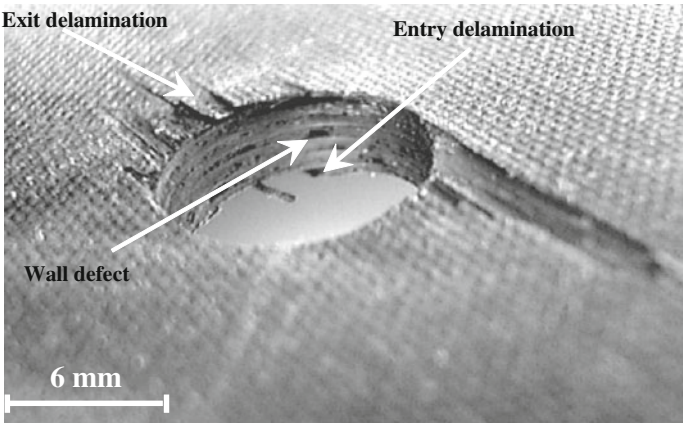

Fig. 2.2 Drilling damages observed on CFRP laminate

depends on the feed. This is explained by the fact that the drill not only rotates but also travels axially during cutting. According to the recent research for drilling of polymer composites the preferred cutting speeds can vary from ≈78 to 155 m/mm, and the point angle from 60° to 135°, helix angle 10 to 36°, clearance angle 6 to 16° can be selected for drilling FRP composite material [2, 3].

It should be noted that whatever the choice of the geometry of the cutting tool, the drilling operation is accompanied with different damages. These damages can degrade the quality of the machined holes and even reduce the life of a bolted or riveted assembly. A description of different damages existing during drilling and mains factors responsible of these defects are given in the subsequent chapters.

The defects (Ref. Fig. 2.2) resulting from the drilling operation when using twist drill can be classified according to their location, (1) at the hole entry, (2) on the wall of the hole and (3) at the hole exit [4].

Literatures related to issues and the factors responsible for drilling of composite laminates using a twist drill [5–9] is discussed in the following sections.

2.3 Analysis of Damages During Drilling of FRP

2.3.1 Defect at the Hole Entry

This defect is linked to the nature of the work material and its curing cycle, tool material and its geometry and the machining parameters. Konig et al. [4] explaining that there is a peeling effect phenomenon on the periphery of the cutting edges (secondary cutting edge of drill called margin) of the twist drill. This phenomenon, peel off the first ply of the laminate, which can directly be related to the rake angle and the helix angle of the drill. This peeling effect increases with

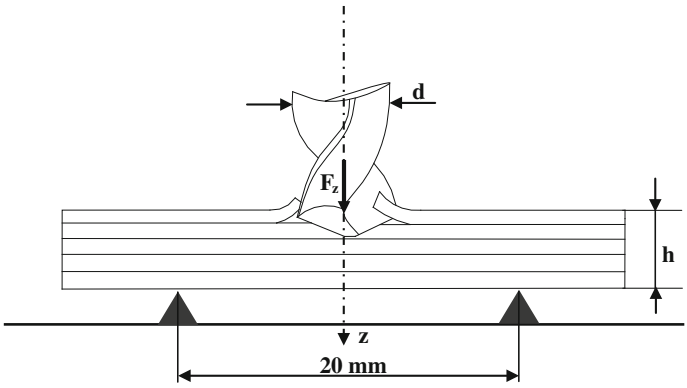

Fig. 2.3 Schematic view of peeling effect at the entry of drill

increasing the helix angle. This debonding phenomenon occurs at the beginning of drilling, specifically when the margin of the drill reaches the interface between the first two plies of the laminate, during the chip formed tends to move under the action of the main cutting face. At this juncture, action alone that opposes the delamination of the first ply is due to the cohesion of the matrix. Using an experimental design, works conducted by Davim et al. [6, 10], show that, size of delamination at the first ply increases with the increasing the cutting speed and the feed of the drill (Fig. 2.3).

2.3.2 Defect on the Wall of the Hole

The defect on the surface of the hole, can be of two types, the first related to the hole shape and the other to the degradation of the matrix on the surface. The first defect, can be explained by the fact that, under the action (loading) of the principal cutting edges of the drill, fibers have an elastic deformation during bending before the brittle fracture. On the cut fibres, it is possible to observe the presence of an inclined facet compared to the cutting direction of the secondary cutting edge (margin cutting edge). The elastic return of broken fibres cause shrinking of the hole and a decrease in the hole diameter, which results in increasing of the friction between the hole and the tool, which reduce the tool life. The experiments show that, this reduction of the hole diameter is influenced by the feed rate, and tool material. The major candidate for the reduction in hole diameter is the nature of the tool material. For example, when drilling is carried out with diamond tool, the hole diameter measured is higher than the diameter of the drill. Nevertheless, with the same machining parameters, drilling with tungsten carbide tool, the hole diameter measured is lower to the diameter of the tool. This disparity on the measured diameters can be explained to the difference between the noise radius of the principle and secondary cutting edges of the drills. With tungsten carbide tool,

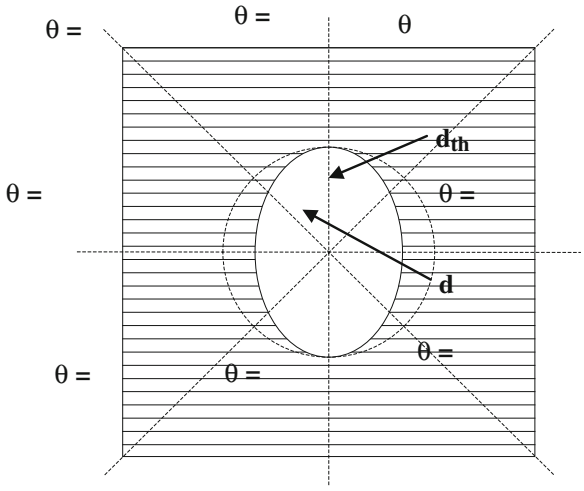

Fig. 2.4 Schematic representation of defect on the surface of hole

d_r : measured diameter,

d_{th} : nominal diameter,

θ : relative angle measured between the plies direction and the direction of the cutting

after grinding we can obtain a noise radius value between 8 and 15 μm, compared to 5–7 μm with the diamond tool.

The second defect is mainly due to the interaction between the chosen feed, tool geometry, anisotropy of the composite material and (with or without) the use of coolant. For example, during drilling at high feed, the damage is higher compared to drilling at low feed (Ref. Fig. 2.4). Matrix degradation and the fibre pull out observed on the wall of the hole are strongly influenced by the relative angle measured between the direction of the fibres and the direction of the cutting speed. When the angle between the direction of the fibres and the direction of the cutting speed ranges from −30° to −45°, the state of the machined surface is of poor quality. This can be explained by the fact that the mechanism of the material removal, depends strongly by the orientation of fibres [11, 12].

In the industry, the quality of the machined surface (wall of the hole) is characterized by the roughness measurements (Ra, Rz, and Rt etc.) However, the values of these mean roughness, are strongly depends on the angular position of measurement in the hole [13] when the hole are generated by conventional machining with a cutting tool (drill). Saleem et al. [14], show that, when drilling is carried out using an abrasive water jet, the damage on the wall of the hole is uniformly distributed. Therefore, the criterion for average roughness initially used for the metallic material, is not appropriate for composite materials [14–16] when the conventional machining is used, whereas it can be used when the machining is carried out using the abrasive water jet. Since there is no specific criterion to measure surface roughness of composite materials are available, the average roughness criteria used for isotropic material during machining is used (Fig. 2.5).

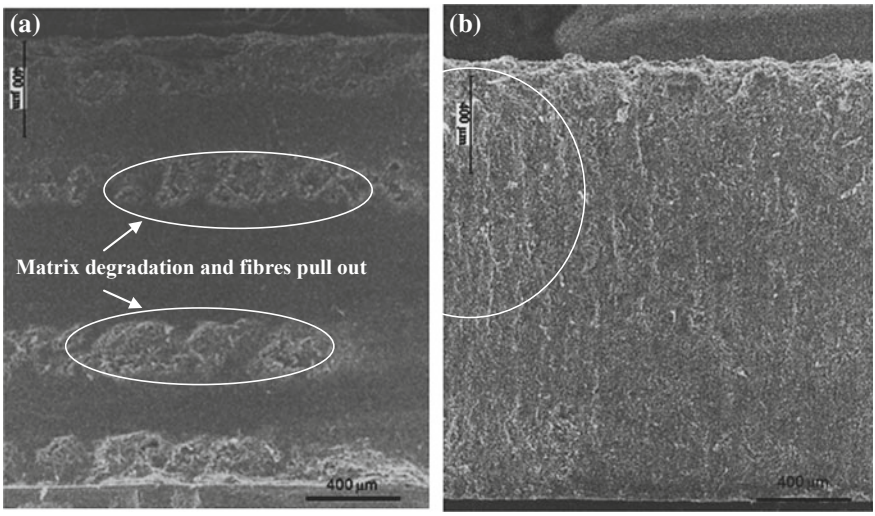

Fig. 2.5 SEM pictures comparing the surface of hole machined on CFRP plate $[+45/-45/+45/-45]_s$ using two different techniques. **a** Drill, $d = 6$ mm, $N = 2{,}020$ rpm, $f = 0.1$ mm/rev. **b** Abrasive water jet machining at $P = 50$ bar

2.3.3 Defect on the Hole Exit

The cutting speed of the drill is maximum at the extreme end of the drill radius, and reduces along the drill radius and is null at the centre of the chisel edge of the tool. Therefore, the material in front of the chisel edge is subjected to an higher axial force resulting from the feed of the tool. The contact pressure of the tool on the material located above the chisel edge increases with the tool displacement. The defect at the hole exit appears when the chisel edge of the drill is in passing the last plies of the laminate. In such case, the thickness of the uncut material located under the tool decreases and leads to a reduction in the bending stiffness (of the uncut material). The critical thrust force exerted by the tool has to be lesser than the adhesion force of the matrix between the interface of plies. Above the force there is a creation and propagation of crack by delamination between the last plies. The de-bonding of the matrix causes the bending and the uncut fibers of the last ply (Fig. 2.6).

The main parameters which influence the value of the thrust force in drilling are:

- The feed rate,
- The point angle and geometry (chisel edge, point angle etc.),
- Tool material,
- State of the tool (Fresh or worn out).

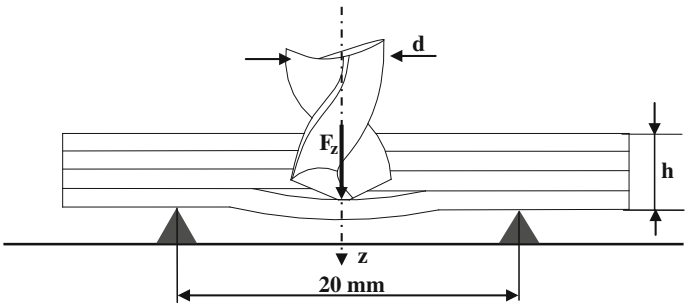

Fig. 2.6 Schematic representation of defect at the exit side of hole

Several experimental studies have shown that the thrust force (Fz) increases with increasing the feed rate (Vf) [7, 10, 17–20]. For example, the experimental results of [18] obtained during drilling of CFRP plate using a twist drill with a rake angle of 30°, clearance angle of 15° and helix angle of 30° show that, when the feed increased from 0.03 to 0.07 mm/rev, the thrust force increase from 36 to 58 N. This increase in thrust force, leads to increase the size of defect at the hole exit. In addition the ANOVA analysis conducted [7] during drilling of CFRP plate using a twist drill, show that, the feed has a contribution on the exit delamination size of 81 %. However, the cutting speed has a negligible influence on exit delamination.

2.4 Variables Affecting the Tool Life

There are many variables affecting the tool life. They are cutting speed, feed, and depth of cut, toot material, tool geometry, work material and work design. Higher cutting speed increases tool temperature and softens the tool material. It thereby aids abrasive, adhesive and diffusion wear. The cumulative effect is an exponential reduction in tool life. The larger the feed, the greater is the cutting force per unit area of chip tool contact on the rake face and work tool contact on the flank face. However, it has been observed that the effect of changes in feed on tool life is relatively smaller than that of proportionate changes in cutting speed. If the depth of cut is increased, the area of the tool-chip contact increases roughly in equal proportion to the change in the depth of cut. Consequently, the rise in temperature is small. Thus, an increase in the depth of cut shortens the tool life to some extent by accelerating the tool wear.

The first section presents an analysis of the drilling operation on GFRP composite material using twist drills. A series of tests was conducted using different cutting conditions namely cutting speed, feed rate, and chisel edge width. It is apparent that the chisel edge is a large contributor to the total thrust force that is responsible for delamination [21]. Decisions related to the optimum drilling

conditions were based on the geometrical accuracy and appearance of the produced holes. The approach followed in this section is to experimentally vary most of the important drilling parameters, in as wide a search as possible, to determine 'optimum' conditions.

2.5 Influence of the Machining Parameters and Tool Geometry on the Machining Quality

2.5.1 Specimen Preparation

Hand lay up process was used to prepare the woven glass fiber reinforced plastic (WFGFRP) specimens. The burning test conducted to check the fiber percentage revealed that the specimens so fabricated possessed 45 % of fiber content by volume. Fiber percentage was controlled by controlling the weight of the fibers (number of layers). E glass fiber mats (360 GSM) were used to reinforce epoxy resins (LY556). Hardener HY951 was mixed with epoxy to cure at room temperature. Necessary care was taken to remove the entrapped air during the lay-up process. Rollers were used for this purpose. A gel coat was applied on the mould prior to the lay-up process. The specimens were macroscopically tested to confirm the absence of defects like voids or delamination. The specimen thickness and the fiber percentages selected for this analysis are within the applicable range. The thicknesses of the specimens varied in the range of 4–5.5 mm. Fiber percentages of 45–65 % by weight of woven fabric are used in aircraft's, marine ordinance and electrical applications. Fiber percentages of 40–70 % by weight of woven roving are used in marine and large container applications.

2.5.2 Experimental Setup

A drill tool dynamometer, was used to measure the axial thrust force and torque during the drilling tests. The proportional charge outputs from the dynamometer were fed to a Tektronix oscilloscope, thus producing a scaled voltage output signal proportional to the applied load. The thrust and torque were continuously monitored throughout the test. The dynamometer was mounted on the table on a vertical CNC machining center. A fixture was used to clamp the laminate at the center of the dynamometer. Figure 2.7 shows the experimental setup.

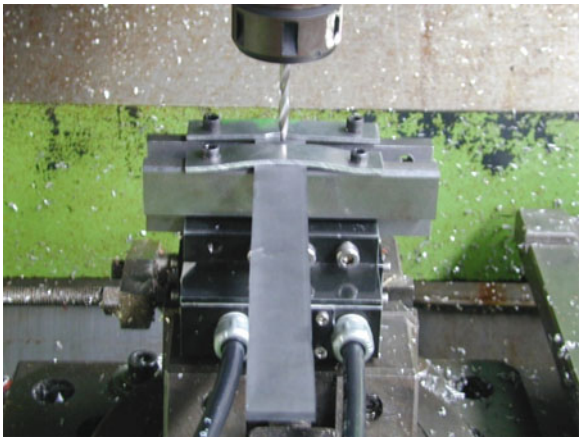

Fig. 2.7 Experimental setup

2.5.3 Cutting Conditions

The main parameters studied are spindle speed, feed rate, and chisel edge width on drilling GFRP composite laminates. A 10 mm diameter high speed steel (HSS-M40) drill with 100° point angle and 30° helix angle was used in conducting experiments. Gindy [22] and Enemuoh et al. [23] reported that 100° point angle is preferred for drilling of FRP composites. Machining of FRP material is carried out for the following conditions

- Spindle speed: 600, 1,200, 1,800 rpm
- Feed rate: 0.05, 0.1, and 0.2 mm/rev
- Chisel edge width: 1.0, 1.5, and 2.0 mm.

As per full factorial design, 27 experiments were conducted with all possible cutting conditions with multiple measurements for each condition.

2.6 Influence of Drilling Parameters on Thrust Force and Torque

It is observed that force increases with increase in spindle speed and feed. Also found that the increase in chisel edge width increases the thrust force. Lower thrust force and torque values were found at 1 mm chisel edge width, which is shown in Figs. 2.8 and 2.9.

The multiple linear equations for thrust force and torque are given in Eqs. 2.1 and 2.2.

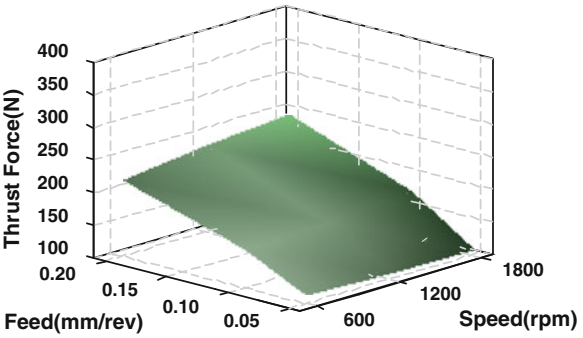

Fig. 2.8 Effect of spindle speed and feed rate on thrust force

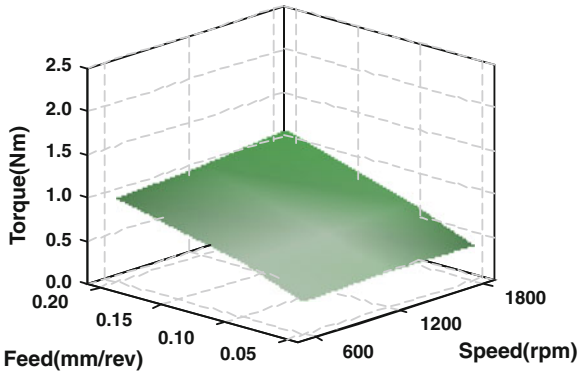

Fig. 2.9 Effect of spindle speed and feed rate on torque

$$\text{THRUST FORCE (N)} = -50.8 + 74.9\,\text{C.EDGE} + 0.0295\ \text{SPEED} + 951\ \text{FEED}$$
$$\text{Correlation coefficient } R^2 = 0.91 \tag{2.1}$$

$$\text{TORQUE (Nm)} = -0.582 + 0.434.\,\text{C.EDGE} + 0.000184\ \text{SPEED} + 5.49\ \text{FEED}$$
$$\text{Correlation coefficient } R^2 = 0.91 \tag{2.2}$$

2.7 Influence of Drilling Parameters on Surface Roughness

The surface roughness (Ra) was evaluated (Ra according to 4287/1) with surface roughness measuring equipment using stylus. For each hole an average of 3 measurements were taken with a cut-off length 0.8 mm. From the Fig. 2.10. It can be inferred that the value of surface roughness (Ra) increases with the feed rate, and decreases with the spindle speed, i.e. to get a better surface finish, it is

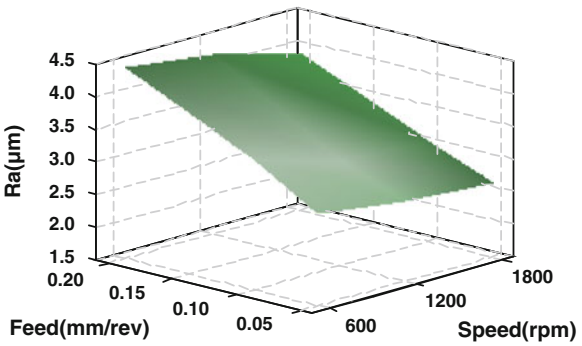

Fig. 2.10 Effect of spindle speed and feed rate on surface roughness

necessary to have a high cutting speed and lower feed. Lesser point angles are preferred as it reduces the chip thickness and leads to get a good surface finish. An average surface roughness of 2–3 μm was found at higher spindle speeds and lower feed rates. The multiple linear regression equation is given in Eq. 2.3

$$\begin{aligned}&\text{SURFACE FINISH (Ra)} = 3.34 - 0.137\ \text{C.EDGE} - 0.00052\ \text{SPEED} + 6.93\ \text{FEED}\\&\text{Correlation coefficient } R^2 = 0.86\end{aligned} \tag{2.3}$$

2.8 Influence of Drilling Parameter on Delamination Factor and Hole Quality

The delamination is evaluated in terms of delamination factor. The delamination factor is the ratio of maximum diameter (Dmax) of the damaged zone to the actual hole diameter (D). The value of delamination factor (DF) can be obtained by the following Eq. 2.4.

$$\text{DF} = \frac{\text{Dmax}}{\text{D}} \tag{2.4}$$

The delamination factor was evaluated by scanning the drilled composite laminates with 400 DPI as demonstrated by Khashaba [24].

From Fig. 2.11, it can be inferred that the increase in feed rate increases the delamination factor; similarly the increase in spindle speed increases the delamination factor. Increase in delamination is found when the feed is increased; this is because of increase in cross sectional area of the chip. Increase in cross sectional area increases the resistance to cutting which in turn increases the thrust force.

The multiple linear regression equation is given in Eq. 2.5.

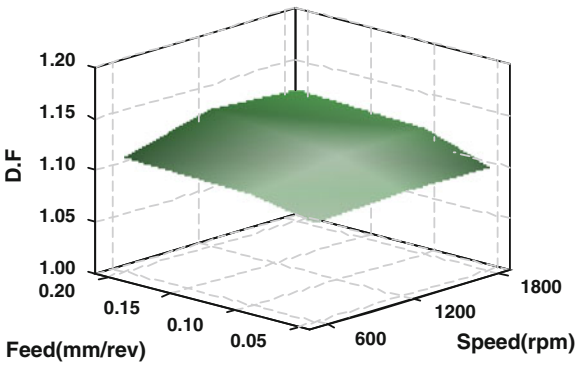

Fig. 2.11 Effect of spindle speed and feed on delamination factor

$$\text{Del. factor} = 1.09 + 0.00389\ \text{C.EDGE} + 0.000005\ \text{SPEED} + 0.164\ \text{FEED}$$
$$\text{Correlation coefficient } R^2 = 0.56 \tag{2.5}$$

It is observed that, if the test sample is supported by a backing plate during drilling, the occurrence of cracking or deterioration of the hole lip can be greatly minimized for almost all values of feeds and cutting speeds. But in industrial environments giving a backing plate is not possible in most of the cases. Experimental results indicate that the thrust force contribution from the chisel edge is a significant component of the total thrust force suggesting that the potential for delamination can be significantly reduced through the use of pilot holes. From the experiment it is found that the force increases with increase in spindle speed and feed. Also it is seen that the increase in chisel edge width increases the thrust force. Lower thrust force and torque values were found at 1 mm chisel edge width. It is inferred that the value of surface roughness (Ra) increases with the feed rate, decreases with the spindle speed, i.e. to get a better surface finish it is necessary to have a high cutting speed and low feed. Lesser point angles are preferred to get a good surface finish which reduces the chip thickness. On an average, surface roughness values of 2–3 μm were found at higher spindle and lower feed rate. It is inferred that the increase in feed rate and spindle speed increases the delamination factor. Increase in delamination is found when the feed is increased this is because of increase in cross sectional area of the chip. Increase in cross sectional area increases the resistance to cut, which increases the thrust force.

2.9 Influence of the Composites Material on the Machining Quality

This section is devoted to the quality of drilling of two types of FRP composite materials. The basic constituents of the laminate structures are provided by the Hexcel Composites Company and are referenced as T2H-EH25 and M21-T700GC

respectively (58 % Vf and ply thickness of 0.25 mm). These two products are roughly equivalent in terms of mechanical properties. However, material M21-T700GC is distinguished by the presence of thermoplastic nodules measuring 20 μm in diameter on average, representing about 13 % of the volume of the matrix in the prepreg. These nodules have the role of initiating networks of cracks on the interface between plies then blocking propagation of those cracks in the laminate. The critical energy release rate in mode I and in mode II of this material is thus improved, as compared with those of the laminate T2H-EH25.

In this part, two types of problems are analyzed. Firstly, the behavior of the machined material (through specific cutting pressure) under the influence of feed per revolution and the diameter of the drill has been studied. To do so, a test campaign was conducted. Having performed acquisition of the thrust force (Fz) for cases of machining on the two materials, varying the cutting conditions, a comparison of the specific cutting pressures between the two materials and a comparison of roughness measurements on the wall of the hole were made in relation to the feed per revolution. Analysis of the extent of defects at exit hole is proposed for both materials taking the influence of feed per revolution into account.

2.9.1 Experimental Procedure

The specimen used for this study has been prepared using 16 unidirectional prepregs and have a quasi-isotropic stacking sequence. The thickness of the plate manufactured with a layer of T2H-EH25 is 4 mm, while that manufactured with the layer M21-T700 GC is 4.16 mm. Drilling is performed using an CNC machine.

The specimen used for this study has been prepared using 16 unidirectional prepregs and have a quasi-isotropic stacking sequence. The thickness of the plate manufactured with a layer of T2H-EH25 is 4 mm, while that manufactured with the layer M21-T700 GC is 4.16 mm. Drilling is performed using an CNC machine. Acquisition of the thrust forces is made using a six-axis force sensor.

The sensor is connected to a strain gauge bridge and a computer to store data. The composite workpiece to be drilled is firmly held in place on a dedicated support. The cutting tool used is made of micro-grain tungsten carbide of grade K20 characterised by three edge sharpening and a pointe angle of 118°. The diameters used are 4, 6, 8 and 10 mm respectively. The cutter rotation speed is set to 1,500 rpm. In Table 1, the mechanical characteristics of the laminate used are presented. The energy release rate in mode I in relation to the (θ) angle between plies is shown in Table 1. The direction (ol) shows the longitudinal direction of the fibres and direction (ot) the direction crosswise to the fibres. Note that table brings together the data provided by the manufacturer (Hexcel Composites) and those derived from the mechanical tests conducted during previous experimental studies.

Table 1 Mechanical properties of T2H-EH25 and M21-T700 GC plates studied with θ interface angle between plies

Mechanical properties	T2H-EH25	M21-T700 GC
El (Mpa)	1,41,000	1,42,500
Et (Mpa)	8,500	9,500
Vf	0.6	0.59
GIc for $\theta = 0°$ (N/mm)	0.16	0.33
GIc for $\theta = 45°$ (N/mm)	0.23	0.44

2.9.2 Results and Analysis

2.9.2.1 Specific Cutting Pressure

To calculate the specific cutting pressure of the two materials studied and identify the influence of the thrust force Fz on defects at hole exit in relation to the diameter of the cutter and feed per revolution, a test campaign was conducted. The feed rates chosen are: 0.01, 0.015, 0.02, 0.03, and 0.05 mm/rev and cutter diameters are: 4, 6, 8, and 10 mm.

Acquisition of the thrust force Fz is made for different diameters and feed rates per revolution. The results shown in Figs. 2.2 and 2.3 are obtained as follows: each point shown on the curve comes from estimation of a mean value made from four measurement points obtained using a new cutter. This way of proceeding allows the influence of the wear effect on the values measured for the thrust force Fz to be minimised. On Fig. 2.12a, showing changes in the thrust force Fz in relation to the drill diameter, it can be seen that for both materials, the thrust force Fz is proportional to the drill diameter. This is certainly largely related to the size of the drill's web that pushes back the material rather than cutting it. The drill web's dimensions depend on the cutter diameter (This dimension is around 1.18 mm for a twist 4 mm diameter drill and about 2 mm for a 10 mm diameter drill). This result concurs with works described in the literature [9]. When examining the

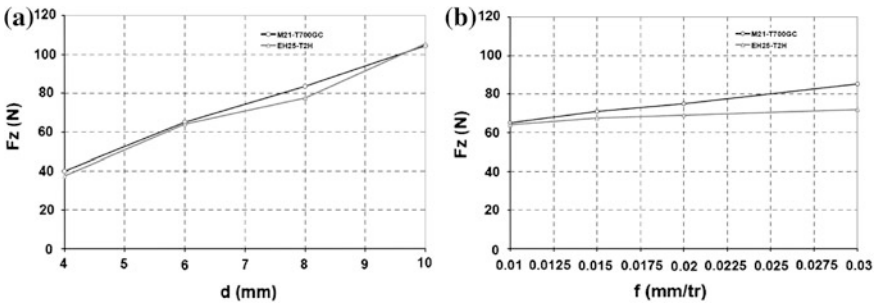

Fig. 2.12 Thrust force F_z, (**a**) versus tool diameter, $N = 1{,}500$ rpm, $f = 0.01$ mm/rev and (**b**) Versus the feed rate; with $N = 1500$ rpm, $d = 6$ mm

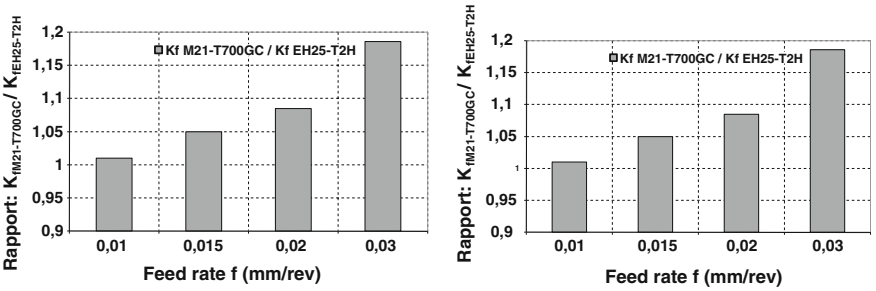

Fig. 2.13 Ratio of the specific cutting pressure for two materials (drill diameter of 6 mm and spindle speed of 1,500 rpm)

influence of feed per revolution in the case of a 6 mm diameter drill, it can be seen that the thrust force Fz is proportional to the feed per revolution for both materials (Fig. 2.12b).

Furthermore, for chosen values of feed per revolution and cutter diameter, the thrust force registered on machining of M21-T700 GC is globally the same as that registered during machining of T2H-EH25. As an example in the most unfavourable case corresponding to a feed rate per revolution of 0.03 mm/rev, the absolute difference between thrust forces for the two materials is 13 N (for a maximum value of 85 N). Globally, Fig. 2.12 shows that the thrust force Fz is directly proportional to feed per revolution "f" and the diameter "d" of the drill. The empirical model proposed by the Centre Technique des Industries Mécaniques (CETIM) for metallic materials translates a change in the thrust force Fz proportional to the specific cutting pressure of the machined material, the diameter and feed per revolution of the drill. This model can thus be used for drilling of carbon/epoxy long fibre composite laminates. The calculated values come from the relation:

$$F_z = K.K_f.f.d \tag{2.6}$$

with d, the drill diameter (mm); K, the reducing ratio that takes into account the geometry of the drill tip (dimensionless); K_f, the specific cutting pressure that is a function of the nature of the material machined, feed per revolution (f) and the drill diameter (This ratio is determined experimentally in N/mm^2).

Using Eq. (2.1) given above, the ratio of the specific pressures of the two materials can be calculated. According to the Fig. 2.13, representing the ratio between the two specific pressures when machining with a new drill of diameter 6 mm and for feed per revolution of the drill of between 0.01 and 0.03 mm/rev, it can be seen that the latter is of order unity. On Fig. 2.14, the ratio between the two specific pressures during machining operations with a feed per revolution of 0.01 mm/rev and with new cutters of diameters going from 4 to 10 mm, is of order unity. However, with this model, the maximum relative deviation between the two specific pressures of the two materials is 8.5 %. This maximum deviation corresponds to a feed per revolution of 0.03 mm/rev.

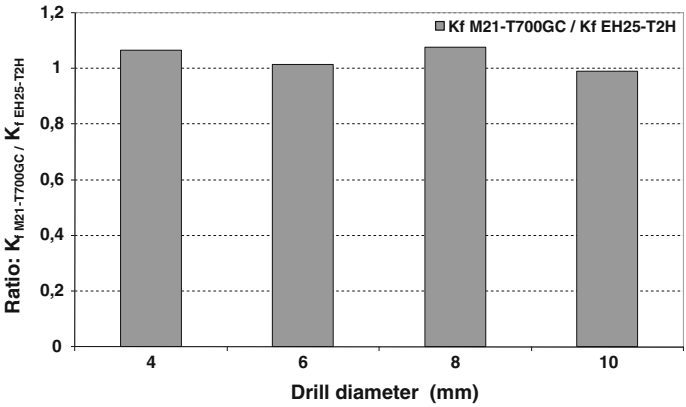

Fig. 2.14 Ratio of the specific cutting pressure for two materials (feed of 0.01 mm/rev at a spindle speed of 1,500 rpm)

2.9.2.2 Influence of Drilling Time on the Thrust Force

From Fig. 2.15, it can be seen that after 2 min of drilling and with a feed per revolution of 0.03 mm/rev, the thrust force recorded during machining of the material T2H-EH25 goes from 72 to 120 N. Now, for material M21-T700 GC, it goes from 85 to 110 N. This variation in load after 2 min of drilling is translated by an absolute deviation between the two materials of about −23 N. A number of works have shown that the wear on the cutting tool is related to the increase in machining time (number of holes drilled) and thus heating of the cutter itself [25]. Wear on the cutter in turn leads to an increase in the thrust force Fz. When drilling

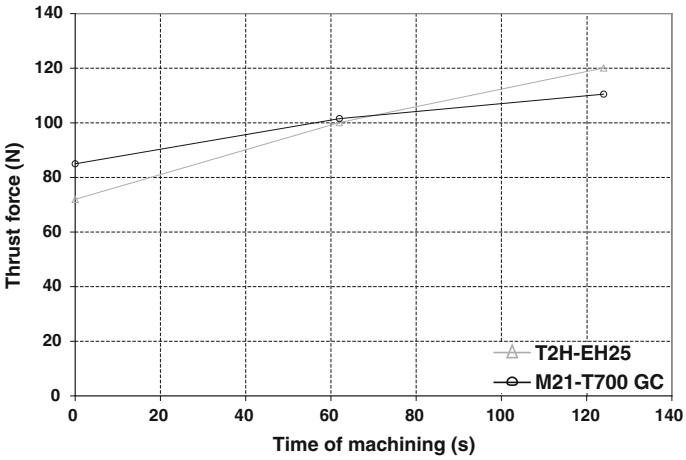

Fig. 2.15 Thrust force F_z versus machining time

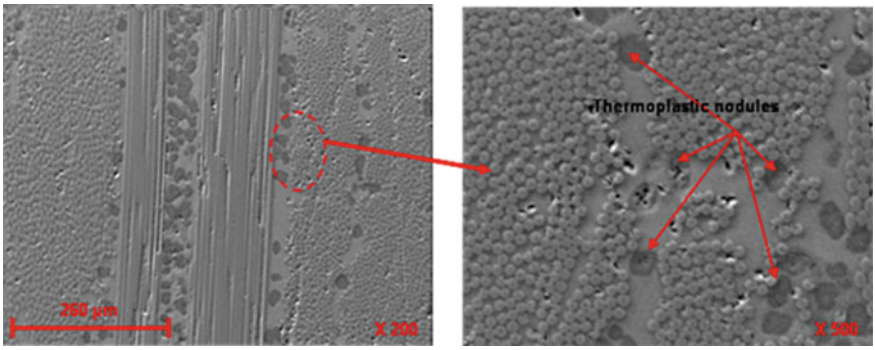

Fig. 2.16 Views of thermoplastic nodules in M21-T700 GC using SEM observations

material M21-T700 GC, the cutter wears at a slower rate than when drilling material T2H-EH25. This is probably due to the presence of the thermoplastic nodules in material M21-T700 GC (see Fig. 2.16). Indeed, these nodules can act as a lubricant in the wall of the hole when cutting, thus protecting the tool's cutting edges against abrasion from the carbon and epoxy resin.

Scanning electron microscope observations on the surface of the hole machined on carbon/epoxy laminate made of M21-T700 GC show a clean surface that spreads the matrix, thanks to the presence of the thermoplastic nodules in the workpiece (see Fig. 2.17a). From the Fig. 2.17b, this is less obvious for a workpiece made of T2H-EH25. Note the presence of torn fibres in the matrix (area surrounded by a border in Fig. 2.16b).

SEM observations at the exit side of hole (Fig. 2.18) shows the torn fibres within the last ply and not in the form of delamination between plies. From this observation, it can be concluded that the thrust force Fz, during drilling because of

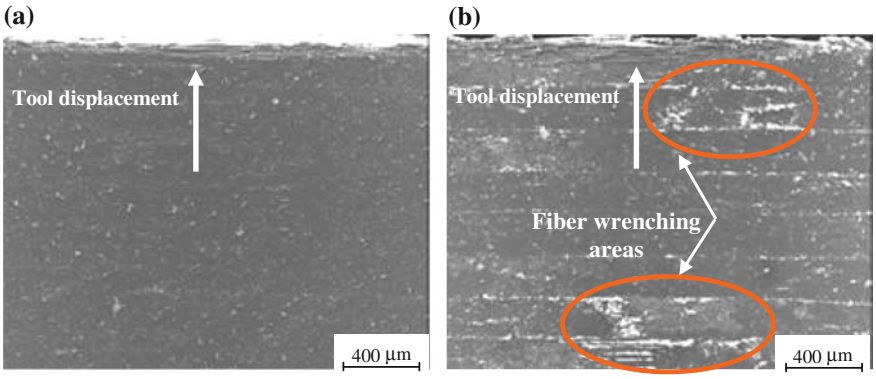

Fig. 2.17 SEM micrographs of the surface. **a** M21-T700 GC plate. **b** T2H-EH25 plate ($d = 6$ mm, $N = 1{,}500$ rpm and $f = 0.02$ mm/rev)

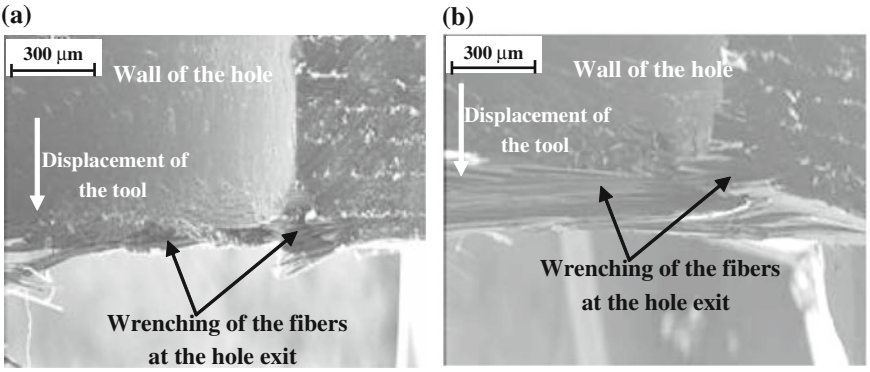

Fig. 2.18 Scanning electron micrographs of the drilled surface. **a** M21-T700 GC plate. **b** T2H-EH25 plate, ($d = 6$ mm, $N = 1{,}500$ rev/min and $f = 0.02$ mm/rev)

the machining parameters, is less than the force Fz that has to be applied to cause delamination between plies. In the following results and analysis, firstly the influence of feed per revolution on the defect at the hole and, secondly, the influence of feed per revolution on the quality of machining on the wall of the hole, exit will be studied using a new drill.

2.10 Delamination at the Hole Exit

The images shown on Fig. 2.19 show the condition of the hole (at drill exit) after the drilling operation. They were obtained as follows: after the drilling operation (with a feed rate of 0.02 mm/rev and spindle speed 1,500 rpm), the laminate plates were scanned with a resolution of 3,000 pixels. Using an image analysis program,

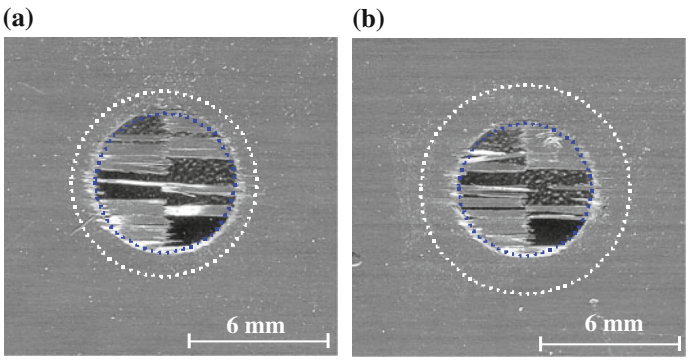

Fig. 2.19 Defect extents at hole exit; (**a**) M21-T700 GC plate, (**b**) T2H-EH25 plate with machining parameters: $f = 0.02$ mm/rev, $N = 1{,}500$ rpm and $d = 6$ mm

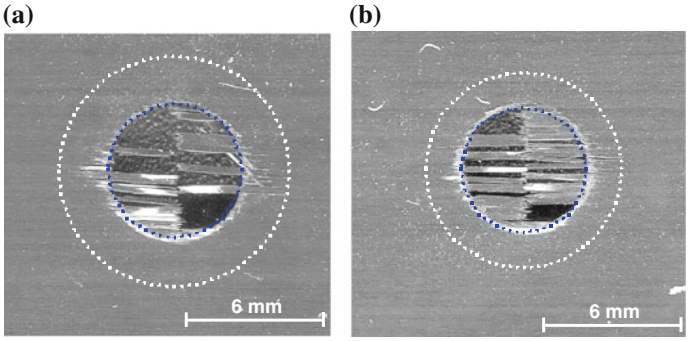

Fig. 2.20 Defect extents at hole exit; (**a**) M21-T700 GC plate, (**b**) T2H-EH25 plate with machining parameters: $f = 0.01$ mm/rev, $d = 6$ mm and $N = 1{,}500$ rpm

two concentric circles are plotted using dotted lines. It can be seen that the extent of delamination on hole exit is greater on laminate T2H-EH25 than on laminate T700M21. In these machining conditions, the factor of delamination for T2H-EH25 is equal to 1.702 and that for M21-T700 GC is 1.587. Obtaining these values benefits from the good resolution of the scanned images. In some cases, it can be seen that the delamination factor of T2H-EH25 is smaller than that for T700-M21. As an example, it can be seen that for a feed rate per revolution f = 0.01 mm/rev that the extent of delamination at hole exit on the laminate of type M21-T700 GC is 1.65 and that for type T2H-EH25 is 1.55 (see Fig. 2.20).

Figure 2.21 shows the distribution of mean values for the delamination factor in relation to feed per revolution for the two materials. Each point on the graph represents an arithmetic mean of 5 points. Looking at this curve, it can be seen that the mean value of the delamination factor for T2H-EH25 is greater than that for M21-T700 GC and this remains true regardless of the feed rate used. This can certainly be explained by the value of the critical energy release rate in mode I that is different from one material to another. According to the analytical and numerical models of [5, 26–28] that allow the critical load responsible for delamination at hole exit to be predicted, this load increases with the energy release rate in mode I (GIc). Thus, when drilling materials M21-T700 GC and T2H-EH25 (GIc of M21-T700 GC being twice as big as GIc of T2H-EH25) for an identical thrust force Fz, the extent of the defect must be less for T700-M21.

For a feed rate per revolution f = 0.01 mm/rev, this leads to a relative deviation of the delamination factor between the two materials of the order of 13 % (this difference is calculated from mean values measured for the delamination factor). According to the works of [7], when drilling a carbon/epoxy laminate with a stack sequence [90°/0°], the increase in feed per revolution of 0.01–0.03 mm/rev leads to a relative deviation of the delamination factor of 10.4 %.

Analysis of the values for standard deviations as shown in Fig. 2.21 shows pronounced scattering of the values measured for the delamination factor. Now, these measurements show that the increase in the critical energy release rate in

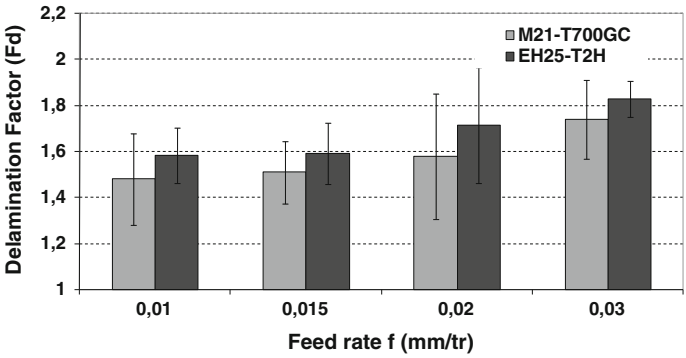

Fig. 2.21 Delamination factor F versus feed rate f with: $d = 6$ mm, $N = 1{,}500$ rev/min

mode I (GIc) of the drilled material does not lead, in all cases, to a reduction in the extent of the defect at the hole exit. This can be due to the influence of dynamic effects that are not catered for in static analytical models.

2.11 State of the Wall of the Hole

A comparison of the surface condition of the wall of the hole for the two materials was made using roughness measurement. Figure 2.22 shows the change in the roughness profile as the stylus is moved on the wall of the hole. It can be seen that the maximum values recorded relate to the central zone. In this central zone, the relative angle between the cutting speed Vc and the direction of the fibres equals to −45°. This trend is exaggerated by the fact that, in this central zone, there are two consecutive plies running in the same direction, which encourages the tearing away of fibres and/or the matrix. These observations have already been mentioned by other authors such as Ramulu et al. [29] and Ghidossi et al. [16]. Figure 2.22

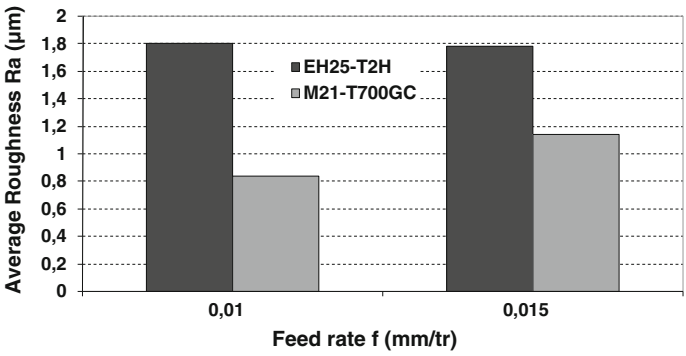

Fig. 2.22 Mean roughness versus feed rate for the two composite materials

shows the change in roughness as a function of the feed rate per revolution of the drill for both the materials studied. The results show that whatever the feed per revolution of the drill, the machined surface of material M21-T700 GC shows a better appearance than that of material T2H-EH25. Having made a comparison of the specific pressure of the two materials as well as of roughness measurement as a function of feed per revolution, it is proposed to proceed with analysis of the extent of the defects at hole exit for the two materials (via the delamination factor concept).

2.12 Summary

Within the scope of the study, analysis of the quality of machining when drilling two types of carbon/epoxy quasi-isotropic laminates shows that:

- The empirical model proposed for homogeneous metallic materials is valid when drilling carbon/epoxy long fibre composite laminates. Using this empirical model, the specific pressure of the two materials is similar when machining using a new drill.
- The defect at hole exit is minimal for material M21-T700 GC regardless of the choice of feed speed. The presence of thermoplastic nodules intended to improve the energy release rate in mode I and in mode II in material M21-T700 GC provides protection for the cutting tool against the abrasive nature of the composite material. The machined surface condition of the laminate M21-T700 GC is better than that of T2H-EH25. In fact, to avoid the damages during drilling of composites material is not sufficient to optimize only the machining parameters and the tool geometry, because composites materials are not a black metal. Nowadays, in the industry fields, during the setup of design only the choice of the composite material is linked to the stress analysis of the part. For this, in order to improve the machining quality of composite part, it is primordial to take into account, in the setup of the design the concept of the machinibility of this material.

References

1. Shaw MC (2005) Metal cutting principles. Oxford University Press, Oxford
2. Kim D, Doan X, Ramulu M (2005) Drilling performance and machinability of PIXA-M and PEEK thermoplastic composites. J Thermoplast Compos Mater 18(3):195–217
3. Zitoune R, Krishnaraj V, Almabouacif S, Collombet F, Sima M, Jolin A (2012) Influence of machining parameters and new nano-coated tool on drilling performance of CFRP/aluminium sandwich. Compos B Eng 43(3):1480–1488

4. König W, Grass P (1989) Quality definition and assessment in drilling of fibre reinforced thermosets. Annals CIRP 38:119–124
5. Hocheng H, Dharan CKH (1990) Delamination during drilling in composite laminates. J Eng Ind 112:236–239
6. Davim JP, Pedro R (2003) Drilling carbon reinforced plastics manufactured by autoclave: experimental and statistical study. Mater Des 24:315–324
7. Tsao CC, Ho-Cheng H (2004) Taguchi analysis of delamination associated with various drill bits in drilling of composite materials. Int J Mach Tools Manufac 44:1085–1090
8. Zitoune R, Périé JN, Collombet F, Piquet R, Lachaud F (2004) Coupe orthogonale sur composites fibres longues carbone/époxy : comparaison entre mesures de champs et calculs numériques (in French). Colloque National de Photo Mécanique 2004, Albi Carmaux (France). ISBN 2-9511591-3-7
9. Krishnaraj V (2006) Study of drilling tool geometry while machining of glass fibre reinforced plastic. Ph.D Dissertation, Anna University, Chennai, India
10. Davim JP, Pedro R, Conceição CA (2004) Experimental study of drilling of glass fiber reinforced plastics (GFRP) manufactured by hand lay-up. Compos Sci Technol 64:289–297
11. Wang DH, Ramulu M, Arola D (1995) Orthogonal cutting mechanisms of graphite/epoxy. Composite part i: unidirectional laminate. Int J Mach Tools Manufac 35(12):1623–1638
12. Zitoune R, Collombet F (2005) Experiment-calculation comparison of the cutting conditions representative of the long fibre composite drilling phase. Compos Sci Technol 65:455–466
13. Konig W, Wulf Ch, Grab P, Willerschied H (1985) Machining of fiber reinforced plastics. Annals CIRP 34:537–547
14. Saleem M, Toubal L, Zitoune R, Bougherara1 H, Cénac F (2012) Influence of drilling process on the mechanical behaviour of cfrp composite plates. Oral presentation, ECCM 15, Italy
15. Arola DD, Ramulu M (1998) Net-shape machining and the process-dependent failure of fiber-reinforced plastics under static loads. J Compos Tech Res 20:210–220
16. Ghidossi PN, El Mansori M, Pierron F (2004) Edge machining effects on the failure of polymer matrix composite coupons. Compos Part A 35:989–999
17. El-sonbaty I, Khashaba UA, Machaly T (2003) Factors affecting the machinability of GFR/epoxy composites. Composite Structures 63:329
18. Lin SC, Chen IK (1996) Drilling carbon fiber-reinforced composite material at high speed. Wear 194:156–162
19. Guegan P (1994) Contribution à la qualification de l'usinage de matériaux composites à matrice organique. Thèse de doctorat n°2025, Génie Mécanique, E.C. Nantes
20. Arola DD, Ramulu M (1997) Net-shape machining and the process- dependent failure of failure of fiber-reinforced plastics under dynamic loads. J Compos Technol Res JCTRER 37(4):379–385
21. Won MS, Dharan CKH (2002) Chisel edge and pilot hole effects in drilling composite laminates. J Manuf Sci Eng 124:242–247
22. Gindy NN (1998) Selection of drilling conditions for glass fiber reinforced plastics. Int J Prod Res 26(8):1317–1327
23. Enemuoh UE, EL-Gizawy SA, Okafor CA (2001) An approach for development of damage free drilling of carbon fiber reinforced thermosets. Int J Mc Tools Mfr 41:1795–1814
24. Khashaba UA (2004) Delamination in drilling GFR-thermoset composites. Compos Struct 63:313–327
25. Ramulu M, Rao PN, Kao K (2002) Drilling of (Al_2O_3) p/6061 metal matrix composites. J Mater Process Technol 124:244–254
26. Tsao CC, Hocheng H (2003) The effect of chisel length and associated pilot hole on delamination when drilling composite materials. Int J Mach Tools Manf 43:1087–1092
27. Zitoune R, Collombet F (2007) Numerical prediction of the thrust force responsible of delamination during the drilling of the long-fibre composite structures. Compos A 38:858–866

28. Zhang L-B, Wang L-J, Liu X-Y (1995) A mechanical model for predicting critical thrust forces in drilling composite laminates. Proc Inst Mech Eng Part B J Eng Manuf 215(2):135–146
29. Ramulu M, Kim D, Kao H, Rao PN (2008) Experimental modeling and analysis of drilling (Al_2O_3) p/6061 metal matrix composites using PCD tool. Int J Mater Prod Technol 32(1):20–41

Part II

Chapter 3
Effects of Drill Points While Drilling of Composites

3.1 Introduction

The mechanism of the material removal in an oblique cutting process such as drilling, the variation of the forces with time and their influence on accompanying damage, the optimal drill point geometry for minimizing the drilling forces and the subsequent damage are some of the directions in which the work in the machining of composite material is progressing [1–10]. Four facet, eight-facet, Jo-point, inverted cone and special geometry are some of the widely used tool designs in drilling composite materials [2]. Three drill geometries are used to study the effect of cutting forces and hole quality on GFRP composite laminates. The first type is a standard twist drill with 118° point angle and 30° helix angle. The second type is Zhirov point drill (Fig. 3.1a), which has a triple lip at each cutting edge, an extra rake ground on the face of the lips, and a split point. The third type is a multifacet drill (Fig. 3.1b). An arc cutting edge with a radius of 1.5 mm is made to increase the rake angle. The arc cutting edge is effective in dividing chip and drill centering. Experiments were conducted using CNC vertical machining center (Mori-Seiki) using full factorial design. A diameter 10 mm drill made of HSS-M40 was used to drill holes on GFRP laminates. A spindle speed of 1,000, 2,000, 3,000 and 4,000 rpm with a feed rate of 0.02, 0.03, 0.04 and 0.05 mm/rev were used in drilling holes. Experiments were conducted using full factorial design. Surface roughness, hole diameter, circularity and delamination at exit were measured and recorded.

3.2 Influence of Cutting Parameter on Thrust Force

From the experiments it was found that increase in spindle speed and feed rate increase the thrust force (Fig. 3.2), especially feed rate; this is because larger the feed rate, higher will be the cross sectional area of the undeformed chip, with greater resistance to chip formation and consequently greater axial thrust force [4, 5].

V. Krishnaraj et al., *Drilling of Polymer-Matrix Composites*,
SpringerBriefs in Manufacturing and Surface Engineering,
DOI: 10.1007/978-3-642-38345-8_3, © The Author(s) 2013

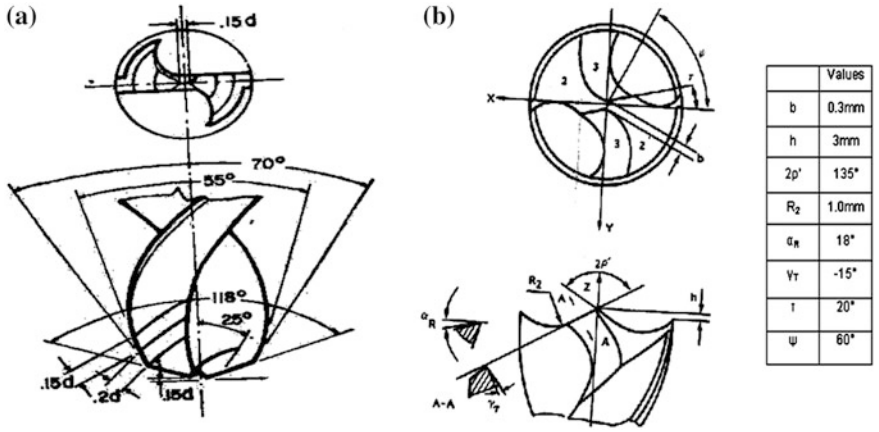

Fig. 3.1 Drill geometries **a** Zhirov point drill and **b** Multifacet drill

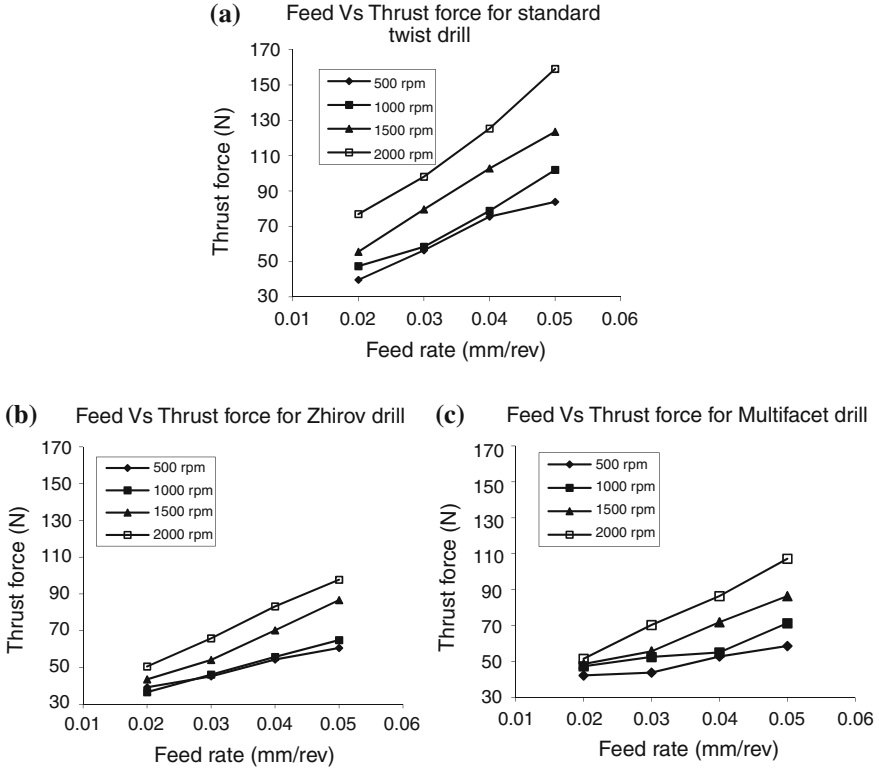

Fig. 3.2 Feed rate versus thrust force **a** Standard twist drill **b** Zhirov point drill and **c** Multifacet drill

Zhirov point drill can drill with lower thrust force for the same operating conditions when compared to standard twist drill and multifacet drill. This is because in the Zhirov drill the chisel edge has been modified with cutting edge and consequently extrusion action is replaced by cutting action. This design allows the feed thrust to be reduced by one-third that is required for standard twist drills. The Zhirov point drill also produces more dimensionally accurate holes because of less deflection in the spindle through a reduction of the thrust force. Multifacet drill (MFD) also generated less thrust force than standard twist drill. The MFD is designed to reduce the cutting force by an arc cutting edge in the cutting lip to increase the rake angle and a reduced chisel edge length to decrease the thrust force. When compared to Zhirov point drill, thrust force generated by MFD was slightly higher.

3.3 Influence of Drill Points on Thrust Force

Figure 3.3 shows the cutting characteristics of the drill points. Sudden increase in cutting force is evident with standard twist drill. This can be attributed to the penetration/extrusion action of the chisel edge of the standard twist drill. Once the work material is penetrated cutting action of the lip starts and the cutting force gradually increases. Then it drops sharply as the tool exits through the opposite side. During the steady portion of the drilling process, significant oscillations of the normal force are observed. For woven fabric/cross ply laminates, the amplitude of variation is lower. While drilling with conventional twist drills, the crack propagation around the drilled hole is found to be more severe when cutting lips pass through the bottom of the laminates.

Cutting action of the Zhirov point is smoother and it starts cutting from the beginning with gradual increase in the cutting force till the entire edges start cutting. The cutting force drops gradually because of the triple edge at the outer lip

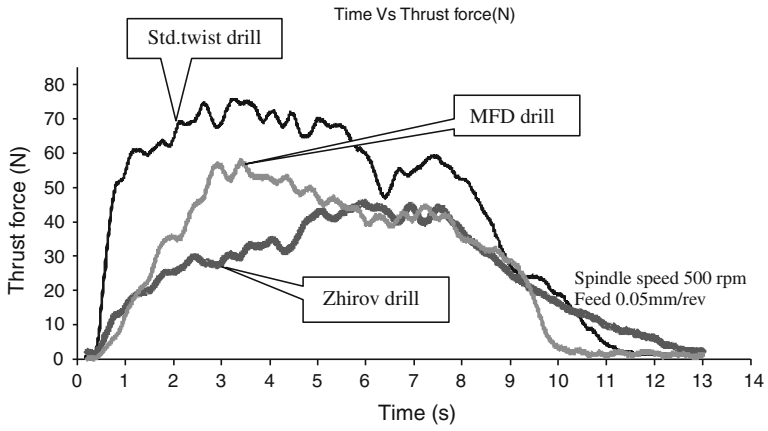

Fig. 3.3 Effect of drill geometries on thrust force

of the drill. Similar crack and fiber pull out was found while drilling using Zhirov point drill when compared to standard twist drill (There was no difference between the Zhirov point drill and standard twist drill as for as the quality of the hole is concerned). The only difference is less thrust force and thin chips when compared to standard twist drill. This was not sufficient to trim the hole neatly around the exit side of the hole.

Multifacet drill picks the top surface of the laminate at three locations, one at the middle and the other two at the outer diameter of the drill (diametrically opposite). When MFD starts cutting the laminate the cutting force reaches a high value possibly because cutting starts at three locations and once it starts cutting the laminate the force drops gradually. In all the three cases after the full engagement of the lip the cutting force starts dropping, perhaps due to softening of the matrix by the heat generated during the drilling process. The cutting force values of MFD are higher compared to Zhirov point but less than standard twist drill. The cutting force variation at the exit is sudden and a button like chip is ejected out [17–19].

3.4 Influence of the Cutting Parameter on Torque

The value of the torque was measured using drilling dynamometer which is interfaced with a system. Figure 3.4 shows the main effects of cutting parameters on the torque. On examining these results, it is found that the torque increased with the cutting speed. However, the increase in torque was much smaller than that in thrust force as cutting speed increases [11–13].

It is found that the torque increased linearly as feed rate increased for all three drill geometries. Zhirov point has a triple lip at each cutting edge, the shortest lip has an include angle of 55°, the intermediate lip has a point angle of 70°, and the largest lip has the standard point angle of 118°. This point style produces wiper chips (chips are thinner) and reduces the torque required to cut the hole.

3.5 Influence of the Cutting Parameter on Surface Roughness

The surface roughness of the holes was measured using (Surfcorder) surface roughness measurement equipment (Ra according to 4287/1). From the Fig. 3.5, it can be inferred that the value of Ra increases with the feed rate. Hence, poor surface will be obtained when the feed rate is increased [4, 5].

When the spindle speed was increased Ra value decreased. Better surface finish can be obtained at higher speed. i.e., to get a better surface finish it is necessary to have a high spindle speed and low feed rate. Zhirov point (0.7–2 μm) and Multifacet (1–2.5 μm) drills are giving low surface roughness. In Zhirov point three lips on flank surface reduce the chip thickness and slot on chisel edge reduces

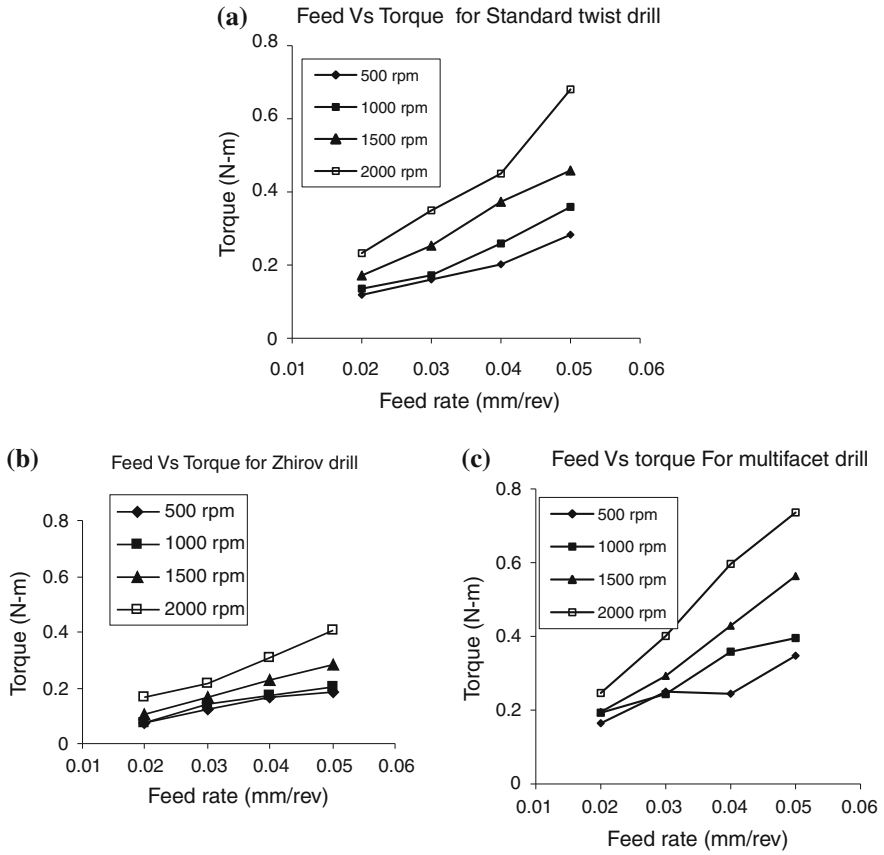

Fig. 3.4 Feed rate versus torque for **a** Standard twist drill **b** Zhirov point drill **c** Multifacet drill

the thrust force. Reduced thrust force gives less vibrations on spindle and surface finish is increased. Whereas in multifacet drill cutting takes place at the periphery like trepanning.

3.6 Influence of the Cutting Parameter on Delamination Factor

3.6.1 Delamination Factor

Delamination near the exit side is induced as the tool acts like a punch, separating the thin uncut layer from the remainder of the laminate. Delamination factor (df) was calculated for each drill points namely standard twist drill, Zhirov point drill

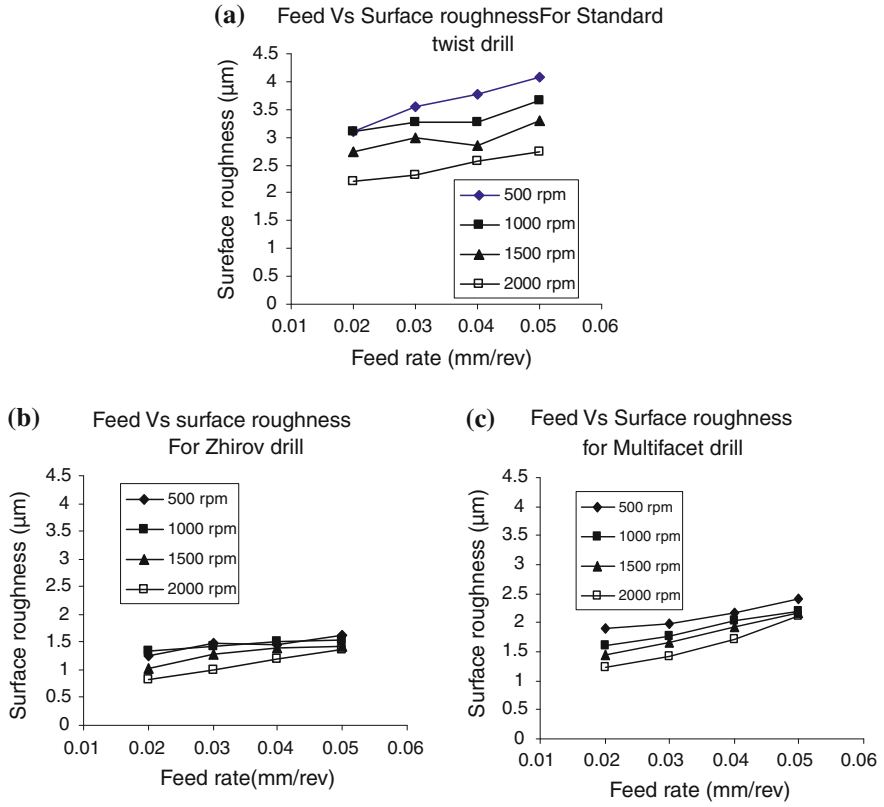

Fig. 3.5 Feed rate versus surface roughness (*Ra*) for **a** Standard twist drill **b** Zhirov point drill **c** Multifacet drill

and multifacet drill. The Fig. 3.6 shows the relationship between the delamination factor and drilling parameters. It is concluded that the delamination factor increases with feed rate and spindle speed. According to the experimental study, multifacet drill presents better performance than standard twist drill and Zhirov point drill, because of its cutting action at the periphery of the holes.

The standard twist drills always give higher delamination for the same drilling conditions. The entry point of hole produced is neat for all the geometries. From the Fig. 3.7 we can observe fibers pull out at exit side of the drilled hole. Damage is more in the case of twist drill [14, 15]. MFD produced clean cut holes at the exit side of the laminate. This is because the cutting mechanism of a multifacet at the last ply is like a trepanning with knife-edge [16].

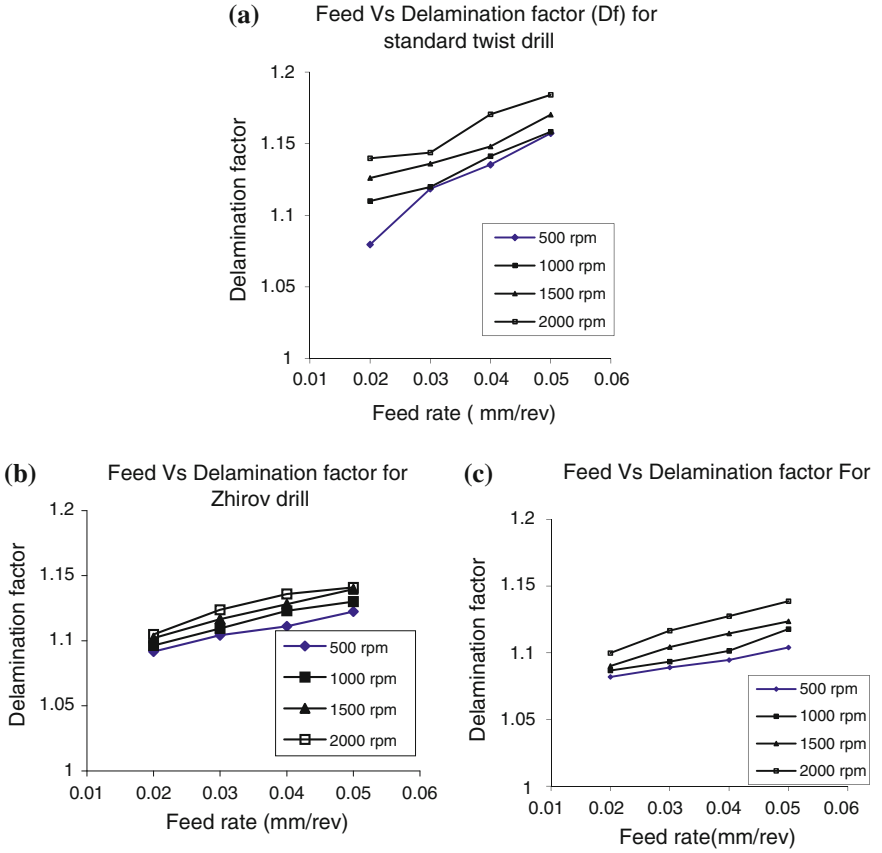

Fig. 3.6 Feed rate versus delamination factor for **a** Standard twist drill **b** Zhirov point drill **c** Multifacet drill

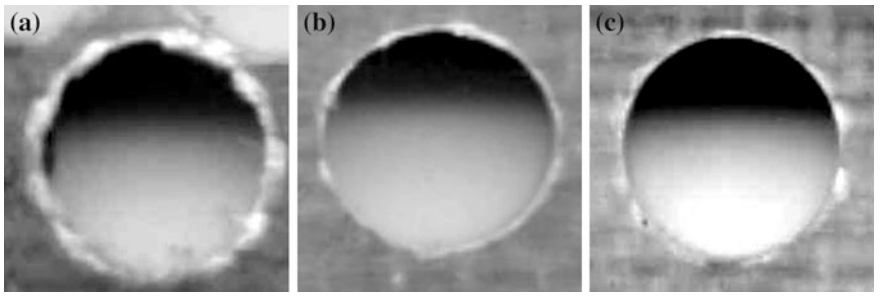

Fig. 3.7 Exit delamination zone for **a** standard twist drill **b** Zhirov point drill **c** multifacet drill

3.7 Influence of the Cutting Parameter on Hole Quality

The holes drilled by HSS drill (φ 10 mm) are measured with the Co-ordinate Measuring Machine (CMM-MITUTOYA) using φ 3 mm Ruby crystal probe. The dimensions of the holes are measured at the middle of the laminate thickness.

Variation of hole diameter up to 0.1 mm is found for the drill geometries considered in this experiments (Fig. 3.8). In Zhirov and multifacet drill points dominant to peripheral cutting action can be seen i.e., can be lead to the observed higher order shrinkage. Circularity can be seen with Zhirov and multifacet drill

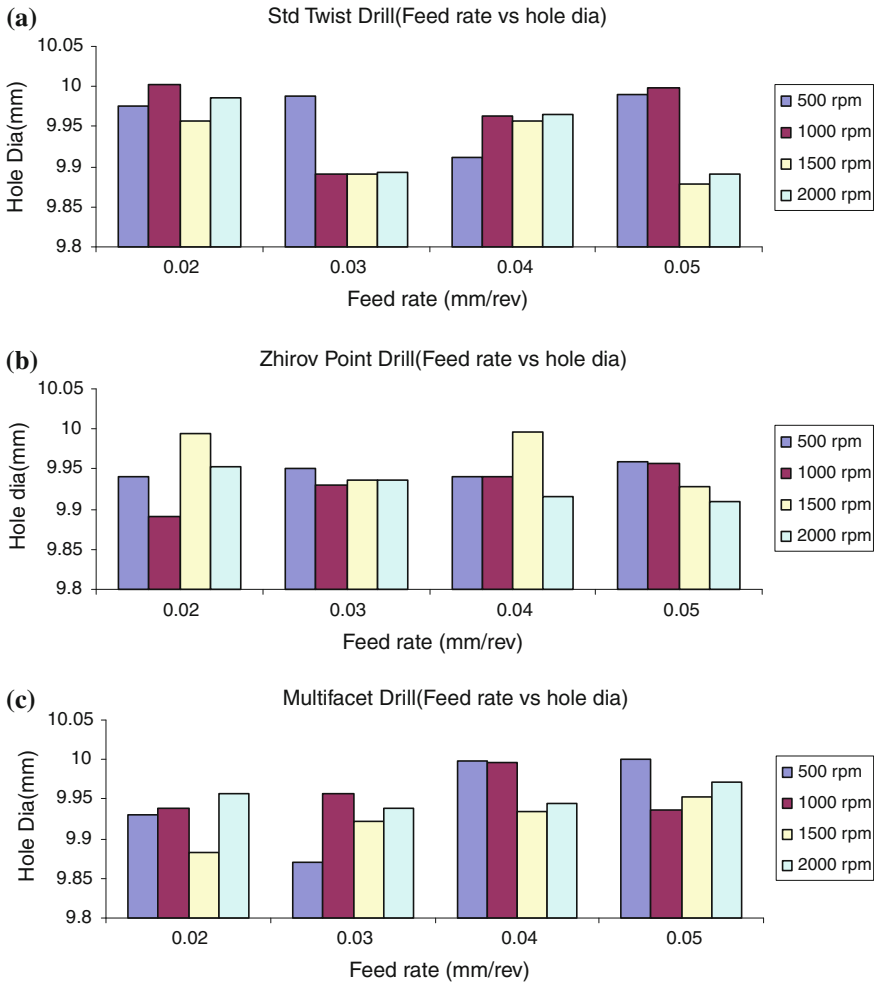

Fig. 3.8 Hole diameter for **a** Standard twist drill **b** Zhirov point drill **c** Multifacet drill

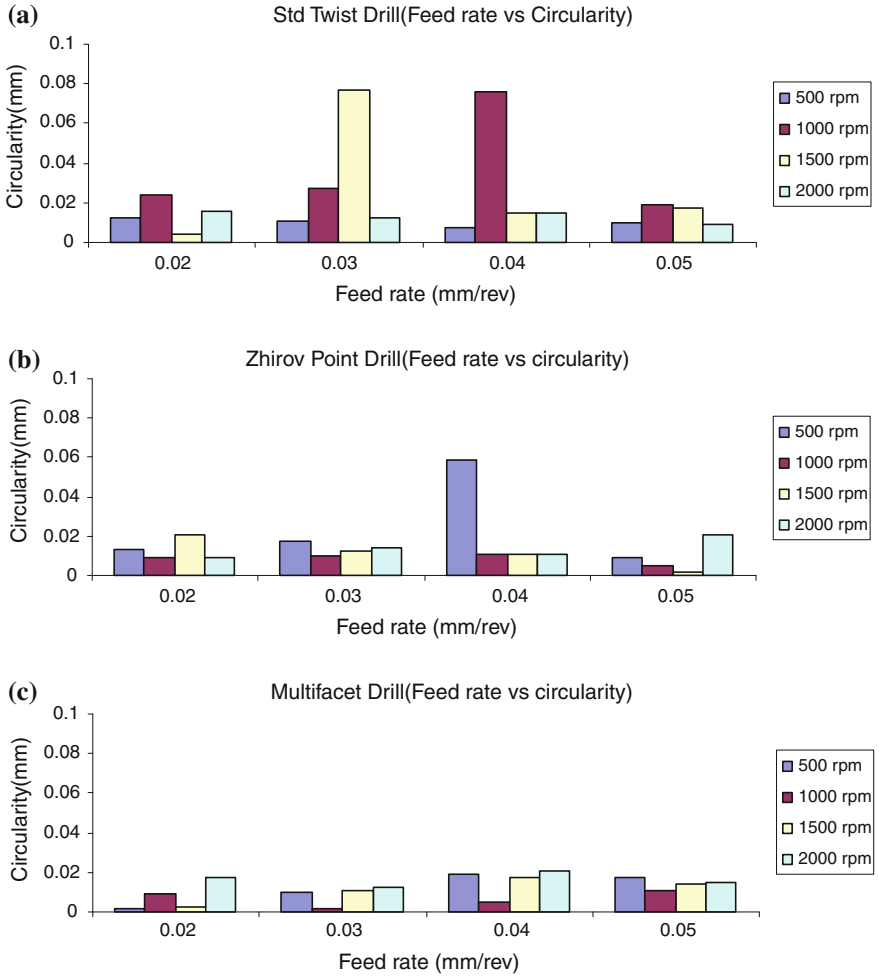

Fig. 3.9 Circularity for **a** Standard twist drill **b** Zhirov point drill **c** Multifacet drill

again attributed to the dominant peripheral cutting action (Fig. 3.9) (Minimum circularity error when drilling with Zhirov point and multifacet drill can be attributed to dominant peripheral cutting).

3.8 Tool Wear Study on Different Drill Points

The major reason for tool wear is the thermal softening of the tool material, and higher order abrasive nature of the chip. The cutting forces are mostly dependent on the status of the cutting edges, which are indirect indicators of the cutting edge

and can also be used as process indicators. With tool wear, thrust force normally increases. So, tool life can be predicted by measuring the thrust force with respect to number of holes. The tool's flank wear was measured using toolmakers microscope with a magnification of 10X.

In standard twist drill, thrust force increased sharply because of initial wear. Initial wear was up to 6th hole. In the range of 20–25 holes, there is a stable trend in the thrust force. The tool life for standard twist drill is around 25 holes and thrust force at the end of 25th hole is 100 N (Fig. 3.10). The powdery chips produced during drilling of composites are quite abrasive in nature owing to the presence of reinforcing fibers. These chips certainly cause more wear at cutting edges and even increase the temperature at cutting edges. 490 μm wear land is observed on the flank after 34 holes are drilled.

In Zhirov point geometry, initially the thrust force increases rapidly from 29 N to 59 N due to wear at the groove edge. Cutting edge near the groove in the Zhirov geometry worn out rapidly those led to rapid increase in thrust force. After 7 holes the wear is uniform and thrust force increases gradually up to 71st hole. After 71st hole thrust force increases rapidly due to an increase in tool wear. Also hole quality is reduced. That shows end of tool life. Uniform wear is observed at the cutting edge near the groove.

In multifacet drill from 1st hole to 5th hole there is an initial wear, so thrust force increases rapidly. In the range of 5–38th holes, there is a stable trend in thrust force due gradual tool wear. Sudden increase in thrust force is observed after 38th hole due to increase in tool wear (Cutting force increased from 60 to 85 N between 36th hole to 42nd hole and beyond 42nd hole the cutting force started increasing steeply). Illustration of variation of thrust force with number of holes drilled indicates higher suitability of Zhirov point drill, where as multifacet drill exhibits lower order thrust force during early phase of drilling.

The dominant wear type in drilling has been identified by microscopic observations of the worn surface of the tool. It is an abrasive form of flank wear in the drill characterized by scratching in the sliding direction, which can be measured as Vb_{max}. An example of this wear type in a drill is presented in Fig. 3.11.

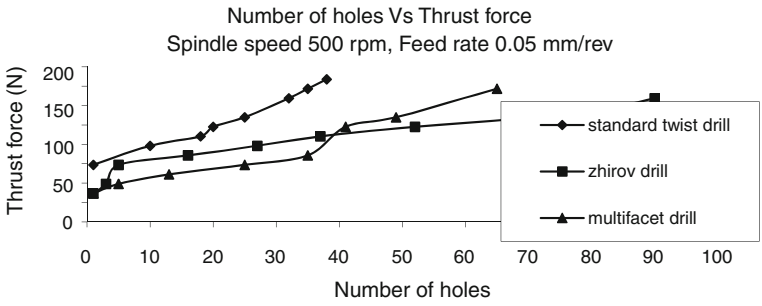

Fig. 3.10 Number of hole versus thrust force for HSS drill geometries

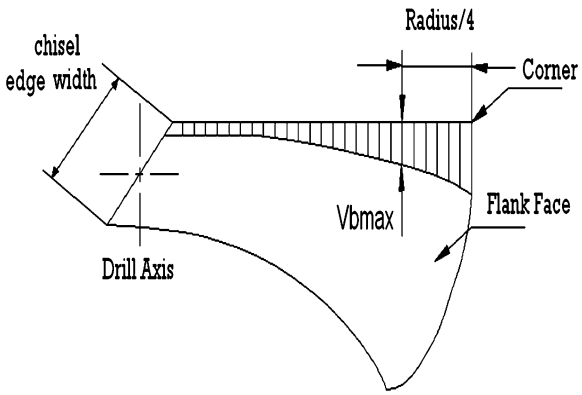

Fig. 3.11 Wear land on the cutting edge of drill

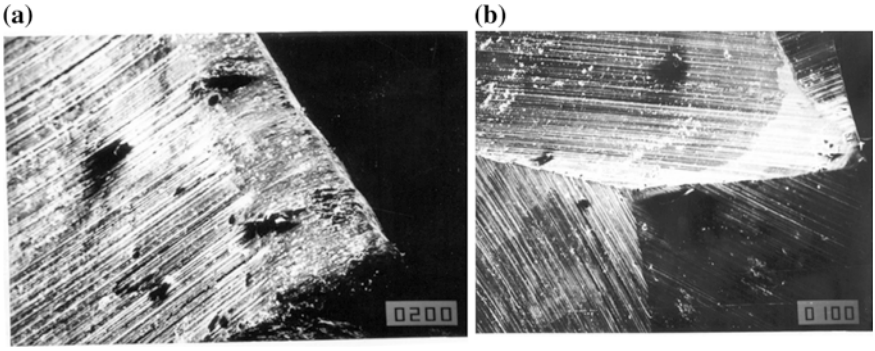

Fig. 3.12 SEM photograph of multifacet drill at **a** Extreme end, **b** Chisel edge

The wear land width is not uniform along the edge. It is smaller near the axis and it grows very sharply near the corner. The resistance to abrasion of the cutting tools material depends directly on the relative hardness of the material involved. The glass fiber used as reinforcement in the FRP is highly abrasive in nature which damages the bonding between cobalt and tungsten carbide. In the standard twist drills abrasion type of wear is predominant.

Figure 3.12 shows the wear pattern of multifacet drill used for drill wear study. It is shown that chipping appears at both the outer corner of arc lip region and the chisel edge region. Otherwise, the drill geometry is about the same as the fresh drill. The appearance of chipping may be because of relatively hard fiber.

3.9 Summary

From a series of experiments it is found that cutting action of the Zhirov is smooth, it starts cutting from the beginning with gradual increase in the cutting force till the entire edges start cutting. The cutting force drops gradually because of the triple edge at the outer lip of the drill. The difference between Zhirov point drill with standard twist drill is less thrust force and thin chips.

Zhirov point drill and multifacet can drill with lower thrust force for the same operating conditions when compared to standard twist drill. Zhirov (0.7–2 μm) and multifacet (1–2.5 μm) drills are giving low surface roughness (Ra). In Zhirov point drills three lips on flank surface reduce the chip thickness and slot on chisel edge reduces the thrust force. Whereas in multifacet drill cutting takes place at the periphery like trepanning instead of extrusion action, hence surface finish is improved.

Delamination factor increases with feed rate and spindle speed. According to the experimental study, multifacet drill presents a better performance than all the other drill geometries, because of its cutting action at the periphery of the holes. The standard twist drill gave higher delamination for the same drilling conditions.

The tool life for standard twist drill is around 25 holes, Zhirov drill it is around 71 holes and for multifacet holes it is around 38 holes. The dominant wear type in drilling has been identified by the microscopic observations of the worn surface of the tool. It is an abrasive form of flank wear in the drill characterized by scratching in the sliding direction.

References

1. Abrate S (1997) Machining of composites. In: Mallick PK (ed) Composites engineering hand book. Marcel Deckker Inc., New York
2. Bhatnagar N, Naik NK, Ramakrishnan N (1993) Experimental investigation of drilling of CFRP composites. Matls Manuf Proc 8:683–701
3. Bhattacharyya A (2000) Metal cutting theory and practice. New Central book agency (P) Ltd., Calcutta
4. Davim JP, Reis P (2003) Study of delamination in drilling carbon fiber reinforced plastics (CFRP) using design experiments. Comp Struct 59:481–487
5. Davim JP, Reis P, Antonio CC (2004) Experimental study of drilling glass fiber reinforced plastics (GFRP) manufactured by hand lay-up. Comp Sci Tech 64:289–297
6. Hocheng H, Dharan CKH (1990) Delamination during drilling of composite laminates. J Eng Industry 112:236–239
7. Hocheng H, Tsao CC (2003) Comprehensive analysis of delamination in drilling of composite material with various drill bits. J Matls Proc Tech 140:335–339
8. Khashaba UA (2004) Delamination in drilling GFR-thermoset composite structures. Comp Struct 63(3):313–327
9. Kohkonen KE, Potdar N (1998) Composite machining. In: Peters ST (ed) Hand book of composites, Chapman and Hall, California, Chap. 27, pp 596–609
10. Komanduri R (1993) Machining of fibre-reinforced composites. ASME Mech Eng 114:58–66

11. Konig W, Wulf Ch, Graß P, Willercheid H (1985) Machining of fibre reinforced plastics. Ann CIRP 38:119–124
12. Persson E, Eriksson I, Zackrisson L (1997) Effects of hole machining defects on strength and fatigue life of composite laminates. Comp Part A, 28(A):41–151
13. Ramkumar J, Malhotra SK, Krishnamurthy R (2004) Effect of workpiece vibration on drilling of GFRP laminates. J Matls Proc Tech 152:329–332
14. Tsao CC, Hocheng H (2004) Taguchi analysis of delamination associated with various drill bits in drilling of composite material. Int J Mach Tools Manf 44:1085–1090
15. Won MS, Dharan CKH (2002) Chisel edge and pilot hole effects in drilling composite laminates. J Manuf Sci Eng 124:242–247
16. Wu SM (1985) Multifacet drills. In: Robert IK (ed) Hand book of high-speed machining technology. Chapman and Hall, New York
17. Krishnaraj V, Vijayarangan S, Davim P (2008) An experimental and statistical study on the effect of drill geometries on force and hole quality in drilling of glass fiber reinforced plastic. Int J Mater Prod Technol 32(2–3):264–275
18. Krishnaraj V, Vijayarangan S (2006) Effects of drill geometry in drilling of glass fibre reinforced plastic using carbide drill. Int J Manuf Eng V:5–9
19. Krishnaraj V, Vijayarangan S, Kaldos A (2006) An experimental study on effect of drill points and drill wear on drilling of glass fiber reinforced plastic at high spindle speed. Int J Manuf Sci Prod 3–4:187–200

Part III

Chapter 4
Effects of Drill Points While Drilling at High Spindle Speed

4.1 Introduction

High speed machining is now recognized as one of the key manufacturing technologies for higher productivity and throughput [2, 10, 14]. It is well known that the most effective way of achieving good quality holes while drilling fibre reinforced plastics is by reducing the thrust and torque [3–11, 14, 15, 17, 19]. High spindle speed reduces the cutting force requirements. So, drilling experiments were conducted with drill geometries, namely standard twist drill, Zhirov-point drill, and multifacet drill, using wide range of spindle speed, and feed rate to analyse thrust force, delamination and surface roughness.

4.2 Experimental Setup

Experiments were conducted using Acumac high-speed spindle (5 kW) mounted on a vertical CNC machine. Figure 4.1 shows the experimental set-up. Due to the high abrasive nature of fiber-reinforced materials, micro-grain carbide (Ø 10 mm-K10) was used in this investigation. Drilling of laminates was carried out for the following conditions using full factorial design. Cutting speed values were selected between 15.7 to 62.8 m/min and 440 to 600 m/min to study the effect of normal and high spindle speed respectively on drill geometries, surface finish and delamination.

$$\text{Spindle speed: } 500,\ 1,000,\ 1,500,\ 2,000 \text{ and } 14,000,\ 16,500,\ 19,000 \text{ rpm}$$

$$\text{Feed rate: } 0.02,\ 0.03,\ 0.04,\ 0.05 \text{ mm/rev}$$

V. Krishnaraj et al., *Drilling of Polymer-Matrix Composites*,
SpringerBriefs in Manufacturing and Surface Engineering,
DOI: 10.1007/978-3-642-38345-8_4, © The Author(s) 2013

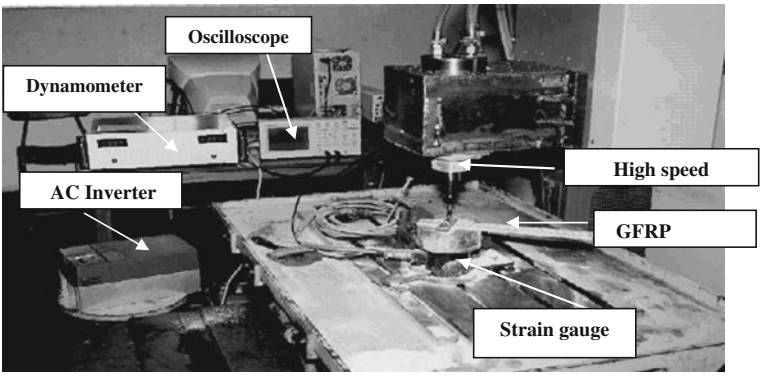

Fig. 4.1 High speed spindle experimental setup

4.3 Influence of Cutting Parameters on Thrust Force

Drilling parameters cause change in cutting forces, which influence the quality of the holes in terms of surface finish, circularity, delamination, fiber pull out, matrix cratering, etc. [3–5, 7–9, 11, 15, 19]. From the experiments it was found that high spindle speed decreases the thrust force [12, 14]. As seen in Fig. 4.2 Zhirov point drill experiences lower thrust force for the same operating conditions when compared to other geometries. This is because in the Zhirov drill the chisel edge has been replaced by cutting edges, therefore extrusion action is replaced by cutting action [1]. The Zhirov-point drill also produces more dimensionally accurate holes because of less deflection in the spindle through a reduction of the thrust force. At lower feed rate (0.02 mm/rev) Zhirov point drill and multifacet generated more or less same thrust force (around 20 N). This value is very less when compared to

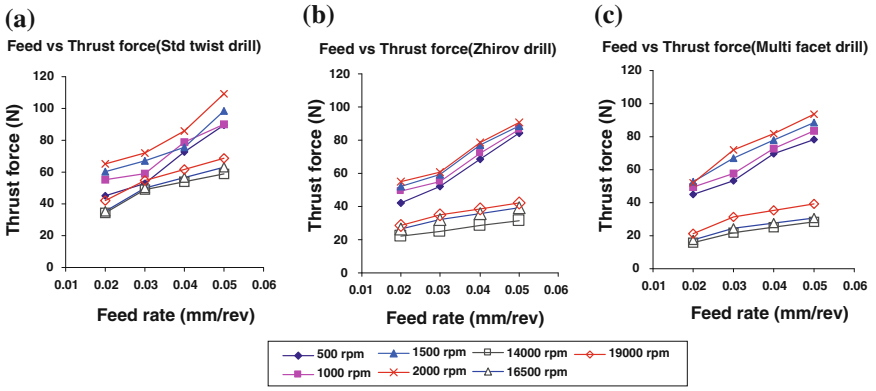

Fig. 4.2 Effect of feed rate and spindle speed on thrust force **a** Standard twist drill **b** Zhirov-point drill **c** Multifacet drill

drilling at normal spindle speed which is around 50 N. For all the drill geometries at high spindle speed the torque values are between 0.1 and 0.2 N-m. Not much variation in the torque values is recorded within the range examined.

4.4 Influence of Cutting Parameters on Delamination Factor

Delamination near the exit side is introduced as the tool acts like a punch, separating the thin uncut layer from the remainder of the laminate. The entry hole produced was neat for all the geometries. However, the fiber pull out at exit was more in the case of twist drill and Zhirov point drill. Multifacet drill produced clean cut holes at the exit side of the laminate. This is because the cutting mechanism of a multifacet at the last ply is like a trepanning with knife-edge. Therefore, exit hole was neat and fuzzy free. A button like chip was ejected at the exit side of the laminate while drilling using multifacet drill. The delamination was evaluated in terms of delamination factor. The delamination factor is the ratio of maximum diameter (Dmax) of the damaged zone to the actual hole diameter (D).

Figure 4.3 shows the relationship between the delamination factor and drilling parameters. It is concluded that delamination factor increases with feed rate and spindle speed [10]. The effect of high spindle speed is significant on standard twist drill, whereas the effect of high spindle speed on delamination factor during drilling using Zhirov point and multifacet is less significant.

Figure 4.4 shows the hole machined in the drilling process for standard twist drill, Zhirov point, and multifacet drill respectively. Multifacet drill presents a better performance than other drill geometries. The special characteristic of the drill is the extreme sickle-form design of the cutting edges. This pre-stresses the fibers in the direction of pull and separates them in the direction of thrust. This results in a clean cut with a smooth surface. The delamination is less compared to other drill geometries.

4.5 Influence of Cutting Parameters on Surface Roughness

After the drilling test, the quality of hole at entry and exit has been examined. The surface roughness (Ra) was evaluated as per ISO 4287/1 [4]. For each test 3 measurements over drilling surfaces were made. Figure 4.5 shows the effect of drill geometry on surface finish. The value of surface roughness increases with the feed rate, and decreases with the cutting speed. Zhirov drill produced better surface finish (4–5 μm) at lower feed rate. The outer most lip produced thin chip which improved the finish of the hole. Multifacet drill also generated better surface finish at lower feed rate when compared to standard twist drill. The effect of spindle speed on surface finish is less compared to feed rate for Zhirov point and

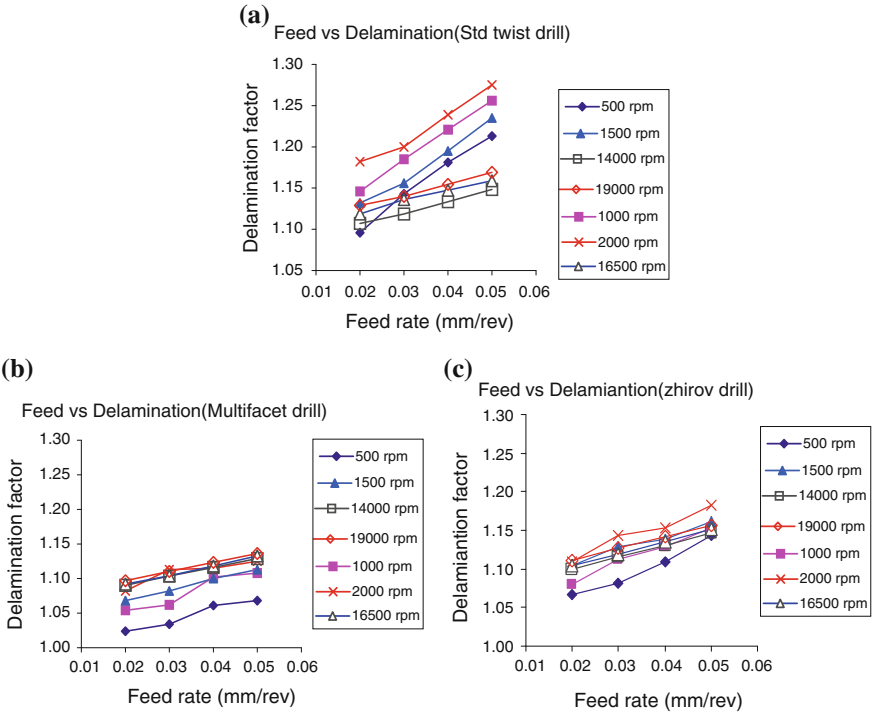

Fig. 4.3 Effect of feed rate and spindle speed on delamination: **a** Standard twist drill; **b** Zhirov point drill; **c** Multifacet drill

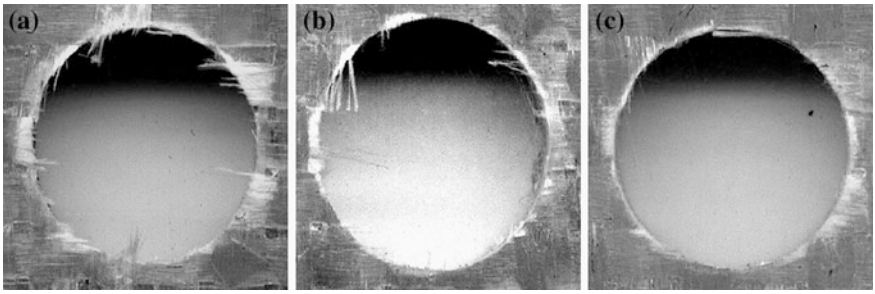

Fig. 4.4 Effect of drill points on delamination (φ 10 mm hole: magnification: 3X) **a** Standard twist drill; **b** Zhirov point drill; **c** Multifacet drill

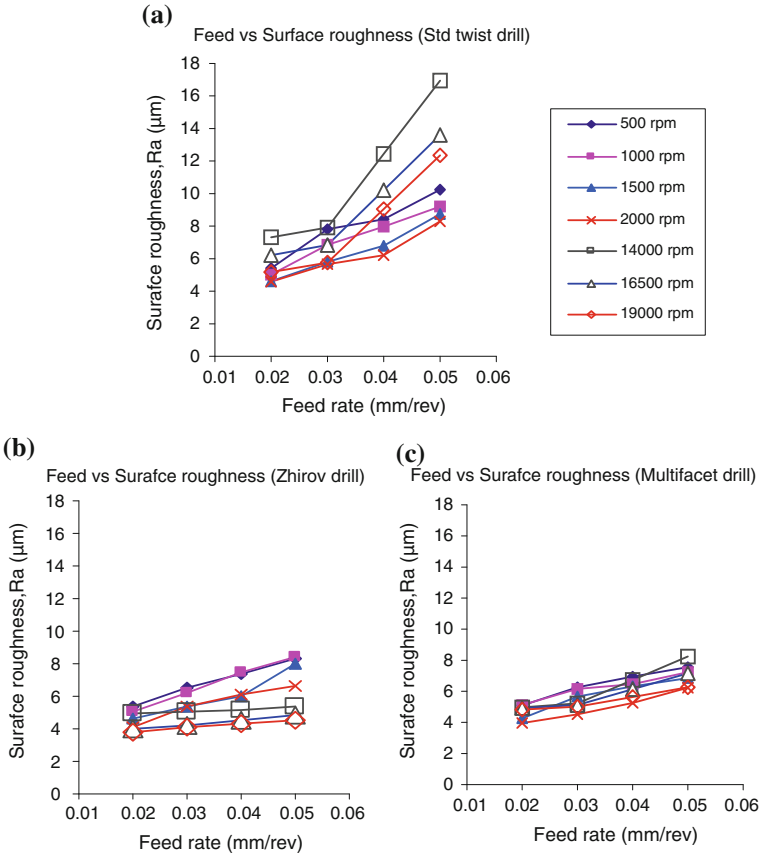

Fig. 4.5 Effect of feed rate and spindle speed on surface roughness **a** Standard twist drill; **b** Zhirov point drill; **c** Multifacet drill

multifacet drill [6, 8, 17]. With high speed drilling a considerable reduction in thrust force can be seen; however the drilled hole exhibits higher order surface roughness and only a marginal difference in delamination factor (Possibly due to higher order drilling temperature). It is seen that for standard twist drill and mulitifacet drill beyond 0.03 mm/rev steeper rise in surface roughness.

4.6 Influence of the Cutting Parameter on Hole Quality

The diameter of the holes drilled by carbide drill (φ 10 mm) is measured with the Co-ordinate Measuring Machine (CMM-MITUTOYA) using φ 3 mm Ruby crystal probe. The dimensions of the holes are measured at the middle of the laminate thickness.

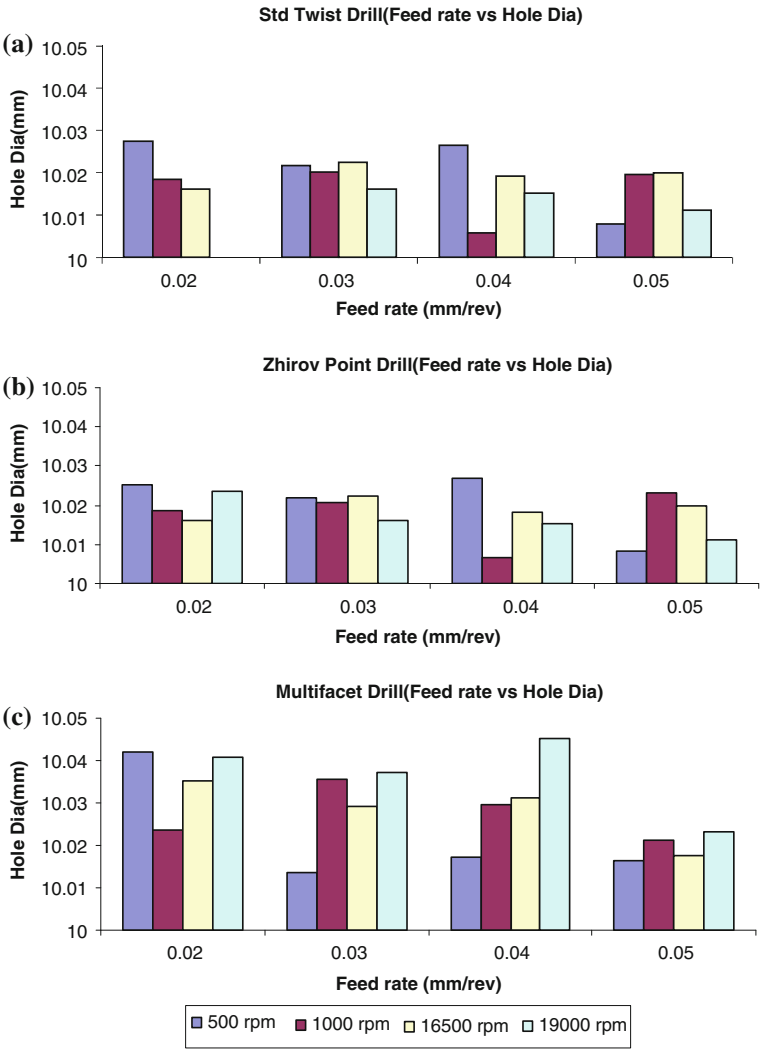

Fig. 4.6 Hole diameter for **a** Standard twist drill **b** Zhirov point drill **c** Multifacet drill

Lower order thrust force, i.e. better cutting action of carbides, higher order material stability, lower order wear, possible lower order cutting temperature on workpiece, all will induce less stress and consequently less relaxing, so mostly over sized holes are seen (Fig. 4.6). Better condition over circularity error unlike the case of HSS. Better circularity values are found when holes are drilled using Zhirov point and multifacet drills (Fig. 4.7). 6–8 μm circularity error in drilling of composite can be treated as negligible.

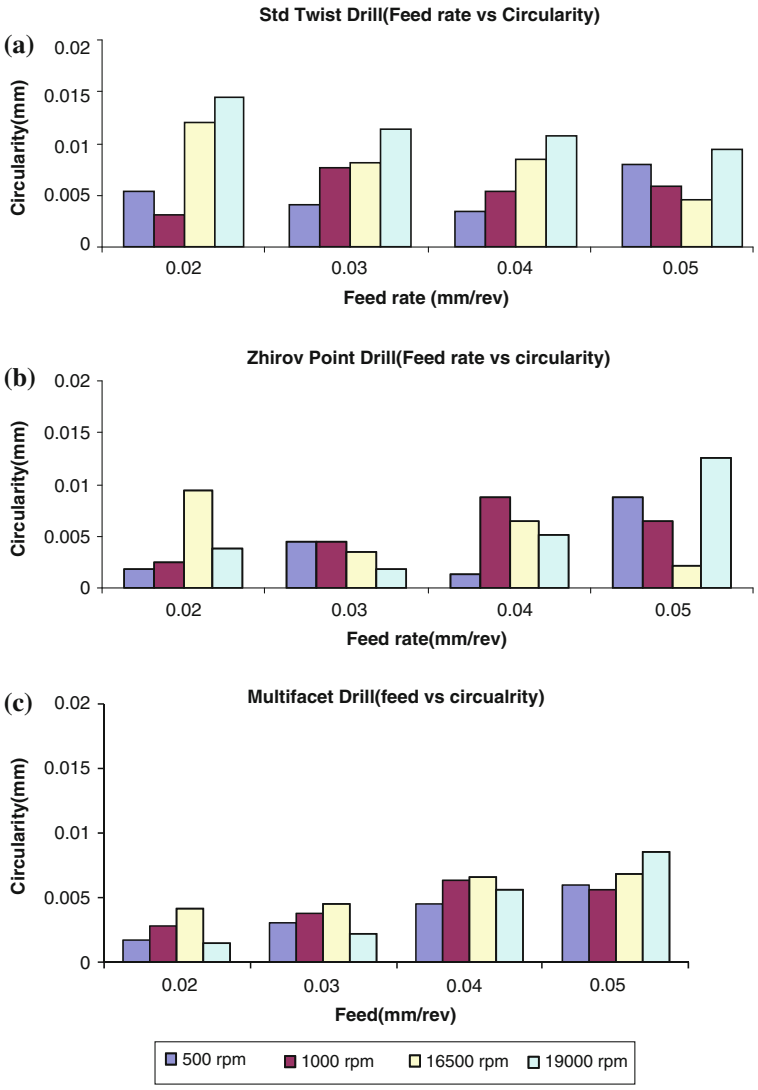

Fig. 4.7 Circularity for **a** Standard twist drill **b** Zhirov point drill **c** Multifacet drill

4.7 Tool Wear Study

In high speed drilling, the major reason for tool wear is the thermal softening of the tool material, and the abrasive nature of the chip. Because of tool wear, thrust force will increase [13, 16, 18, 20]. So, tool life can be predicted by measuring the thrust force with respect to the number of holes. In this tool wear study, carbide drill

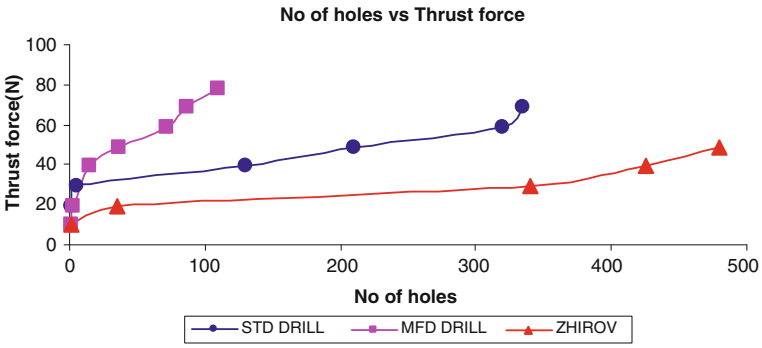

Fig. 4.8 Number of hole versus thrust force for carbide drill geometries

geometries are used at 16,500 rpm (518 m/min) spindle speed and 0.02 mm/rev (330 mm/min) to study the extent of tool geometry at high spindle speeds.

In standard twist drill, the thrust force at the beginning of the cut increased sharply because of initial wear (Figs. 4.8 and 4.9a). Initial wear was up to 10th hole and after that gradual wear took place. Beyond 325 holes the thrust force started increasing steeply. This could be because of rapid wear. Thrust force at the end of 325th hole is 60 N. In Zhirov point drill (Figs. 4.8 and 4.9b), thrust force increased sharply because of initial wear. Initial wear was up to 25 holes and after that gradual wear took place. Beyond 340 holes thrust force started increasing steeply. Thrust force at the end of 340th hole is 30 N. In multifacet drill (Figs. 4.8 and 4.9c) within 10 holes thrust force increased rapidly from 10 N to 40 N after that gradual wear took place. Thrust force at the end of 60th hole is 60 N. After that the force raised steeply because of rapid wear.

Figure 4.10 shows the worn out regions of the drill points. When the tool wear was observed using Tool maker's microscope, uniform wear on the flank region was observed in standard twist drill. After the end of its tool life, a wear land of 0.15 mm was measured on its flank with minute chipping along the lips. In the Zhirov point drill, cutting edge near the groove (Cutting edges ground to replace chisel edge) may worn out rapidly that could have led to rapid increase in thrust force. Flank wear at the extreme end was 0.1 mm. Higher tool wear in multifacet drill at the end of cutting edge was observed, because of its sharp edge at the periphery. In all the drills along the cutting edges minute chipping was observed because of cutting hard glass fibers. Zhirov point could drill with lower thrust force and more number of holes, whereas multifacet drill cuts the hole without any fibre pull out.

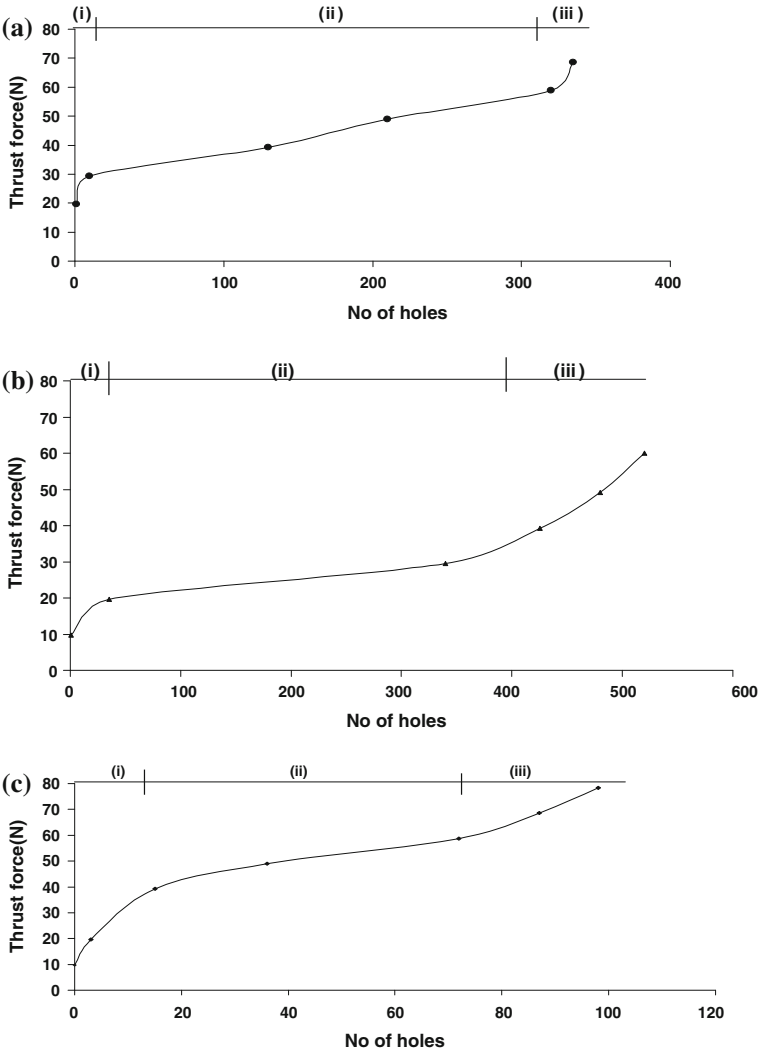

Fig. 4.9 Thrust force versus No of holes (at 16,500 rpm and 0.02 mm/rev). **a** Standard twist drill, **b** Zhirov point drill, **c** Multifacet drill. (*i*)-Intial wear (*ii*)-Normal wear (*iii*)-Rapid wear

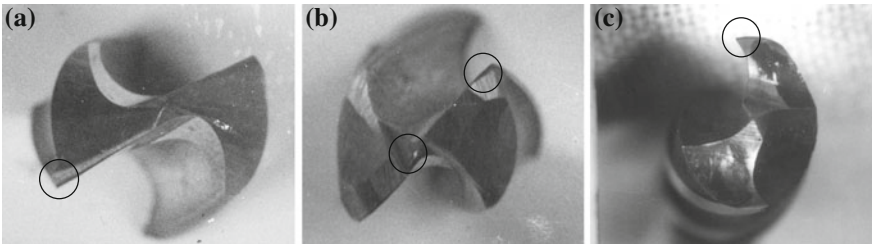

Fig. 4.10 Worn out regions of **a** Twist drill **b** Zhirov point drill **c** Multifacet drill

4.8 Summary

In drilling of composites, high spindle speed and low feed rate improve the machinability aspects within the range examined. The cutting force is less (thrust force and torque both recorded a very low value). The special geometry improves the quality of the hole further, especially Zhirov point drill [8]. From the experimental results (Ref. Fig. 4.8), Standard twist drill and Zhirov point drill were found suitable for producing more number of holes at high spindle speed with low feed rate.

Multifacet drill cuts the hole better than other drill geometries. The special characteristic of the drill is the extreme sickle-form design of the cutting edges. This pre-stresses the fibers in the direction of pull and separates them in the direction of thrust. This results in a clean cut with a smooth surface. The delamination is less compared to other drill geometries.

Zhirov drill produces better surface finish (3–5 μm) at lower feed rate. The outer most lip produces thin chips which improve the finish of the hole. Multifacet drill also generates better surface finish at lower feed rate when compared to standard twist drill. With high speed drilling a considerable reduction in thrust force can be seen, however the drilled hole exhibits higher order surface roughness and only a marginal difference in delamination factor possibly due to higher order drilling temperature.

In standard twist drill, thrust force at the beginning of the cut increases sharply because of initial wear. Initial wear is up to 10 holes and after that gradual wear has takes place. Thrust force at the end of 325th hole is around 60 N. In Zhirov point drill, thrust force increases sharply because of initial wear. Initial wear is up to 25 holes and after that gradual wear has taken place. Thrust force at the end of 340th hole is 30 N. In multifacet drill within 10 holes thrust force increases rapidly from 10 N to 40 N after that gradual wear takes place. Thrust force at the end of 60th hole is 60 N. After that the force rises steeply because of rapid wear.

When the tool wear is observed using Tool maker's microscope, uniform wear on the flank region is observed in standard twist drill. After the end of its tool life a wear land of 0.15 mm is measured on its flank. In the Zhirov point drill, cutting edge near the groove may be worn out rapidly that could have led to rapid increase in thrust force. Flank wear at the extreme end is 0.1 mm. Higher tool wear in multifacet drill at the end of cutting edge is observed, because of its sharp edge at the periphery. In all the drills along the cutting edges minute chipping is observed because of cutting hard glass fibers. From this high speed drilling study, it is concluded that Zhirov point could be used to drill holes with lower thrust force. The life of the Zhirov point is also higher.

References

1. Arshinov V, Alekseev G (1976) Metal cutting theory and cutting tool design. MIR Publishers, Moscow
2. Campos Rubio J, Abrao AM, Faria PE, Esteves Correia A, Davim JP (2008) Effects of high speed in the drilling of GFRP: evaluation of the delamination factor. Int J Mach Tools Manuf 48:715–720
3. Chen WC (1997) Some experimental investigations in the drilling of carbon fibre reinforced composite laminations. Int J Mach Tools Manuf 37(8):1097–1108
4. Davim JP, Reis P (2003) Study of delamination in drilling carbon fiber-reinforced plastics (CFRP) using design experiments. Compos Struct 59:481–487
5. El-Sonbaty I, Khashaba UA, Machaly T (2004) Factors affecting the machinability of GFR/epoxy composites. Compos Struct 63:313–327
6. Enemuoh UE, EI Gizawy SA, Chukwujekwu Okafor A (2001) An approach for development of damage free drilling of carbon fiber reinforced thermosets. Int J Mach Tools Manuf 41:1795–1814
7. Ho-Cheng H, Dharan CKH (1990) Delamination during drilling of composite laminates. J Eng Ind ASME 112:236–239
8. Hocheng H, Tsao CC (2005) The path towards delamination-free drilling of composite materials. J Mater Process Technol 167:251–264
9. Ho-Cheng H, Pwu HY, Yao KC (1993) Machinability of some fiber reinforced thermoset and thermoplastics in drilling. Mater Manuf Proc 8(6):653–682
10. Karnik SR, Gaitonde VN, Rubio JC, Correia AE, Abrao AM, Davim JP (2008) Delamination analysis in high speed drilling of carbon fiber reinforced plastics (CFRP) using artificial neural network model. Mater Des 29:1768–1776
11. Khashaba UA (2004) Delamination in drilling GFR-thermoset composites. Compos Struct 63:313–327
12. Krishnaraj V, Prabukarthi A, Arun R, Elanghovan N, Senthilkumar M, Zitoune R, Davim JP (2012) Optimisation of machining parameters at high speed drilling of Carbon Fibre Reinforced Plastic (CFRP) laminates. Composite Part B 43(4):1791–1799
13. Kim D, Ramulu M (2004) Drilling process optimization for graphite/bismaleimide–titanium alloy stacks. Compos Struct 63:101–114
14. Lin SC, Chen IK (1996) Drilling of carbon fiber-reinforced composite material at high speed. J Compos Mater 194:156–162
15. Mohan NS, Kulkarni SN, Ramachandra A (2007) Delamination analysis in drilling process of glass fiber reinforced plastic (GFRP) composite materials. J Mater Proc Technol 186:265–271
16. Shaw MC (2003) The size effect in metal cutting. Sadhana 28(5):875–896
17. Velayudham A, Krishnamurthy R (2007) Effect of point geometry and their influence on thrust and delamination in drilling of polymeric composites. J Mater Process Technol 185:204–209
18. Velayudham A, Krishnamurthy R, Soundarapandian T (2005) Evaluation of drilling characteristics of high volume fraction fibre glass reinforced polymeric composite. Int J Mach Tools Manuf 45:399–406
19. Wong TL, Wu SM, Groy GM (1982) An analysis of delamination in drilling of composite materials. In: Proceedings of the 14th SAMPE technology conference, Atlanta, (GA), USA, pp 471–483
20. Zitoune R, Krishnaraj V, Collombet F (2010) Study of drilling of composite material and aluminium stack. Compos Struct 92:1246–1255

Chapter 5
Numerical Prediction of the Critical Thrust Force Causing Delamination at the Hole Exit

5.1 Introduction

Delamination at the exit of the hole is considered the most costly damage in the composite structure [1, 4–7, 9–11, 14–21, 22, 23]. This defect leads to a significant loss of the tensile strength and the stiffness of the composite part when it is loaded in compression, shear or fatigue loading [14, 15, 18]. Consequently, this results in a reduction of the loading capacity of the composite part. Several studies have shown that the presence of delamination at the exit side of the hole is mainly due to the axial thrust force developed during the drilling process. This thrust force is mainly related to the interaction between the active part of the cutting tool (cutting edges, chisel edge) and the uncut part of the composite located under the point angle of the drill [5]. However, this thrust force is strongly influenced by the drill diameter, the feed rate of the tool, the nature of material being machined (fibre and resin), the type of web thinning of the tool (point angle, web thickness etc.), and the fibre content [1, 23]. Even drilling at an optimal choice of cutting parameters, the wear of the cutting tool causes an increase in the thrust force which leads to the appearance of delamination at the hole exit.

Two types of models are available in the literature to predict thrust force during drilling. The first one is an empirical model to predict the thrust force as a function of cutting parameters. These empirical models for predicting the thrust forces are similar to those developed in the context of drilling of metallic materials [2, 8, 13]. As a whole, it is based on the identification of the specific cutting pressure of the material to be machined. The second one is an analytical model to predict the critical thrust force responsible for delamination at the exit side of the hole. Beyond this force, there is a high probability of propagation of delamination at the hole exit. These analytical models were inspired by the model developed by Ho-Cheng [5]. Their model development is based on the theory of fracture mechanics, using linear elastic and plate theory. These analytical models are developed from two strong hypotheses. For the first hypothesis, they consider that the critical thrust force is controlled only by the critical energy release rate in mode I (G_{Ic}) of the composite material. For the second assumption, they assume the presence of a

V. Krishnaraj et al., *Drilling of Polymer-Matrix Composites*,
SpringerBriefs in Manufacturing and Surface Engineering,
DOI: 10.1007/978-3-642-38345-8_5, © The Author(s) 2013

circular or elliptical crack near the nominal diameter of the drilled hole. This chapter is composed into two parts. In the first part analytical models available in the literature concerns the prediction of the critical thrust force responsible for delamination at the hole exit during drilling CFRP plates is summarised. In the second part, the elements of a numerical model to predict the critical thrust forces during drilling of composite plate according to the number of plies located under the active part of the drill have been presented. This model is based on analytical models developed by [5, 19, 20] and for isotropic materials [7, 11, 16, 22] for orthotropic materials. In this numerical model, the critical thrust force is controlled by the critical energy release relates in mode I and in mode II of the material to be machined. This represents a step forward compared to the analytical models from the literature which considers only the critical energy release relates in mode I [5, 7, 11, 12, 16, 19, 20, 22]. The originality of the proposed numerical model is the consideration of factors not taken into account by the analytical models. Some of the factors are:

- The influence of the conicity of the drill in the material,
- The presence of a circular crack in the composite located near the chisel edge of the drill,
- The influence of rate of loading induced by the chisel edge and by the principal cutting edges,
- The critical thrust force is controlled by a criterion taking into account the energy release rates in mode I and in mode II of the material concerned.

5.2 Analytical Models from the Literature

5.2.1 Models with the Hypothesis of Isotropic Material

5.2.1.1 Hocheng and Dharan Model (1990)

The first model was developed by Hocheng and Dhahran [5] (Ref. Figure 5.1). During drilling of material, the uncut plies located under the tool (chisel edge) are extruded downwards by the thrust force and undergo elastic deformation. If the resulting stress in the vicinity of the crack tip exceeds a critical value, then the crack propagates. At this point, it is supposed that the force applied corresponds to the critical thrust force.

The assumptions used in this model are:

- The mechanical behaviour of the laminate is considered elastic and isotropic and the delaminated area is supposed symmetrical with respect to the axis of the tool,
- The propagation of delamination at the hole exit is carried out in mode I,

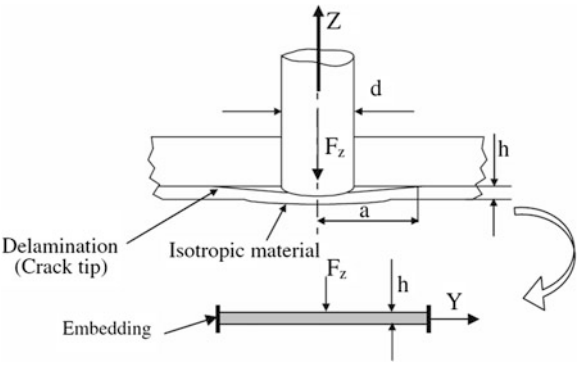

Fig. 5.1 Modeling of the delamination at the exit of the hole according to Ho-Cheng

- The fracture mechanics in the frame of linear elastic is used,
- The crack is considered circular with a radius "a",
- The thrust force of the drill is oriented from the top to the bottom of the plate and its result is applied at the center of the hole,
- The uncut laminate (located under the drill) is subjected to a bending with respect to the hypothesis of small displacements,
- The global bending of the plate is neglected.

The energy balance applied to the structure in the linear elastic is

$$G\pi(2a)\delta a = F_z \partial w - \partial U \tag{5.1}$$

$$G\pi(2a) = F_z \frac{\partial w}{\partial a} - \frac{\partial U}{\partial a} \tag{5.2}$$

with

- U the strain energy of the laminate (J),
- W the local deflection of the part located under the delaminated zone and considered like a plate (mm),
- G the surface energy (J/mm^2),
- Fz the resulting critical thrust force.

Using the plate theory, the authors [5] established a relation to predict the critical thrust force, by considering energy release rate in mode I (G_{Ic}), the elastic mechanical properties of the material (E, υ) and the thickness of the damaged plies (h):

$$F_z = \pi \left[\frac{8 G_{IC} E h^3}{3(1 - \upsilon^2)} \right]^{1/2} \tag{5.3}$$

5.2.1.2 Upadhyay and Lyons Model

Upadhyay et al. [20] introduced two new assumptions compared to the work of Ho-Cheng and Dharan. The first assumption is on the load applied on the area of the uncut plate located under the tool. They made an assumption that the loading is uniformly distributed and not as a concentrated load at the center of the tool. The surface distribution of the loading is considered as circular with radius "a". This radius represents the dimension of the web thickness. In the second hypothesis, the authors consider that under the applied load induced by the drill the bending of the composite plate located under the drill is higher than the thickness of the uncut plies. Therefore, the assumption of large displacements is considered in the model. This assumption is realistic, especially if the area of the composite plate located under the drill is composed of few plies.

By taking these two assumptions into account, the expression of the critical thrust force is given by the Eq. 5.4:

$$F_z = \pi \sqrt{\frac{8G_{IC}Eh^3(1 - 1.464(w_0/h)^2(1 - 0.0488(w_0/h)^2)^2}{3(1 - \nu^2)((1 - 1.708(w_0/h)^2 - 0.107(w_0/h)^4))}} \tag{5.4}$$

with:

- w_0, the maximum deflection at the center of the composite plate (mm),
- E, h, ν and G_{Ic}, are the parameters mentioned in the model similar to Ho Cheng [5].

A comparison of the critical thrust forces (obtained by this model and those given by the model defined by Eq. 5.3) shows only a difference around 12–25 %. The critical thrust forces obtained by the model developed by Hocheng [5] are lower than those measured by experiment and those given by the model Upadhyay et al. [20].

5.2.2 Models with the Hypothesis of Orthotropic Material

The first analytical model to predict the critical thrust force by taking into account of the orthotropy of the composite material was proposed by Jain et al. [6]. Subsequently, many models have been proposed by fellow researchers [11, 16, 22].

Model of Jain-Yang model [7]

$$\mathrm{F_z} = 3\pi \left(\frac{\mathrm{b}}{\mathrm{a}}\right)^{1/4} \sqrt{2\mathrm{G_{IC}D^*}} \tag{5.5}$$

with:

$$D^* = D_{11} + \frac{2(D_{12} + 2D_{66})}{3}\left(\frac{a}{b}\right)^2 + D_{22}\left(\frac{a}{b}\right)^4 \tag{5.6}$$

- D_{ij}, Coefficients of the stiffness matrix of the plate in bending,
- G_{Ic}, the critical energy release rate in mode I,
- a et b, the major and minor radius of the ellipse.

Model of Lachaud et al. [11]

$$F_z = 8.\pi.\left(\frac{G_{IC}.D}{\frac{1}{3} - \frac{D'}{8.D}}\right)^{1/2} \tag{5.7}$$

with:

- G_{Ic} the critical energy release rate in mode I,

$$D = \frac{1}{8}(3D_{11} + 2D_{12} + 4D_{66} + 3D_{22}), \tag{5.8}$$

$$D' = \frac{D_{11} + D_{22}}{2} + \frac{D_{12} + D_{66}}{3}, \tag{5.9}$$

D_{ij}, Coefficients of the stiffness matrix of the plate in bending.

Model of Zhang et al. [22]

$$F_z = \left(\frac{\pi.G_{IC}}{\zeta(C_3 - K)}\right)^{1/2} \tag{5.10}$$

with:

- G_{Ic}, the critical energy release rate in mode I,
- K and C_3, constants dependent on the mechanical characteristics of the composite plate located under the drill.

However, the difference between the numerical model to predict the critical thrust force proposed in this chapter and all analytical models presented above is summarized in the following points:

- the point tool geometry (chisel edge, point angle and cutting length),
- the presence of a crack in the vicinity of the chisel edge of the tool and not near the nominal diameter of the tool,
- the influence of the rate of loading induced by the principal cutting edges and the chisel edge separately,

- the critical thrust force is controlled by a criterion taking into account the critical energy release rate in mode I and in mode II of the composite material,
- the energy of deformation by shear loading.

5.3 Experimental Procedure

Within this study, two types of UD prepreg in carbon/epoxy are used. These raw materials of laminated structures are provided by Hexcel composites and are referenced respectively under, Hexply T2H 268 150 EH25 NS 35 % (noted T2H-EH25) with a 59 % fibre content and a 0.25 mm thick ply and Hexply T700GC 268 M21 34 % (noted T700-M21) with a 58 % fibre content and a 0.26 mm thick ply. Those two products are fairly equivalent from the mechanical properties viewpoint. However, material T700-M21 differs through the presence of 20 μm diameter thermoplastic nodules which represent about 13 % matrix mass rate in the prepreg. These nodules are supposed to improve damage tolerance by initiating a crack network at the interply then controlling the crack propagation within the laminate. The energy release rates of this material in mode I and II increase in comparison with those of T2H-EH25 laminate. The specimens for test present a quasi-isotropic stacking sequence featuring 16 plies $[90^\circ/-45^\circ/0^\circ/+45^\circ]_{2s}$. The drilling of a blind hole is carried out using a CNC machine. In order to avoid delamination while blind-hole machining, the plate to be drilled is supported on its lower face by means of a wood plate. Moreover, the machining parameters are chosen so as to avoid delamination between plies. The machining parameters are based on a small feed rate (the tool feed rate as well as the rotating speed are respectively, 0.001 mm/rev and 1,500 rev/min). The tool is a tungsten carbon micro grain with grade K20 and the principal characteristics of the tool are: (a) Point angle of 118°, (b) Diameter of 4.8 mm and (c) helix angle of 15°. The visual inspection of these blind holes has revealed no delamination or resin crack. We have mentioned in the previous chapters that, the feed rate is the cutting parameter which has a greater influence on the thrust force during drilling with a twist drill, for this reason in this study the influence of the cutting speed on the thrust force, is not taken into account.

The validation of this numerical model is conducted with quasi-static punching tests. The latter are carried out on a standard tensile testing machine INSTRON. The axial load is applied using a twist drill (with a 4.8 mm diameter) which moves in translation in the blind hole. The values of the critical energy release rates in mode I (GIc) and mode II (GIIc) for 0°/45° interface of two studied materials result from the fracture mechanics tests carried out in our laboratory. These tests are performed in accordance with the standard (NF ISO 15024) (Fig. 5.2).

The method of determination of the energy release is based on double cantilever beam (DCB) test. The values obtained GIc and GIIc are in good agreement with the values provided by Hexcel composites. The principal information composed the proposed model are given below.

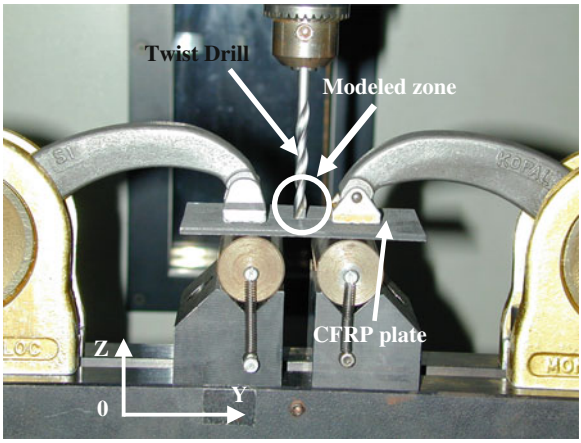

Fig. 5.2 Experimental device for the punching tests

5.4 Numerical Modelling

The numerical model suggested has the advantage of taking into account various aspects. Among them it is noticed that: (a) the consideration of the strain due to the shear forces thanks to the use of an adapted finite element available in the software library of SAMCEF FE code (finite element of type 11).

(b) the second aspect corresponds to the influence of the drill point angle in the material and enables us to represent on the one hand, the presence of a crack at the level of the chisel edge and on the other hand, the influence of the loading distribution on the chisel edge and the principal edges of cut (lips of drill). The resulting thrust force Fz can be decomposed into two components Fz1 and Fz2 (Ref. Figure 5.3), with F_{z1} as the thrust force induced by the contact of the cutting lips with the laminate and F_{z2} as the force corresponding to the contact of the chisel edge with the laminate ($Fz = 2F_{z1} + F_{z2}$). The part of the machined structure is modelled like a volume of circular geometry of external radius Re and

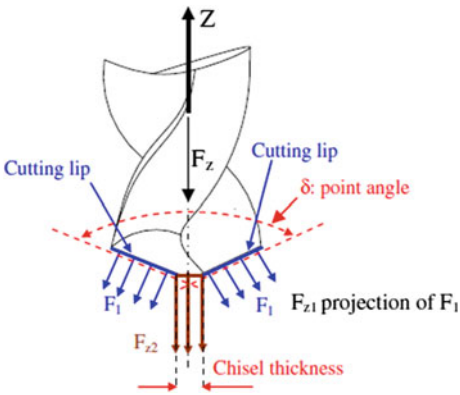

Fig. 5.3 Thrust force induced by the principal cutting edge and the chisel edge

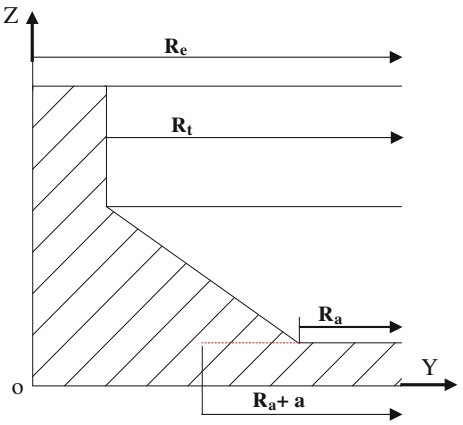

Fig. 5.4 Schematic view of the modelled zone

internal radius R_t (considering that Rt is the nominal drilled hole radius). Figure 5.4 is a schematization of the system section seen in the (YZ) plane. Ra and e respectively represent the chisel edge radius and the thickness of the non-machined plies which are located under the drill chisel edge.

5.4.1 Description of the Numerical Model and Boundary Conditions

Figure 5.5 represents the finite element model of the quasi-isotropic laminate drilling in carbon epoxy. In this modeling, the finite element used is of volumic isoparametric type with degree 2 which is available in the software library of SAMCEF FE code. The interface nodes are located at the middle of the top nodes. The calculation is carried out within a linear static hypothesis with the composite volume assumption. The conditions with imposed boundary correspond to an embedding on the circumference of the hole (of radius Re). A part of the loading is according to the (oZ) direction and is applied on the nodes of the surface generated by the chisel edge at the time of its rotation. The other part of the loading is applied to the conical periphery of the drill (Ref. Figure 5.4). For a crack located on the level of the chisel edge diameter, the principle of determination of the critical thrust force Fz—according to the number of plies under the drill—is based on the calculation of the energy release rate in mode I and mode II. The leading edge of the crack is circular and of radius (Ra + a). The critical value of the thrust force Fz can be obtained if the following energy criterion is checked:

$$(G_I/G_{IC})^{\alpha} + (G_{II}/G_{IIC})^{\alpha} = 1 \tag{5.11}$$

The choice of distribution of the loading quantity (F_{z1} coming through the chisel edge, F_{z2} coming through the cutting lips) is based on literature [8]. The

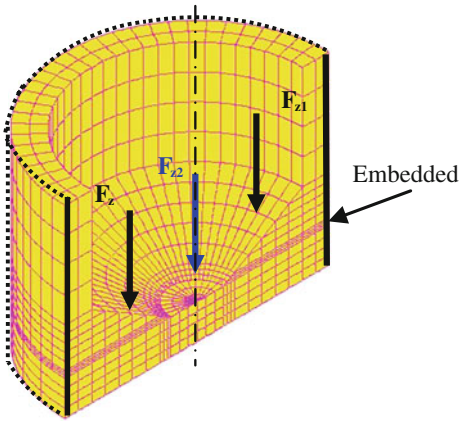

Fig. 5.5 Mesh and boundary condition of the modeled zone

acquisition of thrust forces was carried out with the help of a load sensor of KISTLER type. This identification process was divided into two parts. In the first one, the authors measure the thrust force F_z. In the second one, they make a pilot-hole whose diameter is equal to the dimension of the chisel edge ($2R_a$), then on the same previously-drilled laminate, they machine a hole of diameter ($2R_t$) followed by a measurement of the overall contribution of the two main cutting lips. Figure 5.6 represents the result of this study: for small feed into the material (around 7 mm/min), the part of the thrust force F_{z2} generated by the chisel edge accounts to 40–50 % of the total thrust force F_z.

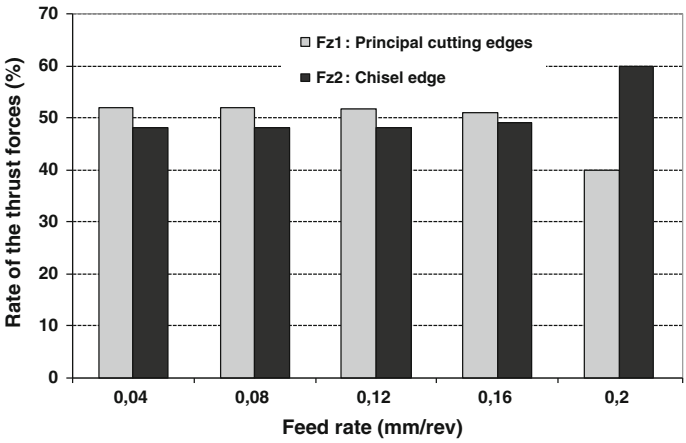

Fig. 5.6 Evolution of the thurst force induced by the principal cutting edge and that induced by the chisel edge during drilling of metallic material using twist drill

This quantitative identification is obtained using dynamic tests (at 7 mm/min tool feed) and this identification is supposed not to change a lot if the tests are carried out in quasi-static context (at 1 mm/min tool feed). As the numerical model proposed is developed in a quasi-static context, validating this model in the same situation seems more relevant.

5.5 Resultants and Discussion

5.5.1 Study of the Influence of Mesh

Firstly, how the choice of the outer radius value (R_e) influences the energy release rate in mode I is studied. To do so, the total number of elements is fixed at 3,480 elements, the dimension of the pre-crack is equal to 0.5 mm and the loading effort on the chisel edge F_{z2} represents 40 % of the total thrust force F_z. Figure 5.7 illustrates G_I variation according to R_e in the case of three plies under the drill and for the two materials under study. The energy release rate in mode I (G_I) is seen as being globally constant for an embedding radius varying from 2.6 to 3.1 mm.

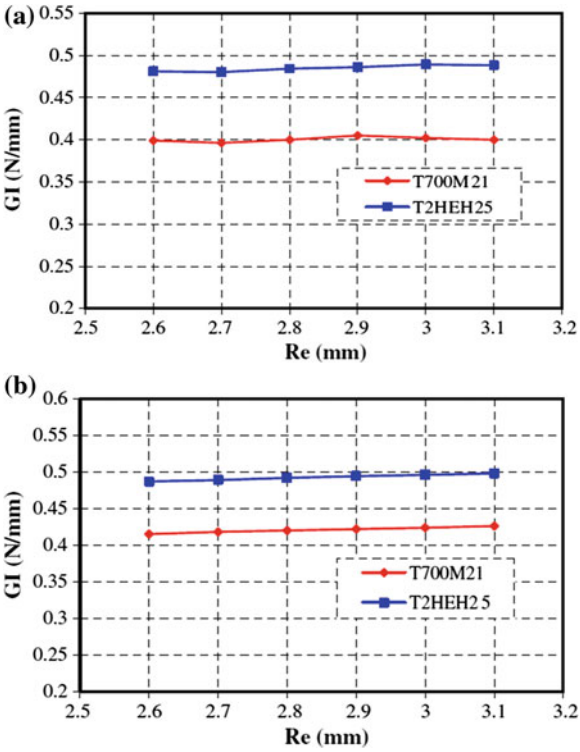

Fig. 5.7 Study of the influence of embedding radius Re on the numerical results with two plies under the drill; boundary conditions: Fz = 500 N, a = 0.5 mm when Fz2 = 40 % Fz. **a** Three plies under the tool. **b** Two plies under the tool

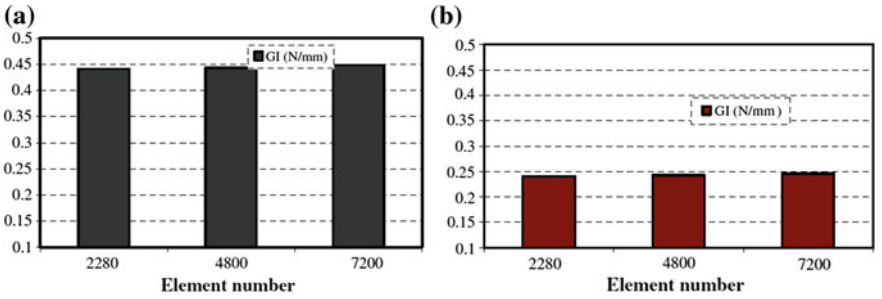

Fig. 5.8 Study of the influence of the total number of elements on the numerical results; boundary conditions. **a** Material T700-M21, Fz = 540 N, a = 0.5 mm with three plies under the drill. **b** Material T2H-EH25, Fz = 230 N, a = 0.5 mm with three plies under the drill

Moreover, in the case of two plies under the drill, it is noticed that the variation of the embedding radius does not lead to a significant variation of the energy release rate in mode I for the two materials (Ref. Figure 5.7a). The value chosen for this study is 2.9 mm. Secondly, the influence of the number of elements on the results is examined. Thus, a 2.9 mm radius Re and a 0.5 mm pre-crack are chosen. Figure 5.8 shows that the use of a number of elements from 2,280 to 7,200 elements has led the energy release rate in mode I to increase by 2 %. This involves T2H-EH25 material. In brief, the total number of elements used in the model has a very little influence on the global thrust force value F_z whatever the material studied (Ref. Fig. 5.8a and b). The final part is devoted to the influence of the pre-crack length "a" on the thrust force "F_z". The total number of elements as well as the outside radius of the model is thus respectively fixed at 4,800 and 2.9 mm. Figure 5.9 features how the pre-crack length influences the global thrust force F_z with three plies under the drill and for the two materials studied: when the pre-crack length varies from 0.25 to 0.8 mm, the thrust force is quasi-constant. Similar observations can be made with two plies under the drill. The numerical results exposed in this study are obtained with a mesh of 4,800 elements, a 2.9 mm embedding radius and a 0.3 mm pre-crack length. It has been checked that the

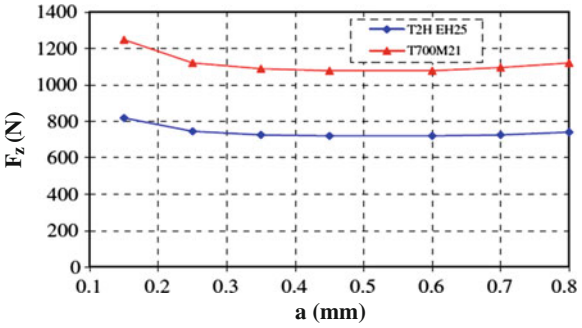

Fig. 5.9 Influence of the crack length (a) on the thrust force (Fz); boundary conditions: three plies under the drill, materials T700-M21 and T2H-EH25, Fz2 = 40 % Fz

fixed parameters (Re, a and the number of elements) are not dependent on the type of the stacking sequence under study.

5.5.2 Macro Scale Analysis

Figure 5.10a represents a comparison experiment/numerical calculation of the thrust forces Fz (for a carbon/epoxy plate of T2H-EH25 material, a 4 mm thickness and a quasi-isotropic stacking sequence of type $[90/+45/0/45]_{2s}$). If the loading taken by the chisel edge drill represents 50 % of the total loading, it is noted that the relative difference between the results provided by the numerical model and those given by the experiment is important (around 50 %). This is checked as soon as the number of the plies under the drill is higher than two. If the loading taken by the chisel edge represents 40 % of the total loading, the results of the numerical model corroborate the experimental measurements. In this case of loading, whatever the number of plies under the drill is, the relative variation remains under 11 %.

However, for material T700-M21 (and when the loading share taken by the chisel edge is 40 %), Fig. 5.10b shows a good correlation calculation/test if the

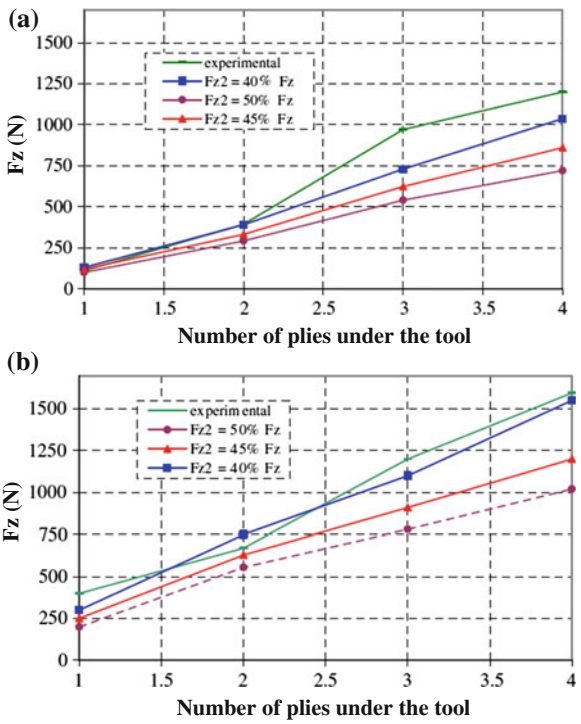

Fig. 5.10 Comparison between the experimental and the numerical critical thrust forces responsible of delamination (**a**) Material T2H-EH25 and (**b**) Material T700-M21

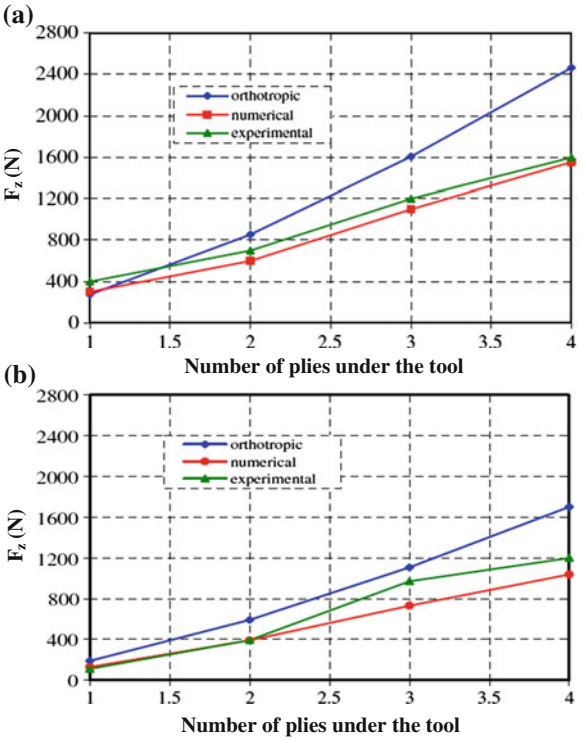

Fig. 5.11 Numerical model/experiment/model (orthotropic) correlation; with the conditions: $F_{z2} = 40$ % of the total Fz. (**a**) T700-M21 material and (**b**) T2H-EH25 Material

number of plies is over one. Moreover, the critical thrust force calculated for material T700-M21 is higher than those calculated for material T2H-EH25 (and that for all numbers of plies under the drill). This can be explained by the presence of thermoplastic nodules in the T700-M21 material which increases the values of energy release rates in mode I and II and therefore the critical outside load which is responsible for the crack spreading.

In Fig. 5.10, the correlation numerical model/experiment/analytical model is presented. The assumption of orthotropic material [11] is considered for the two types of materials under study. For this numerical calculation, the retained distribution of the loading corresponds to a resumption of 40 % by the drill chisel edge and of 60 % by the drill lips. According to Fig. 5.11a, a good correlation is observed between the numerical model and the experiment. The analytical model overestimates the critical efforts responsible for the delamination between the plies whatever the material under study may be. As an example, in the case of material T700-M21 and four plies under the drill, the maximum relative variation registered between the experiment and the analytical model is 42 %. However, in the same situation, the relative difference between the experiment and the numerical model is only 3 %. Similar conclusions are obtained in the case of material T2H-EH25 (Ref. Fig. 5.11b).

5.5.3 Meso Scale Analysis

In Figs. 5.12 and 5.13, the application of the Tsai–Wu criterion is presented for the two studied materials respectively, T2H-EH25 and T700-M21. That corresponds to a situation of calculation in which there are three plies under the chisel edge of the drill and the energy criterion described in the Eq. (5.11) is checked. The Tsai–Wu criterion announces a damage risk in the zone close to the drill chisel edge as well as at the level of the tip crack. The frontiers of the zones drawn with a discontinuous line on these cartographies represent the print of the damage propagation in the vicinity of the crack between plies under the applied load. This cracking propagation announces some delaminated zones which are qualitatively of the same shape as those observed through radiography [3, 23]. In the work of Zitoune et al. [23] drilling of the laminate (without back up) is carried out with a

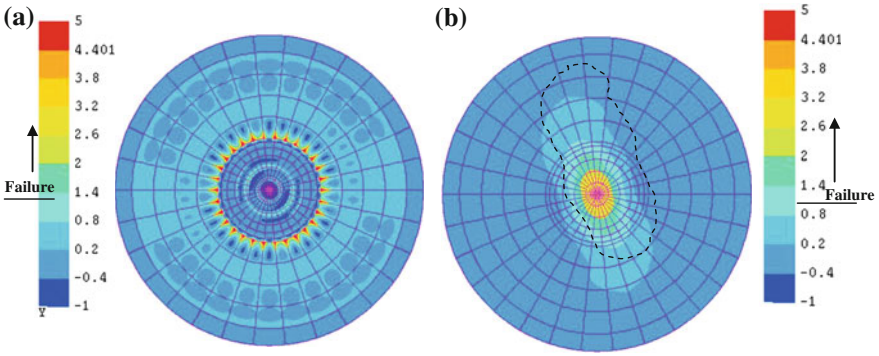

Fig. 5.12 Tsai–Wu criterion for the T2H-EH25 material; (**a**) *top* view, (**b**) *underside* view, machining conditions: three plies under the drill and $F_z = 750$ N

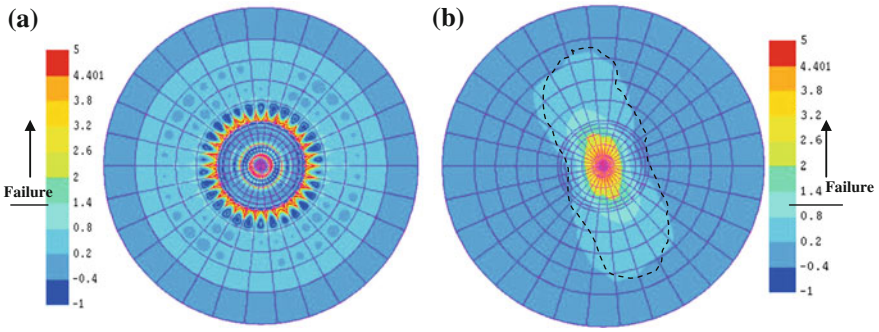

Fig. 5.13 Tsai–Wu criterion for the T700-M21 material; (**a**) *top* view, (**b**) *underside* view, machining conditions: three plies under the drill and $F_z = 1150$ N

high feed rate (1 mm/rev) and the resulting thrust force (1,000 N) is of the same scale as the value calculated in this study. It can be noticed that a feed rate lesser to 1 mm/rev (for example 0.02 mm/rev) implies that the delamination at the exit of the hole widespread within the ply and not in inter-ply zones.

SEM images of the Fig. 5.14 show the presence of delamination at the 90/+ 45 interface in the vicinity of the drill chisel edge. This phenomenon is observed for the various numbers of plies under the drill. That consolidates the assumption of the crack presence at the level of the drill chisel edge. The presence of caulking

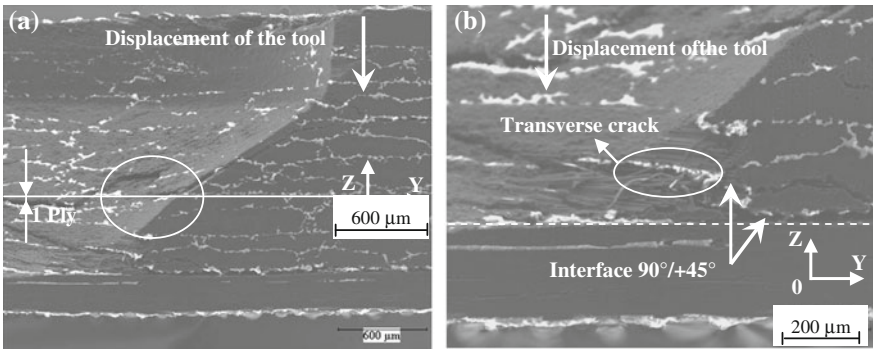

Fig. 5.14 SEM micrographs of the state of the hole after the punching test of the laminate T700-M21 in half cross-section; test conditions: one ply under the drill, (**a**) ×150 magnification and (**b**) ×300 magnification

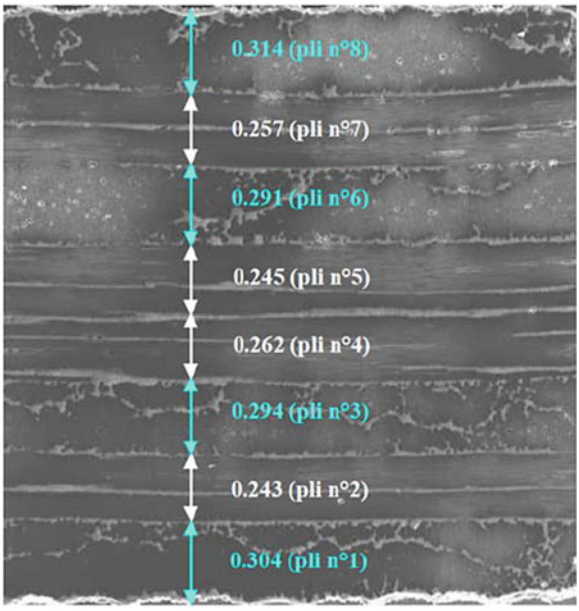

Fig. 5.15 SEM picture of the thickness of composite T700-M21 of stacking sequence $[0/90]_{2s}$ and manufactured in autoclave

can also be observed around the zone of tool/laminated contact due to the tool advance. These caulking zones are certainly the place of an intense pressure and friction between the tool face and the laminate. This friction phenomenon should be taken into account in a modelling.

From these pictures it is observed that, it is difficult to control with precision the position of the chisel edge or the extremity of the drill in the materials. This difficulty is linked the variability of the plies thickness of the composite materials after the setup of curing. In the Fig. 5.15, we represent an SEM analysis of specimens with $[0°/90°]_{8s}$ after the setup of polishing. It is noticed that, the measured thickness of the plies varies from 0.245 to 0.314 mm. These values represent 20 % of gap compared to the theoretical value of the ply thickness mentioned by Hexcel composite.

5.6 Summary

For the analysis of the drilling conditions of long-fibre composite structures, the numerical model that is proposed is based on the fracture mechanics. This modeling enables to restore the critical thrust forces responsible for the formation of the defect at the exit of the hole and for a different number of plies under the drill chisel edge. The validation of this numerical model is carried out thanks to quasi-static punching tests on two types of carbon/epoxy materials. The right correlation has been noticed between the numerically calculated efforts and those which were experimentally obtained. The maximum variation registered is about 15 %. This gap can be related to mechanical proprieties used in the model that are affected by the variability of the ply thickness after the curing phase. A confrontation between the critical thrust forces, numerically obtained, and those obtained thanks to the analytical model is carried out. The proposed model, validated on two types of carbon epoxy laminated, can also be used for other composite materials from UD prepreg. However, its validity has not been fully proved on composite material made of woven fabric. Following the numerical study of the critical thrust force, it would be interesting to exploit them to the most in order to identify the critical feed rates so as to avoid delamination during the drilling phase. This phase can be achieved thanks to the empirical patterns in the literature which give the thrust force according to the tool feed rate. It has been shown that the beginning of the damage due to the tool displacement is located around the chisel edge and not around the nominal diameter. Thus we proposed the development of an analytical model which predicts the critical thrust force by taking into account a crack presence in the vicinity of the chisel edge. The integration of shear effects in that analytical model is also planned.

References

1. Chen WC (1997) Some experimental investigation in the drilling of the carbon fiber-reinforced plastics (CFRP) composite laminates. Int J Mach Tools Manuf 37:1097–1108
2. Dallas DB (1976) Tool and manufacturing engineers handbook. Drilling, reaming and related operation, Chapter 3, pp 1–99
3. Gaitonde VN, Karnik SR, Campos Rubio J, Esteves Correia A, Abrao AM, Davim JP (2008) Analysis of parametric influence on delamination in high-speed drilling of carbon fiber reinforced plastic composites. J Mater Process Technol 203:431–438
4. Hamdoun Z, Guillaumat L, Lataillade J-L (2004) Influence of the drilling on the fatigue behaviour on the carbon/epoxy laminates. ECCM 11 1:301–302
5. Hocheng H, Dharan CKH (1990) Delamination during drilling in composite laminates. J Eng Ind 112:236–239 Transactions of ASME
6. Jain S, Yang DCH (1993) Effects of feedrate and chisel edge on delamination in composites drilling. J Eng Ind 115:398–405 Transactions of ASME
7. Jain S, Yang DCH (1994) Delamination free drilling of composites laminates. J Eng Ind 116:475–481 (Transaction ASME)
8. Kang TH, Carless JW (1971) Cutting force analysis in drilling, ASME Technical paper MR71-170
9. Kashaba UA (2004) Delamination in drilling GRP- thermoset composites. Compos Struct 63:313–327
10. Krishnamoorthy A, Rajendra BS, Palanikumar K (2011) Delamination prediction in drilling of CFRP composites using artificial neural network. J Eng Sci Technol 6(2):191–203
11. Lachaud F, Piquet R, Collombet F, Surcin L (2001) Drilling of composite structures. Compos Struct 52:511–516
12. Lévêque D (1998) Analyse de la Tenue au Délaminage des Composites Stratifiés: Identification d'un Modèle d'Interface Interlaminaire". Thèse de Doctorat de l'Ecole Normale Supérieure de Cachan
13. Montgomery DC (2001) Design and analysis of experiments. Wiley, New York
14. Murphy C, Byrne G, Gilchrist MD (2002) The performance of coating tungsten carbide drills when machining carbon fiber reinforced epoxy composite materials. Inst Mech Eng 216 Part B:143–152
15. Person E, Eriksson I, Zackrisson L (1997) Effects of hole machining defects on strength and fatigue life of composite laminates. Composites Part A Appl Sci Manuf 28(2):141–151
16. Sadat AB (1996) Prediction of delamination load in drilling of graphite/epoxy composites. Eng Syst Design Anal 3:21–27
17. Shaw MC (2005) Metal cutting principles, 2nd edn. Oxford university press, New York
18. Singh I, Bhatnagar N, Viswanath P (2008) Drilling of unidirectional glass fiber reinforced plastics: Experimental and finite element study. Mater Des 29:546–553
19. Tsao CC, Hocheng H (2008) Evaluation of thrust force and surface roughness in drilling composite material using Taguchi analysis and neural network. J Mater Process Technol 203:342–348
20. Upadhyay PC, Lyons JS (1999) On the evaluation of critical thrust for delamination-free drilling of composite laminates. J Reinf Plast Compos 18(14):1287–1303
21. Campos Rubio J, Abrao AM, Faria PE, Esteves Correia A, Davim JP (208) Effects of high speed in the drilling of the delamination factor. Int J Mac Tools Manuf 48:715–720
22. Zhang LB, Wang LJ, Liu XY (2001) Mechanical model for predicting critical thrust forces in drilling composite laminates. Proc I MECH E Part B J Eng Manuf 215:135–146
23. Zitoune R, Krishnaraj V, Collombet F (2010) Study of drilling of composite material and aluminium stack. Compos Struct 92(5):1246–1255

Chapter 6
Effects of Drilling Parameters on Mechanical Strength

6.1 Introduction

The damage generated during the drilling of Fibre Reinforced Plastics (FRP) is detrimental to the mechanical behavior of the composite structure [7]. Degree of damage depends on the feed, spindle speed, tool material and nature of cutting edge etc. [2–4]. This work is focused on analyzing the influence of drilling parameters (spindle speed and feed) on the strength of the glass fibre reinforced woven fabric laminates and further to study the residual stress distribution around the hole after drilling. Holes were drilled at the center of the specimens in a CNC machining center using 6 mm diameter micro grain carbide drill for various spindle speeds (1,000–4,000 rpm) and feed rates (0.02, 0.06, 0.10, and 0.20 mm/rev).

The basic lamina properties such as Young's modulus, Poisson's ratio, and shear modulus are important parameters in predicting the modulus and Poisson's parameters of the laminate. The material properties (Fibre and Matrix) considered for estimating the laminate properties are given in Table 6.1.

The following assumptions are considered in evaluating the mechanical properties.

A woven fabric lamina is considered as two unidirectional plies crossing at 90^{o} angles with each other (two cross plies of 0^{o} and 90^{o} orientation). Woven fabric laminate is considered as an orthotropic laminate. The extensional stiffness matrix for the laminate is given by

$$A_{ij} = \sum_{k=1}^{N} \left(\overline{Q}_{ij}\right)_k (Z_k - Z_{k-1}) \tag{6.1}$$

where,

A_{ij} are the sum of the product of the individual lamina $\overline{Q}_{ij}$ (Transformed reduced stiffness matrix) and the laminae thickness ($Z_k - Z_{k-1}$).

V. Krishnaraj et al., *Drilling of Polymer-Matrix Composites*,
SpringerBriefs in Manufacturing and Surface Engineering,
DOI: 10.1007/978-3-642-38345-8_6, © The Author(s) 2013

Table 6.1 Elastic properties of fibre/matrix

	Young's modulus (GPa)	Poisson's ratio
Glass fibre	85	0.2
Epoxy resin	3.4	0.3

$$[A] = \begin{bmatrix} A_{11} & A_{12} & A_{16} \\ A_{12} & A_{22} & A_{26} \\ A_{16} & A_{26} & A_{66} \end{bmatrix} = \begin{bmatrix} 93.1 & 6.16 & 0 \\ 6.16 & 93.1 & 0 \\ 0 & 0 & 9.232 \end{bmatrix} \times 10^6 (N/m)$$

The estimated laminate properties are given in Table 6.2.

The test specimens with the dimensions recommended as per ASTM standard were cut from the laminate using a diamond wheel.

6.2 Orthotropic Composite Plate with a Circular Hole

Woven fabric composites containing holes or cut-outs are often found in structural applications. Holes in composites will induce stress or strain concentrations and hence will reduce the mechanical properties. The predication of reduction in the mechanical properties caused by holes is important for composite designers. An orthotropic plate containing a circular hole of radius R is subjected to a uniformly distributed tensile stress $\bar{\sigma}$. Under the action of the stress the (through-the-thickness) average normal stress along the x-axis is $\bar{\sigma}_y$ (Fig. 6.2).

According to the point stress criterion, failure occurs in the laminate containing hole "when the stress at some distance d_o away from the hole along the x-axis is equal to or greater than the un-notched laminate strength $\bar{\sigma}_o^f$" (Fig. 6.1).

$$\bar{\sigma}_y(R + d_o, 0) \geq \bar{\sigma}_o^f \tag{6.2}$$

where,

R Radius of the hole (mm)

d_o Characteristic length (mm).

Table 6.2 Elastic properties of laminate

	Longitudinal young's modulus E_{11} (GPa)	Transverse young's modulus E_{22} (GPa)	Poisson's ratio ν_{12}	Shear modulus G_{12} (GPa)
Glass/epoxy laminate	23.173	23.173	0.0662	2.308

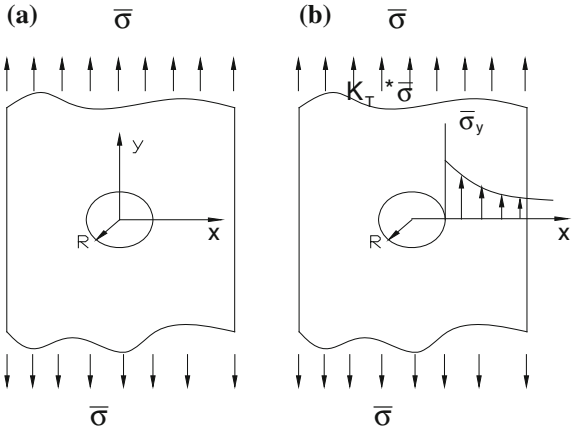

Fig. 6.1 Orthotropic composite plate with a circular hole. **a** Orthotropic plate with a circular hole. **b** Stress distribution along X-axis near the hole

6.3 Failure Strength of Notched Laminate in Tension

The relationship between the strength of the notched specimen σ_a to the strength of the un-notched specimen $\bar{\sigma}_o^f$ is given by

$$\sigma_a = \bar{\sigma}_o^f \left[\frac{2}{2 + r^2 + 3r^4 - (K_T^\infty - 3)(5r^6 - 7r^8)} \right] \tag{6.3}$$

Based on the work of Kollar [5] where, $r = \frac{R}{R+d_o} = \frac{3}{3+4.895} = 0.38$, R = Radius of hole (mm)

$d_o = 4.895$ mm (Found by experiments)

K_T^∞ is the stress concentration factor for an infinite plate with a hole of radius R.

$$K_T^\infty = 1 + \sqrt{\frac{2}{A_{22}} \left(\sqrt{A_{11}A_{22}} - A_{12} + \frac{A_{11}A_{22} - A_{12}^2}{2A_{66}} \right)} \tag{6.4}$$

$$K_T^\infty = 4.45$$

where, A_{ij} = Elements of extensional stiffness matrix component of an orthotropic material [3].

Tensile strength of laminate without hole $\bar{\sigma}_o^f = 205$ MPa, is found experimentally. The tensile strength of the notched laminate using Eq. 6.3 is $\sigma_a^f = \bar{\sigma}_o^f \times 0.9134 = 205 \times 0.9134 = 187.25$ MPa. In order to perform tensile test of notched laminate the specimens were mounted on the frame and proper alignment was made. Thirty two specimens were prepared and holes were drilled at the center of the specimen with different spindle speeds and feed rates. Wedge action grips were

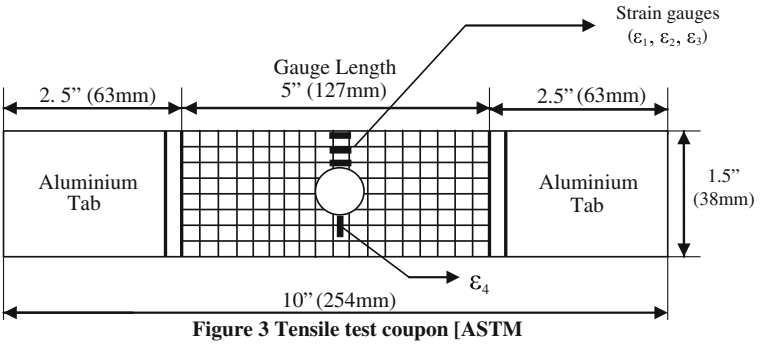

Figure 3 Tensile test coupon [ASTM

Fig. 6.2 Experimental specimen for tensile test

used to grip the specimen at its ends. Figure 6.2 shows the schematic view of the tensile specimen prepared for testing.

The crosshead speed rate of 1 mm/min was used for the movement of the head. The tensile load was applied and the readings of load, deflection were noted at discrete intervals. For notched specimens, the exact solution for the stress distribution in an infinite orthotropic material has been approximated by Lekhnitski [1].

Theoretical stress distribution is given by [5]

$$\overline{\sigma}_y(x,0) = \frac{\sigma_a}{2}\left\{2 + \left(\frac{R}{x}\right)^2 + 3\left(\frac{R}{x}\right)^4 - (K_T^{\infty} - 3)\left[5\left(\frac{R}{x}\right)^6 - 7\left(\frac{R}{x}\right)^8\right]\right\} \tag{6.5}$$

where, R = 3 mm; $K_T^{\infty} = 4.45$; $\sigma_a = 187.25$ MPa. Theoretical stress distribution is calculated at regular intervals from the centre of the hole (5, 11 and 17 mm respectively) and compared with experimental stress values measured using strain gauges mounted at regular intervals along the y axis (i.e. perpendicular to the loading direction).

Experimental stress distribution is given by

$$\sigma_E = \frac{E_{11}\varepsilon_{11} + \upsilon_{12}E_{22}\varepsilon_{22}}{(1 - \upsilon_{12}^2(E_{22}/E_{11}))} \tag{6.6}$$

where,

E_{11}&E_{22} Axial and transverse modulus of woven-fabric laminate without hole

ε_{11}&ε_{22} Axial and transverse strains, υ_{12} = Major Poisson's ratio.

Theoretical stress distribution for the tensile specimen estimated was higher compared to the experimental values. The stress distribution measured for the specimens drilled at lower feed rate was less compared to the specimens drilled at higher feed rate. Figure 6.3 shows the theoretical and experimental stresses.

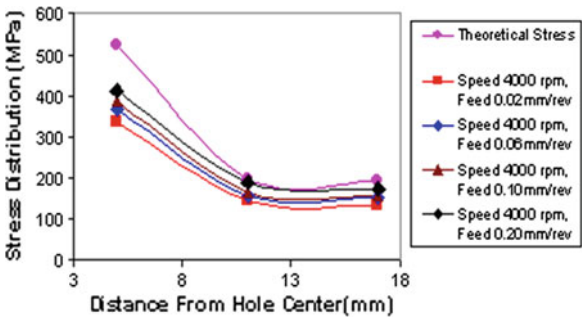

Fig. 6.3 Theoretical and experimental stress distributions for tensile specimen

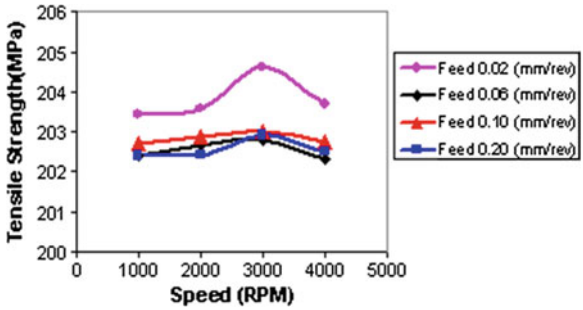

Fig. 6.4 Variation of ultimate tensile strength for notched specimen

The tested specimens showed variation in tensile strength. The specimens drilled at higher feed rate failed at less load compared to specimens drilled at lower feed rate. The values shown in Fig. 6.4 are the average of two identical specimens.

Experimental results showed that the stress concentration and strength of laminates are affected by the cutting speed to feed ratio (V_r/V_t ratio). In particular, larger stress concentrations and damaged zones were observed when lower spindle speed and high feed values are adopted. When high spindle speed and low feed were adopted, the extent of stress concentration and damage reached a minimum.

The specimens drilled at different spindle speeds and feeds have marginal variation on the tensile strength. Even then, the tensile strength of specimens drilled at 3,000 rpm and 0.02 mm/rev, is high compared to the other. The difference between theoretical and experimental tensile strength of the notched laminate could be because of the assumptions made in deriving the equations and variations in the manufacturing of laminates.

6.4 Failure Strength of Notched Laminate in Compression

The compressive test specimens with the dimensions of 38 × 149 mm and gauge length of 12.7 mm were cut from the laminate.

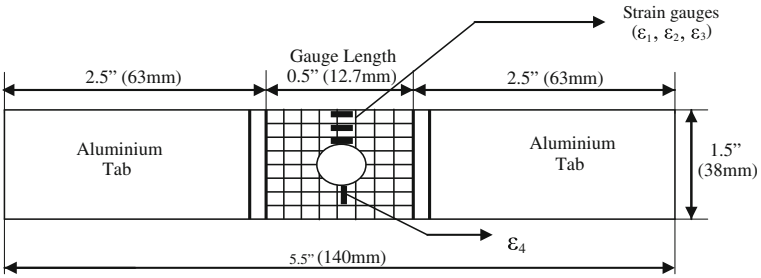

Fig. 6.5 Experimental specimen for compressive test

Figure 6.5 shows the schematic view of the compressive specimen prepared for testing. Thirty two specimens were prepared and holes were drilled at the center of the specimens with different spindle speeds (1,000, 2,000, 3,000 and 4,000 rpm) and feed rates (0.02, 0.06, 0.10 and 0.2 mm/rev). The compressive strength of the notched laminate is estimated using the Eq. 6.3.

where, $r = \frac{R}{R+d_o} = \frac{3}{3+4.9} = 0.38$ and $d_o = 4.9$ mm (Found experimentally)

K_T is the stress concentration factor for an orthotropic plate of finite width

$$K_T = K_T^{\infty} \frac{2 + \left(1 - \frac{2R}{W}\right)^3}{3\left(1 - \frac{2R}{W}\right)} \tag{6.7}$$

where,

K_T^{∞} = Stress concentration factor for an orthotropic plate of infinite width estimated using Eq. (6.4)

W = Width of the orthotropic composite laminate (mm).

The values of K_T^{∞} and K_T are 4.451 and 4.576 respectively.

Compressive strength of the laminate without hole $\bar{\sigma}_o^f = 96.924$ MPa, is found experimentally. The compressive strength of the notched laminate is $\sigma_a^f = 96.924 \times 0.92 = 89.17$ MPa. Figure 6.6 shows the theoretical and experimental stress distribution near the hole and at regular intervals for the compressively loaded coupons drilled at different spindle speeds and feeds.

The hole drilled at lower feed rate generated lower stress values when compared with the holes drilled at higher feed rates. The compressive strength of the specimens tested is shown in Fig. 6.7 and the co-efficient of variation for the specimens drilled at different spindle speeds is 0.4506. Moreover, the failure load of the laminate drilled at spindle speed of 3,000 rpm and 0.02 mm/rev is found to be higher.

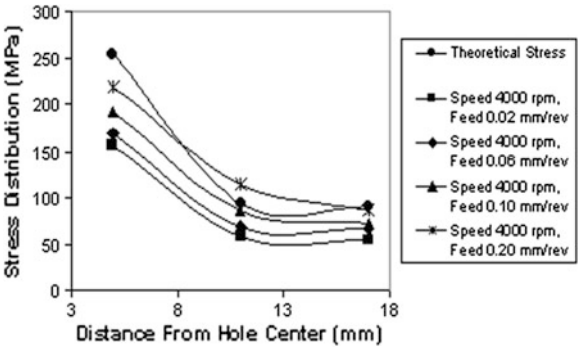

Fig. 6.6 Theoretical and experimental stress distributions

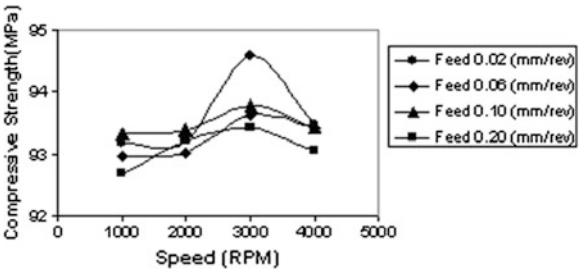

Fig. 6.7 Variation of ultimate compressive strength for notched specimen

6.5 Failure Strength of Notched Laminate in Shear

Woven fabric laminate is cut into $\pm 45^0$ direction and fixed with aluminum end tabs for proper load transfer. Figure 6.8 shows the schematic view of the shear test specimen prepared for testing.

Thirty two specimens were prepared and holes were drilled at the center of the specimens with different spindle speed and feed.

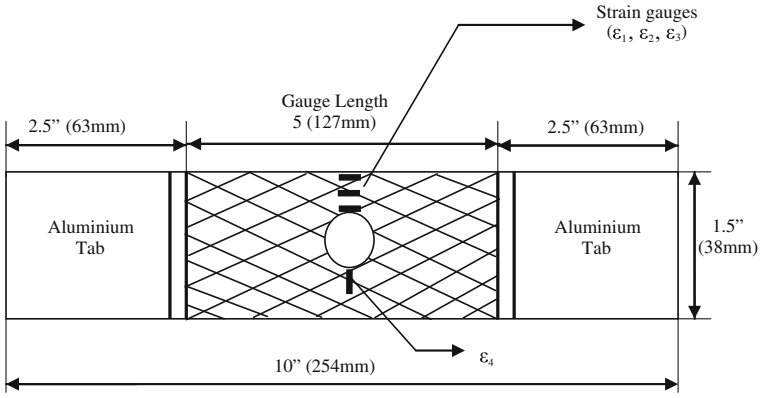

Fig. 6.8 Shear test specimen

Elastic properties of angle-ply Laminate are found experimentally and are given by $E_{11} = 7.784\,\text{GPa}$, $E_{12} = 7.784\,\text{GPa}$, $v_{12} = 0.6863$.
E_{11} = Tensile modulus of (unnotched) laminate in X-direction
E_{12} = Tensile modulus of (unnotched) laminate in Y-direction
v_{12} = Major Poisson's ratio.

Orthotropic stress concentration factors K_T and K_T^{∞} were calculated using Eqs. 7.4 and 7.7 and the values are $K_T = 2.219$, and $K_T^{\infty} = 2.159$ respectively. where, $d_o = 4.895$ mm

$$r = \frac{R}{R + d_o} = \frac{3}{3 + 4.895} = 0.38$$

Shear strength of laminate without hole $\bar{\sigma}_o^f = 68.82\,\text{MPa}$, is found experimentally. The shear strength of the notched laminate is $\sigma_a^f = \bar{\sigma}_o^f \times 0.9134 = 68.82 \times 0.9134 = 62.86\,\text{MPa}$. The testing procedure followed for tensile test is also applicable for shear test. Some selected results are discussed here to show the variation of stress concentration as a function of feed V_t, for cutting speeds V_r.

It can be seen from Fig. 6.9 for the V_r/V_t ratio 50, [4,000 rpm, 80 mm/min (0.02 mm/rev)] the stress concentration produced is comparatively lesser than the other V_r/V_t ratios. This was the trend in tensile test and compressive specimens also.

As can be seen in Fig. 6.10 comparing the ultimate shear strength values for all the specimens, the maximum coefficient of strength variation is 3.1943.

Machining parameters have considerable amount of influence on the shear strength of notched composite laminates. Moreover, the failure load of the laminate drilled at spindle speed of 3,000 rpm and 0.02 is found to be higher.

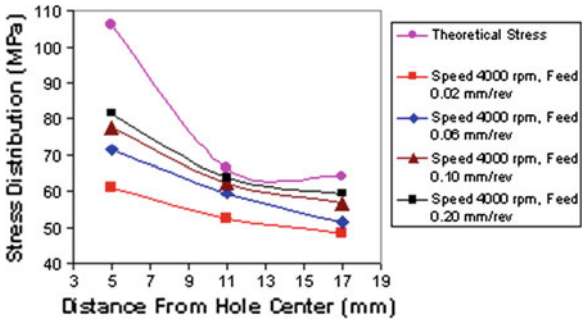

Fig. 6.9 Theoretical and experimental stress distributions for shear specimen

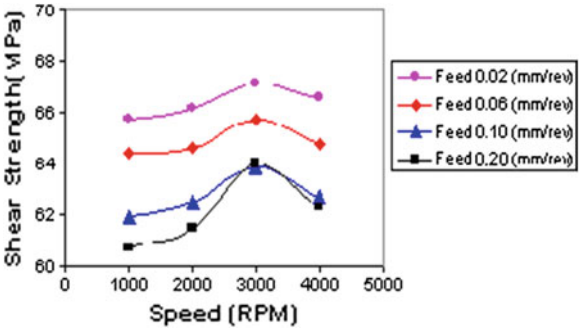

Fig. 6.10 Variation of ultimate shear strength for notched specimen

6.6 Failure Strength of Notched Laminate in Bearing

The purpose of this test is to determine static bearing strength of the composite laminate and to show the bearing stress versus deformation of the hole. Higher strength materials will generally give higher bearing strengths. Bearing strength test is applied where the rivets, bolts, or similar fastenings are to be used in joining members of sections. Bearing load is applied by means of a pin of circular cross-section, which pierces the laminate perpendicular to the surface.

A woven fabric laminate is cut as per the specified dimensions and the aluminum end tabs are fixed at one end (Fig 6.11).

Thirty two specimens were prepared and holes were drilled at the other end with different spindle speed and feed. A fixture and a pin are used to apply the bearing load on the through hole of the specimen. The specimen is placed in between the grips of the machine and tensile load is applied. The readings are taken at the intervals of 1 kN. The bearing stress σ_b is directly calculated from the applied axial load using Eq. 6.8.

$$\sigma_b = \frac{P_b}{td} \tag{6.8}$$

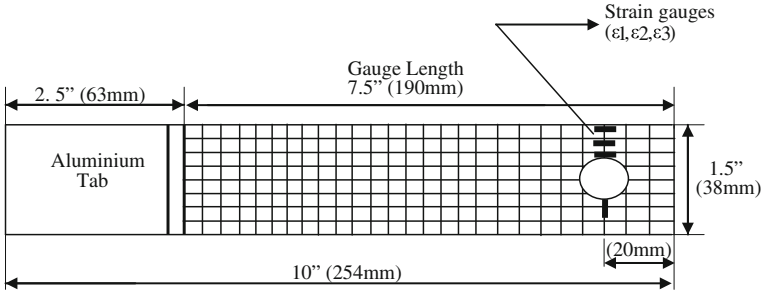

Fig. 6.11 Bearing test specimen [ASTM D953]

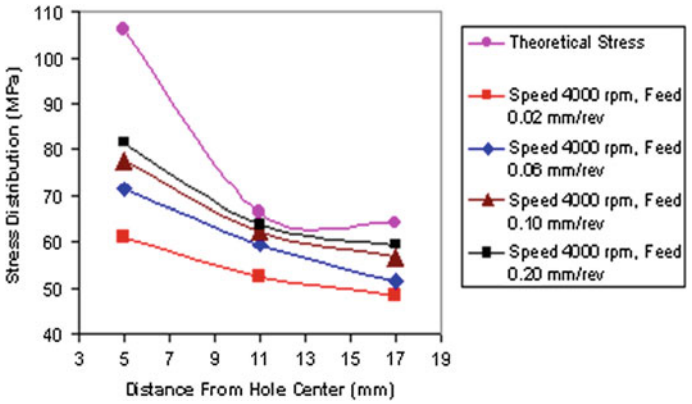

Fig. 6.12 Theoretical and experimental stress distributions of bearing specimen

where,

P_b Bearing load (N)
d Bearing hole diameter (m)
t Specimen thickness (m)

The bearing strength (S_b), which is the stress at which the first failure load occurs and can be identified on the load value in the load-indicating dial.

It is seen from Fig. 6.12 that for the ratio of $V_r/V_t = 50$, [4,000 rpm, 80 mm/min (0.02 mm/rev)] the stress concentration produced is comparatively less than the other V_r/V_t ratios. This was the trend in the earlier tests also. By comparing the ultimate bearing strength values for all the specimens (Fig. 6.13), the hole drilled with 3,000 rpm, 0.02 mm/rev gives highest strength, which is also having the same V_r/V_t ratio of 50 (i.e. 3,000 rpm/60 mm/min).

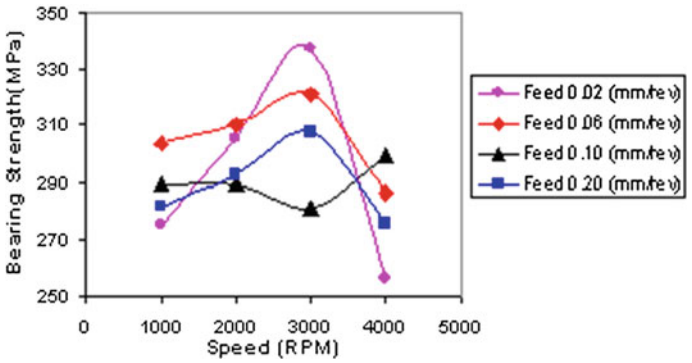

Fig. 6.13 Variation of ultimate bearing strength for notched specimen

The maximum coefficient of strength variation is 7.76. From the experimental results, it is concluded that the machining parameters have influence on the bearing strength of composite laminates.

6.7 Summary

Drilling parameters cause change in cutting forces, which lead to difference in quality of the holes in terms of surface finish, circularity, delamination, fibre pull out, matrix cratering, etc. It is observed from the literatures that the damage increases with both cutting parameters (Spindle speed and feed), which means that the composite damage is bigger for higher cutting speed and for higher feed whereas, at lower spindle speed and lower feed rate, cutting action may not be steady. While drilling if thrust force increased above its critical value delamination is initiated which decreases the strength of the structure.

At spindle speed of 3,000 rpm and feed rate of 0.02 mm/rev, the thrust force generated was less, when compared to all the other speed and feed rates. Even at 4,000 rpm and 0.02 mm/rev the thrust force generated was slightly higher. This could be due to ploughing action at high spindle speed, and higher impact forces of fibres at high spindle speed. The strain distribution measured for the specimens drilled at lower feed rate was less compared to the specimens drilled at higher feed rate.

The specimens drilled at different speed and feed rates showed (Fig. 6.14) variation in tensile strength, compressive strength, shear strength and bearing strength.

The specimens drilled at higher feed rates failed at less load compared to specimens drilled at lower feed rates. So it is concluded that at a spindle speed of 3,000 rpm and feed rate of 0.02 mm/rev, the mechanical strength is high compared to other spindle speeds and feeds [6]. To reduce the problem of machining it is also

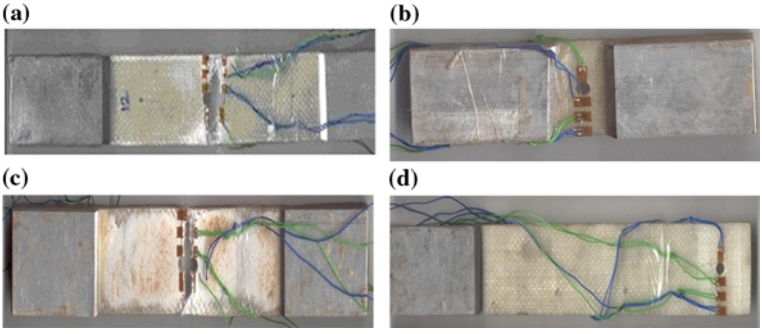

Fig. 6.14 **a** Failed tensile specimen. **b** Compressive test specimen. **c** Failed sear specimen. **d** Bearing test specimen

possible to produce holes during the process of manufacturing composite parts. In the following section behavior of composite plates with drilled and moulded holes are detailed.

References

1. Carlsson LA, Byron PR (1987) Experimental characterization of advanced composite materials. Prentice-Hall, New Jersy
2. Davim JP, Pedro R (2003) Drilling carbon reinforced plastics manufactured by autoclave—experimental and statistical study. Mater Des 24:315–324
3. Erik P, Ingvar E, Leif Z (1997) Effects of hole machining defects on strength and fatigue life of composite laminates. Compos A 31:141–151
4. Koënig W, Wulf Ch, Grass H, Willerscheid H (1985) Machining of fibre reinforced plastics. Ann CIRP 345:37–47
5. Kollar LP, Springer GS (2003) Mechanics of composite structure. Cambridge University Press, Cambridge
6. Krishnaraj V (2006) Study of drilling tool geometry while machining of glass fibre reinforced plastic. Ph.D Dissertation, Anna University, Chennai, India
7. Nilsson S, Bredberg A, Asp LE (2009) Size effects on strength of notched CFRP laminates loaded in bending. In: Proceeding of ICCM 17

Chapter 7
Behavior of Composite Laminates with Drilled and Moulded Hole Under Tensile Load

7.1 Introduction

Nowadays, composite materials are used within primary load carrying aircraft structures. Recent examples are Boeing 787 and Airbus A350XWB where the composite weight content has increased to 50–60 % [22]. However, joining of a composite part on a structure often requires manufacturing holes in order to place bolts or rivets. To obtain these holes, different processes can be implemented such as drilling or moulding. Drilling process concerns a conventional machining procedure where the composite materials are machined to produce hole. Nonetheless, it implies destruction of fibre continuity, large stress concentration and delamination at the hole entry and the hole exit [16, 7, 32]. Such result of damages can cause significant reduction in both tensile and compressive strength of composite structure [26, 27].

The destruction of the fibre continuity leads to the damage on the surface wall of the hole. According to the works of [32, 2, 30], this damage is affected by the interaction between the principal cutting edges of the drill and fibres orientation of the material machined. The results indicate that the machining quality of the wall of the hole is affected partly by the choice of cutting depth (feed rate of the tool) and the angle (θ) measured between the direction of fibres and the direction of cutting speed. For values of θ between $-45°$ and 90°, important damages are observed. These damages are mainly related to the rupture of fibres that is made by bending and shearing of the fibres of the composite part.

Several works have been published on the analysis of delamination at the entry and the exit of the hole. A number of works show that this damage is influenced by the choice of the machining parameters, the geometry of the cutting tool tip, and the nature of its material. All these authors are in agreement for that, the delamination located at the hole exit is caused mainly by the thrust force of the drill [1, 6, 8–11, 17, 18, 24, 29, 33]. For that various authors have been interested to the prediction of the thrust force analytically and numerically. The first analytical model based on the linear fracture mechanics is proposed by Hocheng and Dharan [14]. A 3D finite element analysis, based on fracture mechanics allowing to predict

V. Krishnaraj et al., *Drilling of Polymer-Matrix Composites*,
SpringerBriefs in Manufacturing and Surface Engineering,
DOI: 10.1007/978-3-642-38345-8_7, © The Author(s) 2013

the critical thrust force (for a two lip twist drill) responsible for this damage have been developed. In this modelling, the drill point geometry, the thrust force produced by the main cutting edges and the thrust force generated by the web of the drill are taken into account. The critical thrust forces obtained using this model is compared with those given by the analytical models developed by Hocheng [14]. The results show that the analytical model underestimates the critical thrust forces. Another numerical model has been developed by Zitoune [34]. This modelling is based on the damage mechanics with consideration for the various criteria for damage initiation.

As discussed by Torres et al. [27], conventional drilling leads to a reduction on the mechanical properties of composites structures. This reduction can be quantified by Residual Strength Diagrams which plot the strength of structure as a function of the hole diameter. They found that strength can be represented as an exponential function of hole's size and the orthotropic strength factor which involves the material properties. On the other hand, moulding consists of placing a pointed steel punch to spread out the fibres during the composite lay-up with an aim to leave a hole after polymerization. This process distributes locally the fibre placement at the edge of the hole.

The stress field around the hole in a composite plate under tension has been widely studied in the literature. Several analytical criteria for drilled and notched composites have been developed to predict failure modes. The principal assumption is that there is a stress concentration in damage vicinity which is a function of the material properties, specimen geometry and service loads. However, many of these criteria idealize the model by simplifying the material and geometry heterogeneities that can be observed near the edge of the hole. One of the most used failure criterion for drilled composites is the Point Stress Criterion (PSC) proposed in [25, 31]. This criterion defines a zone of stress intensification in the hole's surroundings as a function of the hole's radius. A similar approach was published by Tercan 2007 to determine the critical crack length at the edge of the hole. Additionally, a modification of PSC, called PWG and published in [5, 23], which assumes an exponential sensitivity of stress when a hole exists. With the same basis, the Damage Zone Criterion (DZC), which involves a maximum stress region around the hole was proposed by [12]. For non-local criterion, an approach called Fracture Characteristic Volume (FCV) was developed to take into account the stress gradient effect on the fracture of the composite laminate [13]. All these criteria and other several fracture models for composites with circular holes and cracks have been reviewed [4] to establish the more influent variables for this problem. Finally, the experimental technique of interferometry was applied by Toubal et al. [28] to determine the strain field and the stress concentration in woven fabric composites with circular hole under a longitudinal tensile load.

Few works concern specimens with moulded holes made of woven fabric, moreover, no literature is available on specimens made of unidirectional carbon fibres. Although the moulded holes require a specific mould for manufacture, the final outcome is comparable to the solution with drilled holes, and the cost of the

mould can be amortised over a period of time. Experimental works were carried out by Ng et al. [21], Lin et al. [20], Lin and Tsai [19], Hufenbach et al. [15] on the behaviour of composite panels and assembly with moulded hole under tensile load. In these studies a numerical procedure is used to predict the notched strength of the specimens with moulded hole. The results showed a strength dependency to the hole's diameter. For the same hole size, the predicted failure strength of specimens with moulded holes using numerical analysis have a higher value which are slightly higher than the experimental ones. On the other hand, the experimental study proposed by [20] leads to larger failure strength, smaller the initial stiffness and larger the failure strain of [0°/90°]s laminates with a moulded hole compared to those with a drilled hole. Lin et al. [19] uses experimental and numerical methods to study the failure of bolted joints of glass woven composites with drilled and moulded holes. Failure tests are conducted with the sequence [0°/90°]s and [±45°]s of woven glass/polyester roving specimens with different hole sizes and ratios E/D (distance from the hole centre to the edge on the hole diameter). For E/D = 1, the results exhibit the fracture strength of the moulded specimens of about 30–50 % higher than those with drilled specimens. The same order of magnitude between them exits when the ratio is E/D > 2.

In this section, a comparison between two categories of perforated specimens loaded in tension has been presented. The holes of the first category are obtained by drilling and by moulding for the second category. The studied specimens are quasi isotropic made of unidirectional prepreg materials. In order to analyze the behaviour of the specimens in the vicinity of the hole, the strain field measurement with the three-dimensional Digital Image Correlation (DIC) technique is carried out. The results obtained with 3D DIC technique are compared with the strain gauge measurements. The pictures obtained by a CCD-camera are used to describe the damage mechanisms of the plates with drilled and moulded holes. In order to understand better the causes of damages produced near the moulded holes during the tensile tests, the void content and fibre content has been quantified using normalized and no normalized methods (image processing).

7.2 Experimental Procedure

Unidirectional prepregs of 0.25 mm made of carbon/epoxy composite are used for preparing CFRP specimen. The raw materials of laminated structures are provided by Hexcel composites and are referenced as UD HexPly® T300-M10 with 56 % fibre content. The Table 7.1 presents the mechanical properties of the UD CFRP prepreg obtained following the mechanical standard ASN-A 4102. The stacking sequence of the composite parts is quasi-isotropic. The UD prepreg used for manufacturing is contained between two rigid moulds. On these two rigid moulds, holes were machined and fitted with pointed steel punch which has been used to spread the fibres during the manufacture process of the composite plate and getting

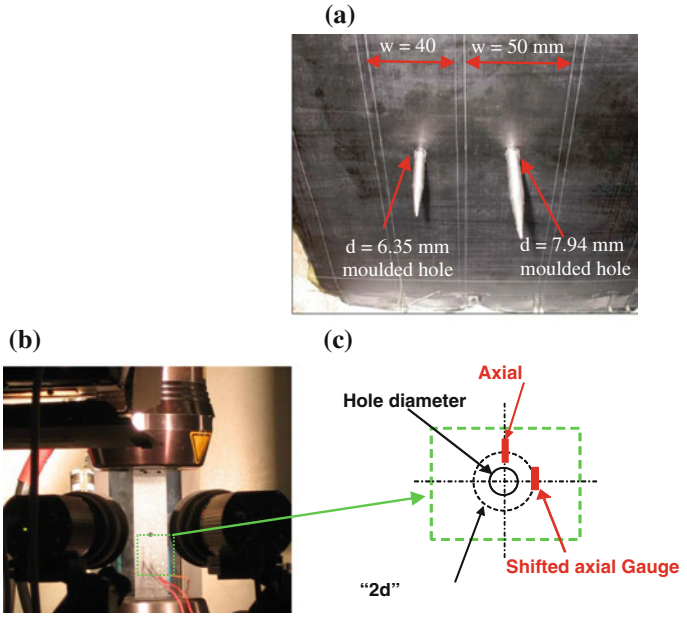

Fig. 7.1 Specimens for the tensile tests related to **a** mother plate from the mould, **b** Experimental device with DIC, **c** Scheme of the gauges position

Table 7.1 Mechanical properties of (T300/M10) carbon/epoxy unidirectional composites

Young's modulus (GPa)	Shear modulus (GPa)	Compressive modulus (GPa)	Poisson's ratio
$E_{11} = 125$, $E_{22} = 7$	$G_{12} = 3.2$	115	$\nu_{12} = 0.3$, $\nu_{21} = 0.016$, $\nu_{13} = 0.3$
Tensile strength (MPa)	In plane sheat strength (MPa)	Compressive strength (MPa)	Fiber content (%)
$\sigma_{11} = 1{,}600$ $\sigma_{22} = 80$	$\tau_{12} = 90$	1,400	56

a circular space after polymerization (Fig. 7.1a). The displacement of the pointed steel are activate when the resin reach the viscous phase. Vacuum and pressure are applied and maintained during the period of solidification.

In order to reduce the variability due to the manufacturing process all the specimens tested are obtained from the same mother plate. Two sets of specimens were tested (Fig. 7.1a). The first set concerns the specimens with moulded holes with diameter values of 6.35 and 7.94 mm. The second set includes the drilled hole specimens with the diameter values of the moulded holes. The diameter values used in this study are usually employed in the aeronautical field. For all specimens tested

the ratio between the hole diameter and the part width (d/w) is equal to 0.15 mm (Fig. 7.1a). The drilling is performed with a tungsten carbide drill (Twist drill).

A randomly distributed pattern is painted on the surface of the specimen for the strain field measurements thanks to Digital Image Correlation (DIC) technique (Fig. 7.1b). Moreover, on the same surface, two strain gauges (Fig. 7.1c) are pasted in the loading axis and located at a distance D (hole diameter) from the hole, which allows the axial strain measurement at two different places. Tensile tests were performed by means of an (Instron) UTM with a load capacity of 100 kN (Fig. 7.1b) at a speed of (2 mm/min). In order to better understand the different damage modes observed between drilled and moulded holes, the void content and fibre content analysis have been carried out using two methods. The first is normalized ASTM D3171 based on the dissolution of the specimen in sulphuric acid [3]. The second method is based on the image processing technique.

In order to quantify the variability of the void content as well as the fibre content in the vicinity of the moulded hole inducted by the manufacturing process, because of the need of the local information, here it is proposed the use of a method based on the technique of image processing. With the normalized method a mean value can be measured relative to the analysed material volume.

The technique of image processing principle consist of taking several SEM pictures of the plan "Pi" (i = number of plan). For this, specimens must firstly be prepared by polishing (See Fig. 7.2). Thanks to image processing the fibre content and the void content can be calculated statistically. In the SEM picture, voids, fibres and resin appear at different colours: white for fibres, grey for resin and black marks for voids. Using image processing software, it is simple to make only voids appear. The main idea here is to modify pictures in a binary form, which in fibres and matrix are associated with a white colour, and voids with black. In practice, it consists in setting a threshold to dissociate voids from the rest of the picture. Using this technique, voids surface content is equal to the ratio between black surface and the whole surface of the picture. The same principle is used to obtain the fibre ratio from all coupons.

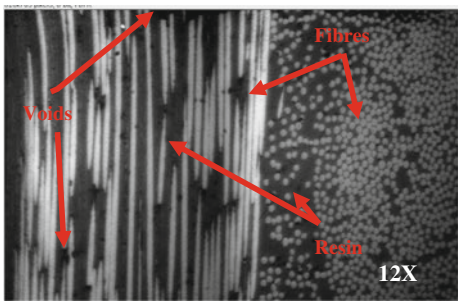

Fig. 7.2 SEM observation of the specimen thickness with 12X magnification

7.3 Results

7.3.1 Behaviour Analysis

Figure 7.3a shows the evolution of load versus measurements by the axial gauge for the drilled and moulded hole specimens with a 7.94 mm diameter (D). Failure strength for moulded hole is 30 % higher than the drilled hole. In addition, the axial gauge allows a local rigidity detection of the material in the moulded hole specimen which is smaller than the one detected on the drilled plate. After a detailed analysis, presence of a resin rich zone in the vicinity of the axial gauge is detected. The presence of the resin rich zone is related to the manufacturing process of the specimen with moulded hole which spreads the fibre around the hole. This analysis is verified by the X-Ray images obtained from specimens with moulded holes manufactured from textile structure [15].

Load versus strain curves given by the shifted axial gauge revealed that the local rigidity for moulded holes is higher than that of drilled holes (Fig. 7.3b). This difference can be explained by the fact that, in the area where the shifted axial gauges are pasted, the fibres are higher because of the stretched fibres o produce moulded hole. All the tested plates present the same results as presented in Fig. 7.3. Table 7.2 lists the average values of the failure strength for different studied specimens. It is found that the moulded hole specimens have higher residual strength compared with the drilled hole specimens. This gain is around 33 % for all specimens tested with 6.34 and 7.94 mm diameters.

The strain field, measured using the DIC technique, is confronted with strain gauges data. For the drilled hole, it is observed a good agreement between the two measuring techniques, with the maximum difference being about 5 %. With regard to the moulded hole specimens, the strain measurements are in good agreement with those obtained by the strain gauges when the applied load is lower than 28 kN (Figs. 7.4, 7.5). When the load reached 28 kN, damaged zones on the surface of the specimen are observed. This damage can be observed by the delamination of

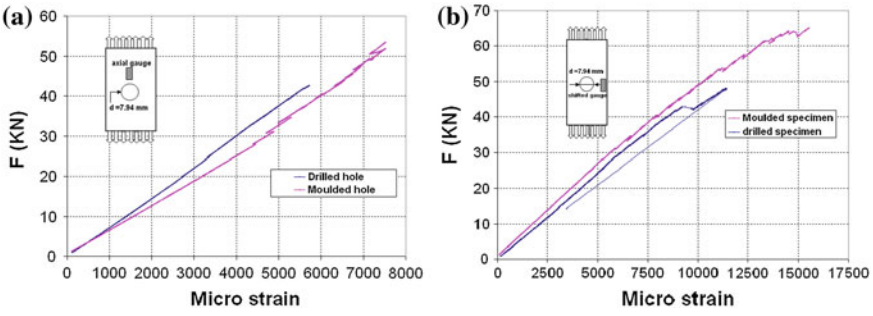

Fig. 7.3 Load versus gauges strains for specimens with moulded hole and drilled hole with 7.94 mm of diameter related to **a** axial gauge, **b** shifted axial gauge

Table 7.2 Average failure stress values for the different studied specimens

Diameters: d (mm)	Failure stress with drilled hole: σ (MPa)	Failure stress with moulded hole: σ (MPa)
6.34	349 ± 16	459 ± 35
7.93	386 ± 35	514 ± 40

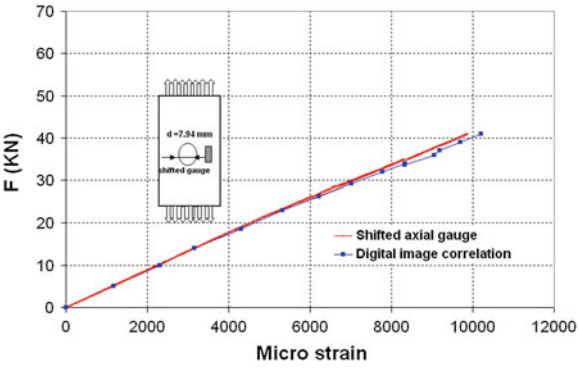

Fig. 7.4 Load versus strains, measurement comparison between DIC technique and strain shifted gauge related to drilled specimen with a 7.94 mm drill diameter

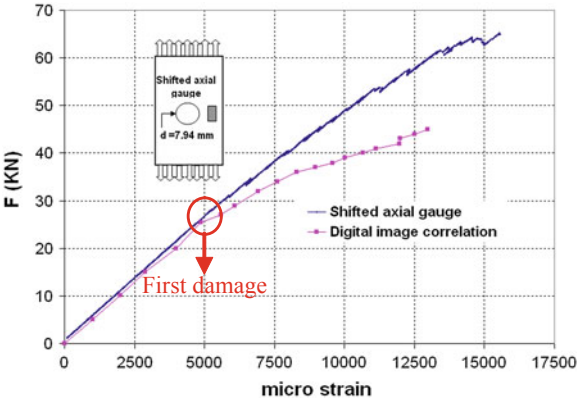

Fig. 7.5 Load versus strains, measurement comparison between DIC technique and strain shifted gauge related to moulded specimen with a 7.94 mm hole diameter

the above ply. This delamination affects the measurements taken, resulting into difficulties to achieve an accurate image correlation.

Image analysis provided by CCD camera shows a difference between the damage mode observed for the specimen with moulded hole and drilled hole for 7.94 mm diameter. Figure 7.5 shows a first damage occurrence for the specimen with moulded hole with the appearance of a crack oriented in the same direction as the 0° ply (or loading axis (OY)). This crack, observed at a given load value of 28 kN, is located at 1 mm at the edge of the hole (Fig. 7.6a). As the applied load increase, it is observed a second crack initiation (second damage) on the second edge of the moulded hole (at the right edge) and then a propagation of these two cracks in a parallel direction with regards to the fibre axis (Fig. 7.6a). With a load

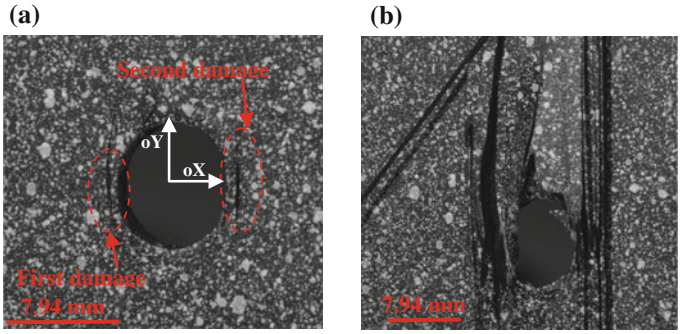

Fig. 7.6 Damage progression for different loading levels with 7.94 mm moulded hole related to **a** 47 kN loading, **b** 64 kN loading

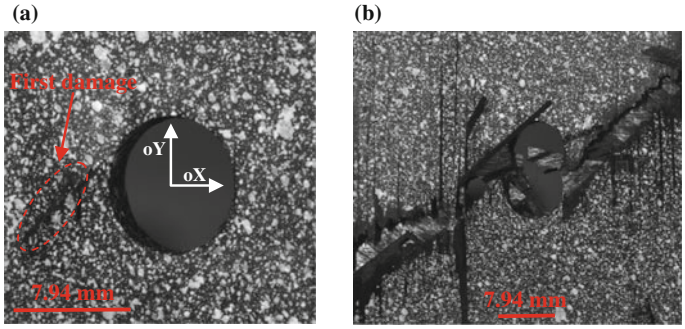

Fig. 7.7 Damage progression for different loading levels with 7.94 mm drilled hole related to **a** 42.5 kN loading, **b** 49 kN loading

value of 64 kN, the damage increase appears as a separation of the higher ply (Fig. 7.6b).

The CCD recorded sequences during the tensile test related to the drilled hole specimen show a different failure mode from that observed with a moulded hole. For a loading force lower than 42.5 kN, no damage is noticed. From 42.5 kN, a first damage (as a crack shape) oriented at 45° to the loading axis (OY) is observed (Fig. 7.7a). This crack remains stable until an amplitude of 48 kN (no propagation is observed). Moreover, when the loading reached 49 kN, a sudden failure of specimen is noted (Fig. 7.7b). All tested specimens present the same failure mechanisms. This mode of damage is similar to the drilled plates under tensile load [26].

It is noticed that, the damage mode versus the applied load for our moulded holes specimens (quasi-isotropic stacking sequence) made of UD prepreg is different compared to drilled holes, similarly the damaged are different for the moulded holes using woven fabrics with the same stacking sequence [21, 20, 15].

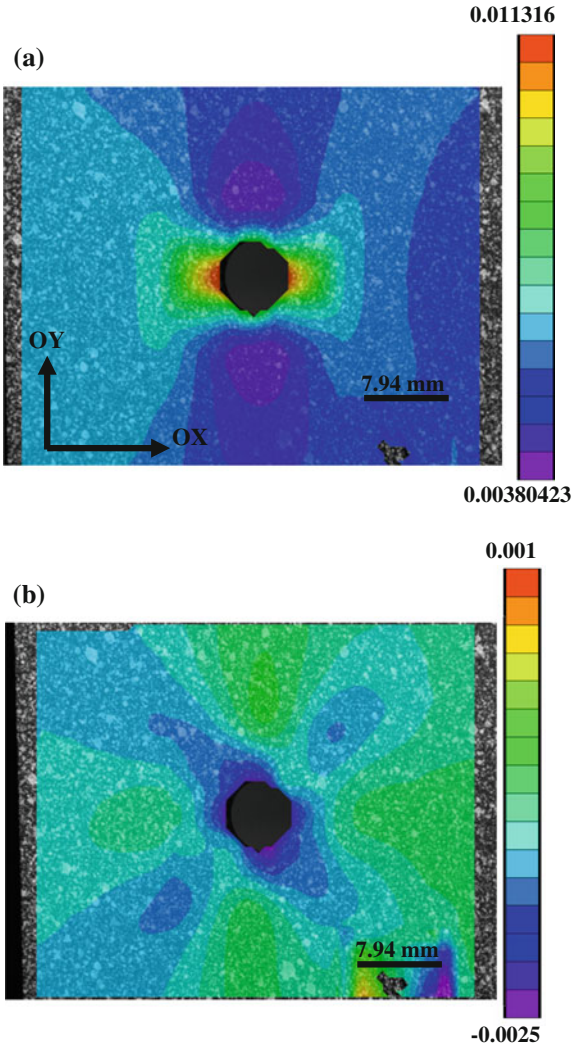

Fig. 7.8 Strain field distribution by the DIC technique for a 7.94 mm drilled hole specimen and a 25 kN loading amplitude related to **a** strain along the OY axis (ε_{yy}), **b** strain along the OX axis (ε_{xx}) (correlation carried out with 33-pixel of ZOI)

This difference can be explained due to the fibres trajectory near the hole as well as the amount of void content and fibre content in the vicinity of the hole.

Figure 7.8 shows the strain field distribution on the surface of a drilled hole specimen for a loading amplitude corresponding to 25 kN. These images are obtained with a 33-pixel size. In Fig. 7.8a, it is observed a positive strain along (OY) axis everywhere and a maximum value located at the edge of hole. For the strain field cartography along the transverse axis (OX), we notice the negative measured values (Fig. 7.8b). These strain results are caused by the Poisson modulus effect. However, for the same loading level, the strain amplitudes recorded on a drilled hole specimen are higher compared with those recorded on

moulded hole specimens (Figs. 7.8, 7.9). For a load of 25 kN, the axial strain ε_{yy} measured by the DIC for a plate with drilled hole is around 11,356 μdef. For the same test conditions and similar correlation parameters (DIC), the strain measured on specimen with moulded hole is around 6,000 μdef. For moulded holes, the fibre content is more important in the vicinity of the hole. This discrepancy can be linked to the difference in the local mechanical proprieties.

With the test conditions of the DIC image analysis carried out on the moulded hole specimens presented on the Fig. 7.9 (ZOI of 33 pixels), it is noticed that the transverse strain (along OX axis) presents a negative sign on all the structure. However, the crack opening phenomenon is observed around the hole thanks to the images provided by CCD camera. It results into a stress field with a positive sign

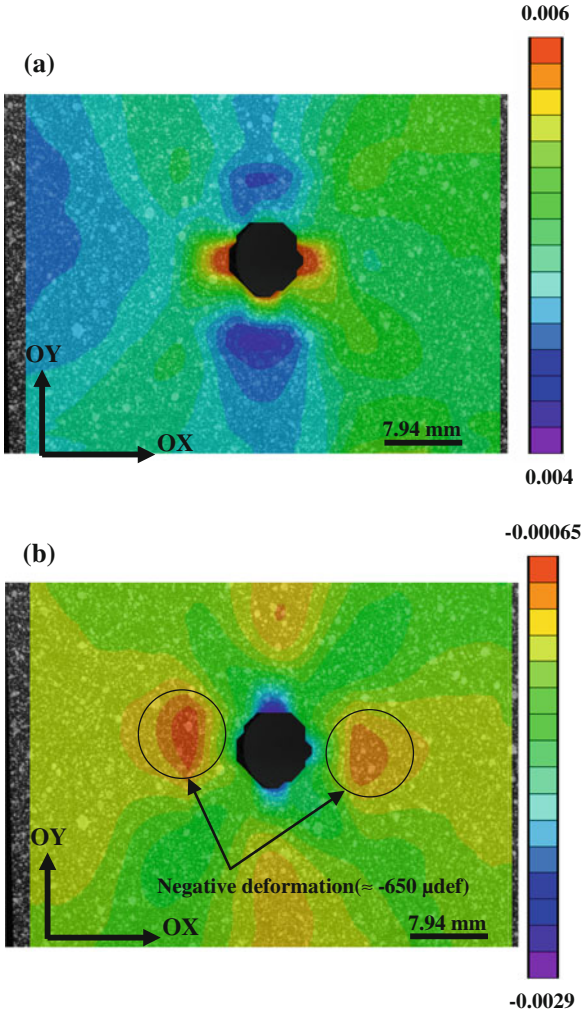

Fig. 7.9 Strain field distribution by the DIC technique for a 7.94 mm moulded hole specimen and a 25 kN loading amplitude related to **a** strain along the OY axis (ε_{yy}), **b** strain along the OX axis (ε_{xx}) (correlation carried out with 33-pixel of ZOI)

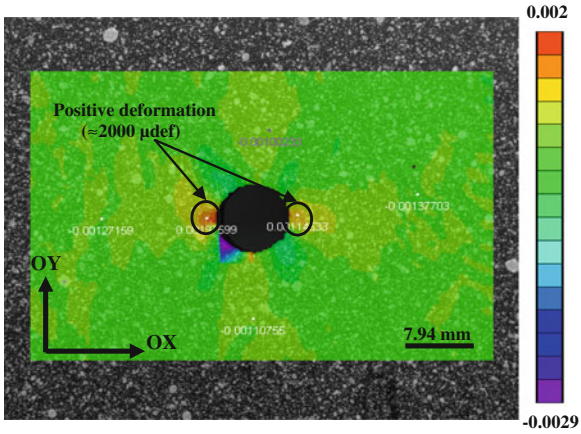

Fig. 7.10 Strain field distribution (ε_{xx}) by the DIC technique for a 7.94 mm moulded hole specimen and a 25 kN loading amplitude with the condition of correlation of 19 pixel of ZOI

along the OX axis. For this reason, additional correlation is carried out by means of a 19 pixels numerical gauge (ZOI). With this conditions, the result shows that, on one hand a positive transverse strain (along OX axis) near the hole is measured and it is in agreement with the opening crack phenomenon observed during the tensile test (Fig. 7.10); on the other hand the physical information is lost and this can be induced by the measurement noise or the quality of the specimens random pattern.

7.3.2 Fibre and Void Content Analysis Near the Moulded Hole

The use of the normalized method and no normalized method on five specimens cut far from holes give almost identical results. In this case, the mean values are respectively 4 and 56 % for the void content and the fibres content. The values of relative deviation are 0.5 % for the void content and 1 % for the fibres content. It can be assumed that this non-standardized method gives accurate results.

As shown in Figs. 7.11, 7.12, the results of this optical technique are presented for four positions (5, 6, 9 and 10) located respectively at 11.5, 9, 3.7 and 1.2 mm from the moulded hole centre in the Ox direction. From the Fig. 7.11 there is a small increasing of the fibre content and the void content measured in the plane 6 compared to these measured in the plane 5. At this step, it can be noted here that fibre ratio increase when the measurement comes near the hole, in both x and y directions. The maximal fibre content found is 57 % and it is measured close to the

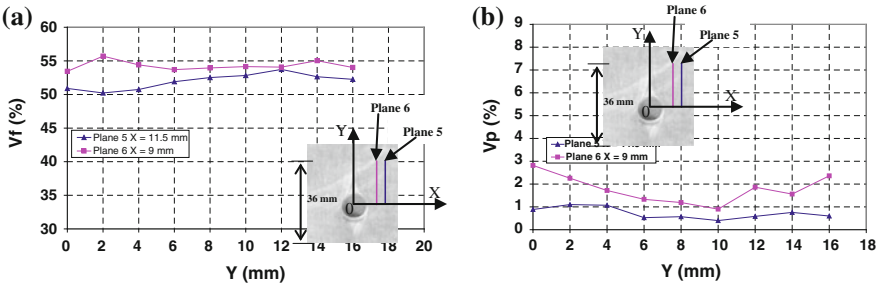

Fig. 7.11 Evolution of the fibre content and the void content along the loading direction (oY) in plane 5 and 6, **a** fibre content, **b** void content. Moulded plate with diameter of 6.35 mm

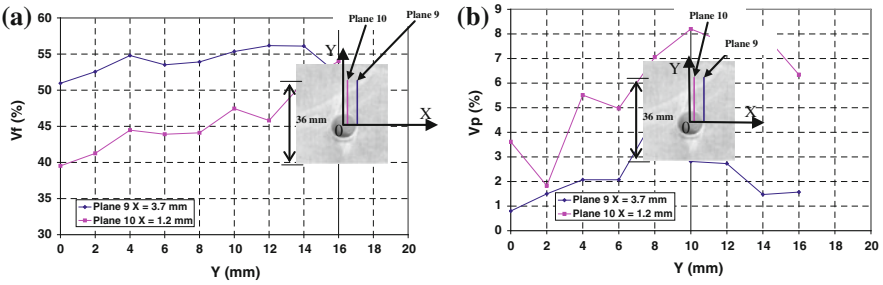

Fig. 7.12 Evolution of the fibre content and the void content along the loading direction (oY) in plane 9 and 10, **a** fibre content, **b** void content. Moulded plate with diameter of 6.35 mm

hole. At this location, picture analysis show that voids content is about 7 %. Modifications of void and fibre content can explain the onset of cracks during loading and fibre spread due to a lake of matrix.

7.4 Summary

This paper presents experimental results of drilled holes and moulded holes of composite specimens with quasi-isotropic stacking sequence made from UD prepreg and subjected to tensile loading. Based on the experimental analysis, the following conclusions were drawn.

1. The fracture strength for moulded hole specimens is higher than those obtained for drilled hole specimens. This difference is greater than 30 %. Although the fibre content around the moulded hole is higher than the drilled hole, it has been noted from strain gauge data that the local rigidity in tension for drilled specimens is higher than moulded specimens.

2. Moreover, the digital images obtained by the CCD Camera show different damage mechanisms between drilled holes and moulded holes specimens. For a plate with drilled hole, a sudden fracture is noticed and for the plate with moulded hole a progressive fracture is observed.
3. The strain fields measured by the DIC have shown that the maximum deformation (εyy) of drilled hole is twice higher compared to those of moulded hole. Also, the strain field cartography obtained from the test data leads to the strain along the transverse direction (OX) influenced by the size of the numerical correlation gauge. All the results obtained with the numerical correlation gauge corresponding to the 19-pixel size are in good agreement with the damage mechanisms observed by means of the CCD Camera.
4. The difference of the mechanical behaviour observed as well as the difference of the damage mode illustrated between the specimens with drilled and moulded hole were explained by the local measurement of the fibres content and void content carried out by the optical technique. In the plates with moulded holes, the void content in the vicinity of the hole is 8 % higher compared the void content far the hole.

References

1. Antoniomaria DL, Alfonso P, Francesco V (1996) Tool wear in drilling thermoset and thermoplastic matrix composites. Eng Syst Des Anal 75:41–46
2. Arola D, Ramulu M, Wang H (1996) Chip formation in orthogonal trimming of graphite/epoxy composites. Compos Part A 27A:121–133
3. ASTM D3171-99 (2004) Standard test methods for constituent content of composite materials. ASTM Int
4. Awerbuch and Madhukar (1985) Notched strength of composite laminates, predictions and experiments. J Reinf Plast Compos
5. Baselga Arino S, Maza Frechin M (2006) Methods for modelling the ultimate strength of orthotropic plate with a central hole under uniaxial tension. J Mater Sci 41:4365–4372
6. Campos Rubio J, Abrao AM, Faria PE, Esteves Correia A, Paulo Davim J (2008) Effect of high speed in the drilling of glass fiber reinforced plastic: evaluation of the delamination factor. Int J Mach Tool Manuf 48:715–720
7. Davim JP, Pedro R (2003) Drilling carbon reinforced plastics manufactured by autoclave—experimental and statistical study. Mater Des 24:315–324
8. Davim JP, Reis P (2003) Study of delamination in drilling carbon fiber reinforced plastics (CFRP) using design experiments. Compos Struct 59(4):481–487
9. Dharan CKH, Won MS (2000) Machining parameters for an intelligent machining system for composite laminates. Int J Mach Tools Manuf 40:415–426
10. Durão LMP, De Moura MFSF, Marques AT (2008) Numerical prediction of delamination onset in carbon/epoxy composite drilling. Eng Fract Mech 75(9):2767–2778
11. Erik P, Ingvar E, Leif Z (1997) Effects of hole machining defects on strength and fatigue life of composite laminates. Compos A 31:141–151
12. Eriksson and Arronson "Strength of tensile loaded graphite/epoxy laminates containing cracks, open and filled holes. J Compos Mater
13. Hochard C, Lahellec N, Bordreuil C (2007) A ply scale non-local fibre rupture criterion for CFRP woven ply laminated structures. Compos Struct 80:321–326

14. Hocheng H, Dharan CKH (1990) Delamination during drilling in composite laminates. J Eng Ind 112:236–239
15. Hufenbach W, Adam F, Kupfer R (2010) A novel notching technique for bolted joints in textile-reinforced thermoplastic composites. 14th European conference on composite materials, Paper ID: 461. Budapest, Hungary. 7–10 June 2010
16. Koënig W, Wulf Ch, Grass H, Willerscheid H (1985) Machining of fibre reinforced plastics. Ann CIRP 345:37–47
17. Krishnaraj V (2006) Study of drilling tool geometry while machining of glass fibre reinforced plastic. Ph.D Dissertation, Anna University, Chennai
18. Langella A, Nele L, Maio A (2005) A torque and thrust prediction model for drilling of composite materials. Compos A 36:83–93
19. Lin JH, Tsai CC (1995) Failure analysis of bolted connections of composites with drilled and moulded-in hole. Compos Struct 30:159–168
20. Lin JH, Tsai CC, Shie JS (1995) Failure analysis of woven-fabric composites with moulded-in holes bolted connections of composites with drilled and moulded-in hole. Compos Sci Technol 55:231–239
21. Ng SP, Tse PC, Lau KJ (2001) Progressive failure analysis of 2/2 twill weave fabric composites with moulded-in circular hole. Compos: Part B 32:139–152
22. Nilsson S, Bredberg A, Asp LE Size effects on strength of notched CFRP laminates loaded in bending. In: Proceeding of ICCM 17
23. Pipes and Wetherhold (1979) Notched strength of composites materials. J Compos Mater EUA
24. Singh I, Bhatnagar N, Viswanath P (2008) Drilling of uni-directional glass fiber reinforced plastics—experimental and finite element study. J Mater Des 29:546–553
25. Tercan M, Asi O, Aktaş A (2007) Determination of the critical crack length of notched weft-knitted glass fiber variable width composite plates. Compos Struct 77:111–119
26. Torres M, Gonzalez JL, Hernandez H (2009) Residual strength and fracture path for drilled epoxy-glass composites. Adv Mater Res 65:89–96
27. Torres M, Gonzalez JL, Hernandez H (2009) Fracture behavior characterization of composite tubes with hole defects under tensile load. Suplemento de la Revista Latinoamericana de Metalurgia y Materiales S1(3):1183–1188
28. Toubal L, Karama M, Lorrain B (2005) Stress concentration in a circular hole in composite plate. Compos Struct 68:31–36
29. Tsao CC, Ho-Cheng H (2005) Effect of eccentricity of twist drill and candle drill on delamination in drilling of composite materials. Int J Mach Tools Manuf 45:125–130
30. Wang DH, Ramulu M, Arola D (1995) Orthogonal cutting mechanisms of graphite/epoxy composite, Part I unidirectional laminate. Int J Mach Tools 35(1):1623–1638
31. Whitney and Nuismer (1974) Stress fracture criteria for laminates composites containing stress concentrations. J Compos Mater
32. Zitoune R, Collombet F (2005) Experiment-calculation comparison of the cutting conditions representative of the long fibre composite drilling phase. Compos Sci Technol 65:455–466
33. Zitoune R, Collombet F (2007) Numerical prediction of the thrust force responsible of delamination during the drilling of the long-fiber composite structures. Compos A 38:858–866
34. Zitoune R, Collombet F, Piquet R, Lachaud F, Pasquet P (2005) Experiment-calculation comparison of the cutting conditions representative of the long fibre composite drilling phase. Compos Sci Technol 65:455–466